CENTRE FOR MINERALS RESEARCH

UNIVERSITY OF CAPE TOWN

EVALUATING THE EFFECT OF OPERATING VARIABLES ON ENERGY CONSUMPTION IN STIRRED MILLS

Mussa Lisso

(BSc. Chemical Engineering)

A dissertation submitted to the Faculty of Engineering and the Built Environment at the University of Cape Town, in fulfilment of the requirements for the degree of Masters of Science in Engineering

October 2013

“For every complex problem there is an answer that is clear, simple, and wrong.”

H. L. Mencken

PLAGIARISM DECLARATION

I hereby declare that the work presented in this MSc. thesis is mine. Any thoughts and postulations used in this thesis that were obtained from the body of literature were appropriately referenced.

_____

Mussa M. Lisso

ACKNOWLEDGEMENTS

Above all, I would like to thank God for being my guide and protector through every step of the way.

I further take this opportunity to acknowledge the people who immensely contributed to the success of this thesis.

I would like to thank my supervisor A/Prof. Aubrey Mainza for his guidance and assistance during the period of my MSc project. I would also like to thank members of the Centre for Minerals Research (CMR) team for assistance in the laboratory work conducted at University of Cape Town (UCT).

Abundant appreciation to Bismark Sarpong for his invaluable assistance during my milling tests at mintek and also sample processing at UCT's CMR laboratories. Special thanks to Warren Little and Lucy van de Ruit, for some of the test work data.

I would also like to express my gratitude to members of the Minerals Processing Division (MPD) at Mintek in Johannesburg. Special thanks to Getrude Marope and Ntokozo Shabalala, for their assistance and support when carrying out my test work at Mintek.

Last but not least, I would like to thank my parents for their endless support. In addition, great appreciation to my siblings Nyakwesi, Ibrahim and Zebida for dispatching hope and emotional support throughout my MSc programme.

ABSTRACT

High grade ores have largely been depleted and those currently being treated are low grade, complex and sometimes finely disseminated, requiring fine grinding to liberate valuable minerals. For fine grinding applications, conventional tumbling mills are energy intensive. More energy efficient technologies such as stirred mills have been developed and widely used for fine and ultra-fine grinding.

In this study, the effects of residence time, solids concentration, impeller speed, impeller type, media size and media density on energy consumption in a batch vertical stirred mill were investigated. The effect of energy on mill performance was assessed using the perfect mixing mill model. In addition, the effect of media stress intensity on grind and energy efficiency at constant residence time was also investigated.

It was found that irrespective of the method of altering the energy input, the fineness of grind improved with increase in the specific energy input. This suggests that energy is the key driver for size reduction. The perfect mixing model can be used to assess mill performance and the breakage rates generally increased with increase in the specific energy input, impeller speed and solids concentration.

The media stress intensity approach is useful in assessing mill performance in stirred mills at constant residence time. The fineness of grind improved when the media stress intensity was varied from 4.41×10^{-3} to 27.41×10^{-3}Nm. In addition, the specific energy required to produce material below 25µm and 38µm decreased with an increase in the media stress intensity. When slurry density effects were considered, an optimum stress intensity was observed with respect to specific energy required to produce material below 25µm and 38µm.

It was recommended that additional test work be carried out to investigate the effect of media size in the range -6.7mm + 2mm on energy efficiency. It was also recommended that tests be carried out at impeller speed between 600rpm and 1500rpm to assess how mill performance increases even at relatively high impeller speeds. In addition, a model predicting the specific energy using the impeller speed and solids concentration can also be developed.

Table of Contents

List of Figures

List of Tables

List of Symbols

m_i: mass fraction of material in the mill in size class i at time t

S_i: size-discretized selection function which gives the fraction of material broken down from i^{th} size class per unit time

b_{ij}: size-discretized breakage distribution function for material appearing in size class i from size class j.

S_N: Stress Number

N_c: Number of grinding media contacts

N_p: Number of product particles in the mill

P_s: The probability that sufficient stress is applied to a particle trapped between grinding media

SI: Stress intensity

SI_{GM}: Stress intensity of the grinding media

d_{GM}: Grinding media diameter

ρ_{GM}: Grinding media density

v_t: Tangential velocity

RPM: Revolutions per minute

SG: Specific gravity

wt%: Weight per-cent

SE: Specific energy

P_{80}: size at which 80% of product material passes

CHAPTER ONE: INTRODUCTION

The origins of the processes of comminution, a primary step in mineral processing, stretch as far back as the medieval era (Gaudin, 1939). Through comminution, minerals of value locked in host rocks are liberated in preparation for harvesting through subsequent downstream processes such as froth flotation and leaching. For several years, the general consensus in the mineral processing industry has been that comminution is the most energy demanding and, consequently, the most cost intensive step (Wills, 1997). Adequate liberation of valuable minerals from host ore bodies has become increasingly difficult over the years as ore grades have significantly dropped over time. In order to achieve sufficient liberation of minerals of value, it has become necessary to grind below traditional product requirements of 80% passing 75μm mesh size (Jankovic, 2003).

Comminution circuits have been dominated by tumbling mills for both coarse and fine grinding because of their ability to process large throughputs. Tumbling mills such as ball mills have been proven to be energy intensive in the fine and ultra-fine region of the grinding spectrum. Until recently, the mineral processing industry has been reluctant to deviate from using traditional comminution circuits for fine grinding. However, there has been growing concern over the excessive energy demands of tumbling mills which result in significantly high operating costs in comminution. In South Africa, Eskom estimates show that the mining industry consumes 15% of their annual electricity output. Of this 15%, the gold mining sector consumes 47%, platinum mines, 33% and other mine 20% (Eskom, 2013). According to Ntsele and Allen (2012), 30% of the energy consumed in a concentrator is used in crushing and grinding of ores. This has a negative impact on the operating costs due to the increasing cost of electricity. This has driven the development of new milling technologies in an attempt to address these energy issues. In addition, efficient energy utilisation could also help reduce Green House Gas (GHG) emissions (Ntsele and Allen, 2012).

The development of stirred milling technologies has found wide acceptance in the platinum industry due, mainly, to the improved energy efficiencies for fine and ultra-fine grinding compared to tumbling mills. Other benefits of stirred mills are low installation and maintenance costs, the ability to utilize inert grinding media and the ability to operate at high speeds, which results in high power intensities. A number of stirred mills have been developed but the major categories are horizontal and vertical stirred mills. It has been

postulated that the breakage mechanisms in these stirred mills are similar although slight differences may be related to stirrer types, operating rotor speed, method of media retention and equipment size (Kwade, 1999a). Stirred milling technologies have been introduced to main stream inert grinding (MIG) and ultra-fine grinding (UFG) circuits with acceptable success (Rule *et al*., 2008). The introduction of stirred milling technology in existing circuits has been challenging, mainly due to additional capital costs required for supporting equipment and instrumentation. An informed judgment regarding the customization of existing circuits to accommodate fine grinding technology is necessary. This can be achieved by identifying and assessing the most important variables affecting the fine grinding of minerals using stirred mills. Some of the variables identified include the rotor speed, grinding media size and density, grinding media load, slurry density and stress intensity. A number of researchers (He and Forssberg, 2006; Jankovic, 2003; Kwade, 1999a; Weller and Gao, 1999; Zheng *et al*., 1995, Mankosa *et al*., 1989; Mankosa *et al*., 1986) have assessed the influence of some of these variables on fine grinding when using stirred milling technologies. Stirred milling technologies are preferred to tumbling mills for fine grinding mainly because of their ability to utilize inert grinding media and high speed stirring of charge with reasonable energy demands.

1.1. Research Objectives

The proposed study focuses on fine grinding with a vertical stirred mill as the enabling technology. The motivation for using vertical stirred mills in this study is that they are the least studied compared to other types of stirred mills such as the Isamill. The main aim is to assess the influence of energy input on the performance of the mill by varying some design and operating variables. To achieve this, the following sub-objectives were formulated:

- Investigate the influence of altering the energy input through changing residence time, impeller speed and design, solids concentration, media size and media density on mill performance.
- Assess the performance of the stirred mill at different energy inputs using the perfect mixing model.
- Using the media stress intensity model to assess mill performance.

1.2. Hypotheses

The hypotheses tested in this thesis are:

- The fineness of grind in a batch vertical stirred mill increases with increase in the specific energy input regardless of the method of specific energy variation because energy input is the key driver of size reduction.
- The breakage rates in a batch vertical stirred mill decrease with decrease in size because the particle strength increases with decrease in particle size.
- The specific energy consumption decreases with increase in the media stress intensity at constant residence time.

1.3. Key Questions

The following key questions were formulated:

- How does the residence time, impeller speed, solids concentration, media size and density and impeller type affect the specific energy in a batch vertical stirred mill?
- Can the perfect mixing model be applied to assess performance of stirred mills at different input energy levels?
- How does the stress intensity at constant residence time, affect the energy and grind efficiency in a batch vertical stirred mill?

CHAPTER TWO: LITERATURE REVIEW

This chapter offers a review of literature related to fine grinding and stirred milling technologies. Articles related to breakage mechanisms as well as the factors affecting fine grinding using stirred mills have been reviewed.

2.1. Fine Grinding

Fine grinding has been widely applied in several industries which include pharmaceutical, chemical, paint and pigments, foods and mineral processing. The definition of fine grinding varies in the different industries because the product standard in these industries is different. For instance, in the paints and pigments industry, particles finer than 1µm are considered fine while the fine grinding domain in the mineral processing industry is described as particle sizes less than 30µm (Jankovic, 2003). The review presented focuses on fine grinding in the platinum industry.

The Bushveld Igneous Complex, located in the North West of South Africa, is the world's largest deposit of platinum group minerals. The region is host to several platinum bearing reefs which include Merensky, Upper Group 2 (UG2) and Platreef. The Merensky and UG2 reefs are currently extensively exploited for noble metals such as platinum group metals. Currently, six Platinum Group Elements (PGE) are known and are considered to be minerals of economic value (Xiao and Laplante, 2004). These include ruthenium, rhodium, palladium, osmium, iridium and platinum.

The flotation of Merensky and UG2 ores is said to be similar entailing bulk sulphide flotation to recover PGE-rich sulphides and liberated PGM sulphides (Feng and Aldrich, 1999). However, the behaviours of the two systems are different. The PGM grain sizes for Merensky and UG2 ores are different. UG2 ore possesses a finer PGM grain size compared to Merensky (Liddell *et al*., 1986). Due to various challenges associated with processing these ores, extensive research is currently being conducted to find ways to improve PGM liberation and reduce gangue recovery in the final concentrate.

Declining ore grades coupled with extremely fine grained complex ores has made fine and ultra-fine grinding critical for the enhancement of liberation. The most common concentration philosophy is having two milling stages in series, each followed by a flotation stage. This is commonly known as MF2 (mill-float-mill-float) and is illustrated in Figure 1.

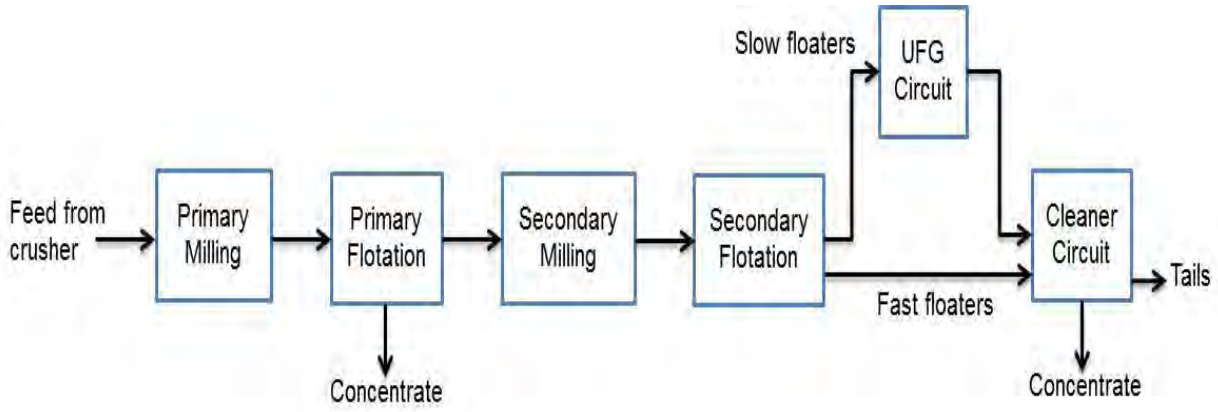

Figure 1: Common concentration philosophy (Fourie, 2008)

2.1.1. Sulphide Mineralogy of the Merensky Reef

The merensky reef, a geological occurrence in the Bushveld Igneous Complex, is a source of Merensky ore which is platinum bearing. The mineralogy of Merensky is complex. Noble metals of the platinum group have been observed to be associated with Base Metal Sulphides (BMS). The BMS content of the reef has been reported to be approximately 1% (Wiese *et al*., 2006). According to Liddell *et al*. (1986), the major base metal sulphide has been reported to be pyrrhotite (~45%). This is closely followed by pentlandite (~32%) and chalcopyrite (~16%). Low amounts of pyrite have been reported (2 - 4%) with other sulphides occurring in trace amounts (Liddell *et al*., 1986).

2.1.2. PGM mineralogy of Merensky

Majority of PGM minerals are associated with base metal sulphides (Liddell *et al*., 1986). Mineral association of PGM in merensky are mainly with pentlandite. The PGM mean grain size has been recorded as 236µm (±45µm) by Liddell *et al*. (1986).

2.2. Fine Grinding Enabling Technologies

A number of milling technologies have been implemented in the fine grinding realm of comminution. The governing criteria for assessing the efficiency of fine grinding enabling machines is often based on the specific energy utilisation and product quality.

2.2.1. Conventional Milling Technologies

Tumbling mills, specifically ball mills, have been conventionally used for fine grinding (Shi *et al*., 2009). Figure 2 shows a schematic of a ball mill detailing its major components. These mills are designed such that a horizontal cylindrical vessel loaded with steel grinding media and ore, rotates, lifting the vessel contents and dumping them to breakage on impact. Figure 3 shows snapshots of two media motion patterns, cascading and cataracting. According to Sun *et al*. (2009), cascading happens when media is lifted up the mill shell and on reaching a certain height, falls along a charge ramp. This results in rock breakage. Cataracting describes media rising up the mill shell to a certain height and follows a trajectory on descent. This leads to breakage of rock material upon impact on the mill shell (Sun *et al*., 2009). Attrition breakage has also been considered as one of the breakage mechanism in tumbling mills (Napier-Munn *et al*., 2005). This occurs when a small particle is trapped between two larger particles that are moving parallel to their plane of contact leading to preferential breakage of the smaller particle (Napier-Munn *et al*., 2005).

The particle strength has been known to increase with decrease in particle size (Tavares and King, 1998). This is because the size of the largest micro-cracks within the particle must decreases when the particle size is reduced (Tavares and King, 1998). This makes fine grinding a non-trivial method of improving liberation. Ball mills have been found to be uneconomical for fine grinding. A significant drop in energy efficiency has been observed when utilizing ball mills for grinding to product sizes of less than 30µm (Jankovic, 2003) making them unattractive for economic liberation.

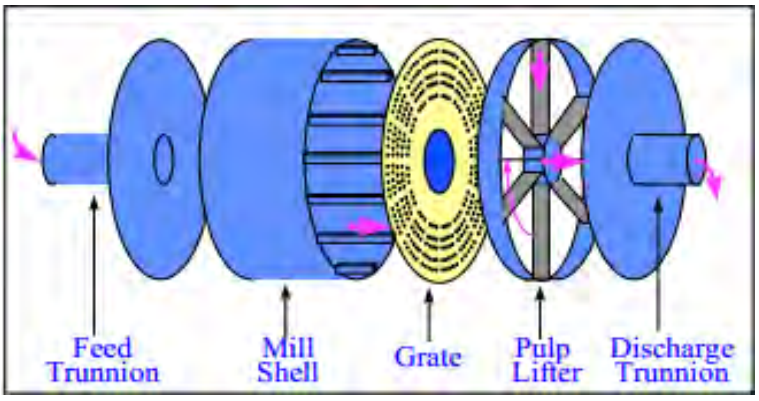

Figure 2: Illustration of a typical SAG mill (adopted from Latchireddi and Rajamani, 2006).

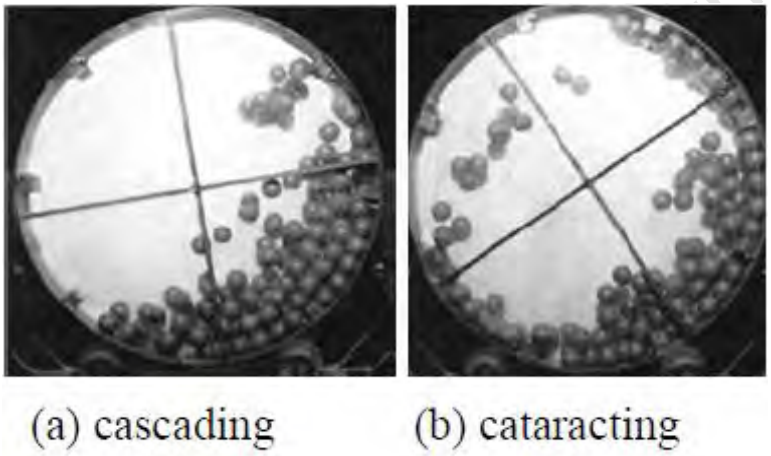

Figure 3: Snapshots of media motion in a tumbling mill (adopted from *Sun et al*., 2009).

2.2.2. Stirred Milling Technologies

Stirred mills are currently the *de facto* enabling technologies for fine and ultra-fine grinding (Rule, 2011; Rule *et al*., 2008; Pease *et al*., 2005). Nevertheless, the application of stirred milling technologies is largely dependent on economic and product quality factors. Figure 4 (after Jankovic, 2003) shows the energies required to achieve a range of grinds for ball mills and stirred mills. As the grind size approaches the fine grinding region, the energy requirements for ball mills increase exponentially. In contrast, stirred mills appear to utilize less energy to achieve the same task in terms of grind size and have hence been preferred for fine and ultra-fine milling.

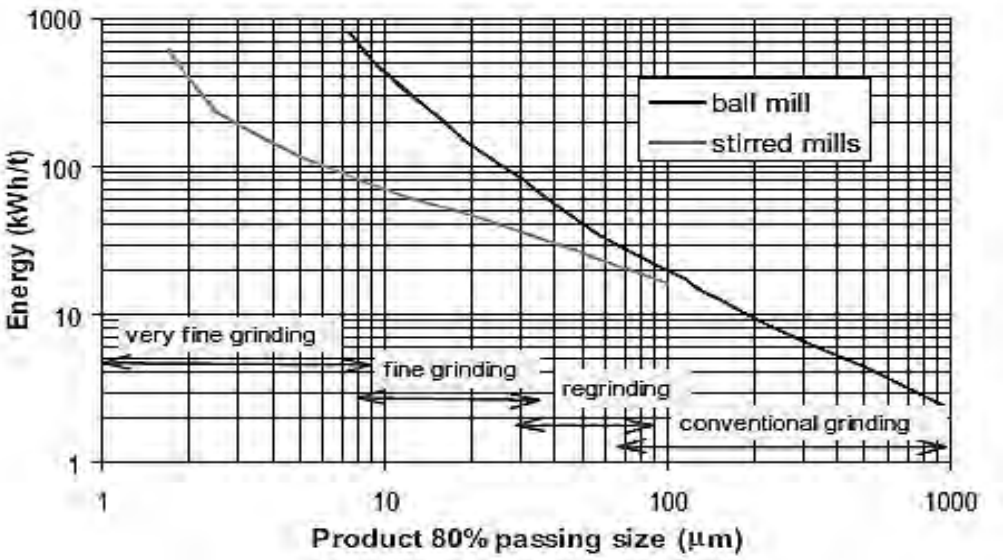

Figure 4: Energy consumption at different grinding stages (adopted from Jankovic, 2003).

A number of stirred mills have already been developed. These include, tower mills, vertimills, Isamills and the Stirred Media Detritors (SMD). The main differences in their designs mainly lie in the orientation of the mill grinding chamber as well as stirrer design. The Isamill mill for instance is a horizontal stirred mill utilizing a disk type stirrer. The SMD however, is a vertical stirred mill utilizing a pin type stirrer.

2.2.2.1. Tower Mills

The Tower mill was manufactured by Kubota in Japan and became the first low speed stirred mill to find application in the mineral processing industry (Jankovic, 2003). The tower mill possesses a distinctive stirrer comprising of a double helical screw that is used to move charge during operation (Napier-Munn *et al.*, 2005). Tower mills are typically operated at rotor speeds of 40 – 50rpm (Napier-Munn et al., 2005). Steel balls are often used as grinding media with media sizes ranging from 9-20mm (Weller and Gao, 1999). Figure 5 is a simplified schematic of the tower mill.

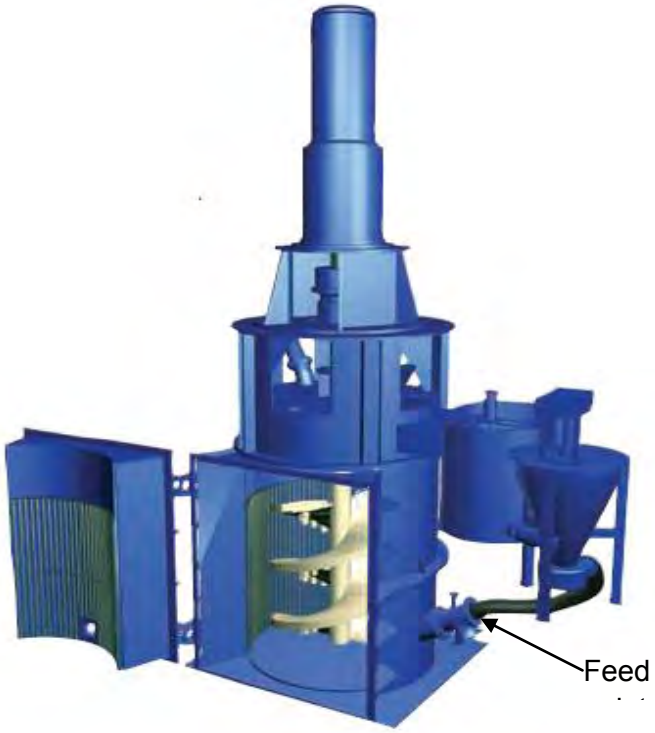

Figure 5: Schematic of a tower mill (adapted from Litcher and Davey, 2006)

The fresh material is fed into the mill via a feed pot located at the bottom of the mill as shown on Figure 5. The motion of helical stirrer lifts the charge up the milling chamber resulting in fairly high grinding activity in the mill (Sinnott *et al*., 2011). The tower mill relies on a media settling zone at the top of the milling chamber which allows product material to exit the mill. This settling zone is key to the operation of the mill because the mill speed is limited by gravity. If the stirrer speed increases to an extent that the vertical forces exceed gravity, the charge moves upwards and media over flow occurs. With a limited operating speed, the size reduction in tower mills is limited to 20-35µm (Napier-Munn *et al.*, 2005). Tower mills are industrially operated in closed circuit in order to enhance size reduction and energy efficiency. Operational limitations like the stirrer speed pose challenges for use of tower mills in ultra-fine grinding. Tower mills are therefore more suitably used as a bridge between the fine end of ball milling and coarse end of other stirred mills (Napier-Munn *et al.*, 2005).

2.2.2.2. Vertimill

The Vertimill is similar in design to the tower mill (Jankovic, 2003). It is exclusively offered by Metso, who first introduced the vertimill in metalliferous mining (Metso, 2010). This type of vertical stirred mill provides a number of advantages for fine grinding, including low capital and maintenance costs, high energy efficiency and low media consumption. Typical feed

sizes have been reported as 100 - 300μm, with the resulting product size ranging from 100 - 15μm (Litcher and Davey, 2006: 71). Vertimills typically utilize high density ceramic or steel grinding media (Metso, 2010) and predominantly operated as wet mills in concentrate regrinding (Litcher and Davey, 2006: 71). Up until 2010, about 382 units had been installed worldwide with standard units sizes ranging from 15 – 3000HP (Metso, 2010). Table 1 shows various applications of the Vertimill in Australia (Kalra, 1999). Figure 6 shows a schematic of the Metso vertimill (Ntsele and Allen, 2012).

Table 1: Applications of the Vertimill in Australia (after Kalra, 1999).

Company	Size & Qty	Product Material	Product 80% Pass	t/h	Application	Year
Granny Smith, Placer	VTM-500-WB	Gold ore tailing	20	12	Regrinding	95
Pegasus Gold, Mt Todd	VTM-1250-WB × 2	Gold ore	15	34	Regrinding	96
BHP Cannington	VTM-800-WB × 2	Zinc and Lead rougher	20	30.9/ 38.2	Regrinding	96
BHP Cannington	VTM-200-WB	Silver	20	9.8	Regrinding	96
MIM Ernest Henry	VTM-1250-WB	Copper ore	45	155	Regrinding	97
Newcrest Cadia	VTM-650-WB	Gold ore	53	54	Regrinding	97
Wanadium Australia	VTM-800-WB	Magnetite	75	67	Regrinding	99
Worsley Alumina	VTM-300-WB	Lime Slaking	45	18	Slaking	99

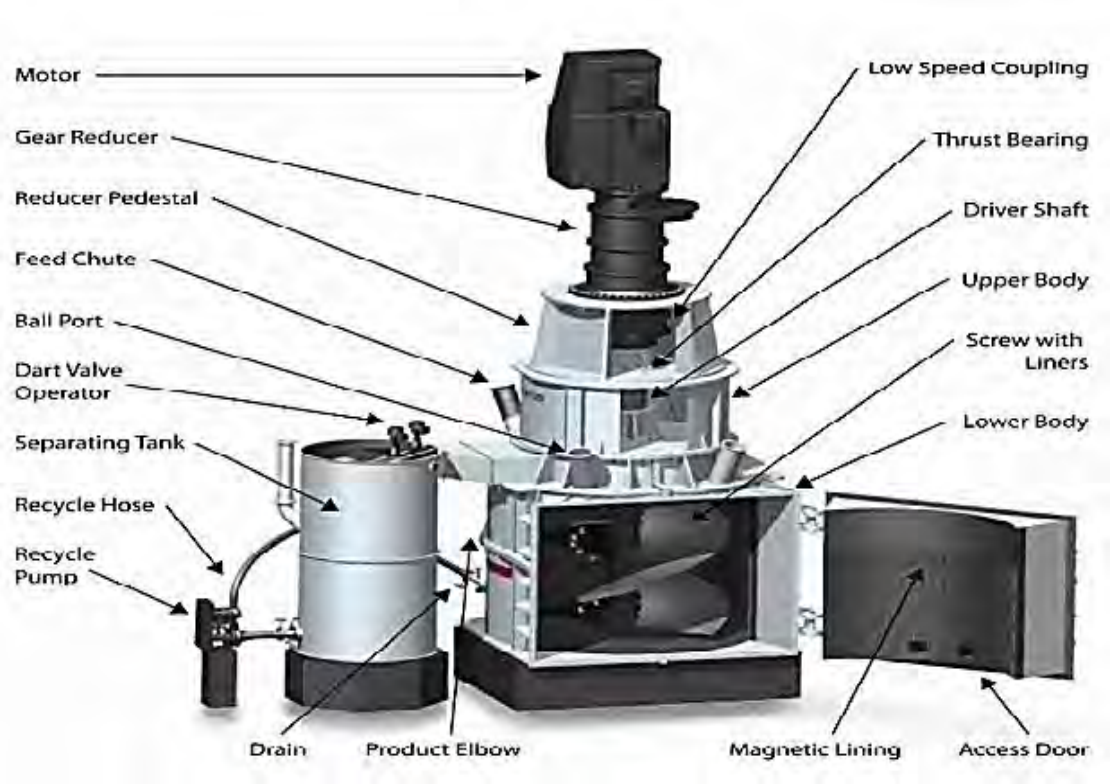

Figure 6: Schematic of the vertimill manufactured by Metso (Ntsele and Allen, 2012).

2.2.2.3. Isamill

The Isamill is a horizontal stirred mill consisting of a concentrically positioned rotor with disc stirrers that enable movement of charge in the mill at high speeds. The mill was originally invented by Mount Isa Mines of Australia in collaboration with Netzsch Feinmahltechnik GmbH of Germany. The Isamill has found wide acceptance in both mainstream inert grinding (MIG) and ultra-fine grinding (UFG) circuits (Rule *et al*., 2008). The driving force for the invention of the Isamill at Mount Isa Mines was the fine grain ores which had to be ground to less than 10µm in the most cost effective way (Pease *et al*., 2005). The Isamill horizontal chamber is often maintained at pressures of about 100-200 kPa to ensure an even distribution of grinding events (Gao *et al*., 2002). The disc peripheral speed in Isamills is as high as 21-23 m/s which is essential for fluidizing charge, resulting in efficient grinding in the milling chamber. Isamills are currently available in a variety of sizes ranging from laboratory scale size, like the M4 (4 litre milling chamber), to the M10000 (10000litre milling chamber). Figure 7 shows some of the differently sized isamilling chambers.

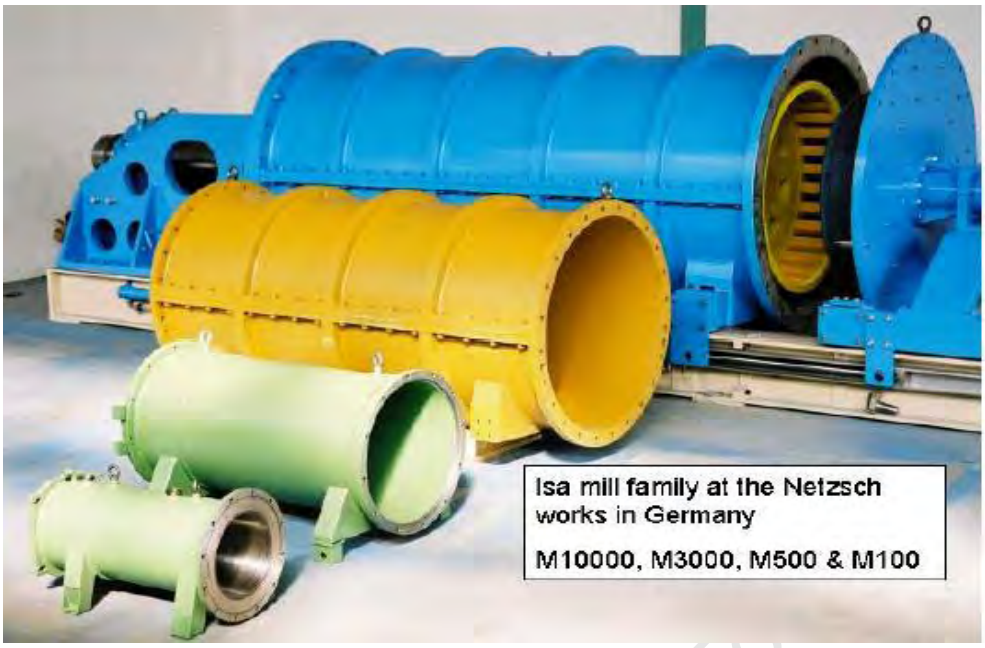

Figure 7: Isamill family (Pease *et al*., 2005).

The high power intensity, about 350kW/m^3, observed in an Isamill mill chamber results in high breakage events which improve energy efficiency. Another major advantage of the Isamill is the ability to utilise fine inert grinding media of 1 - 4mm (Fourie, 2008). With fine grinding media, the number of media is increased and consequently the media-particle collisions are significantly increased (Gao *et al*., 2002). It is reported (Gao *et al*., 2002) that the use of Isamills has a number of advantages which include:

- Ability to operate at high stirrer speeds, resulting in improved grind and energy efficiency.
- Ability to utilise inert grinding media such as ceramics, sand or slag, preventing contamination of product material that might be detrimental to downstream separation processes.
- Cheap materials of construction of inner components with low wear rates, resulting in low maintenance costs.

Figure 8 shows a simplified schematic of the Isamill system.

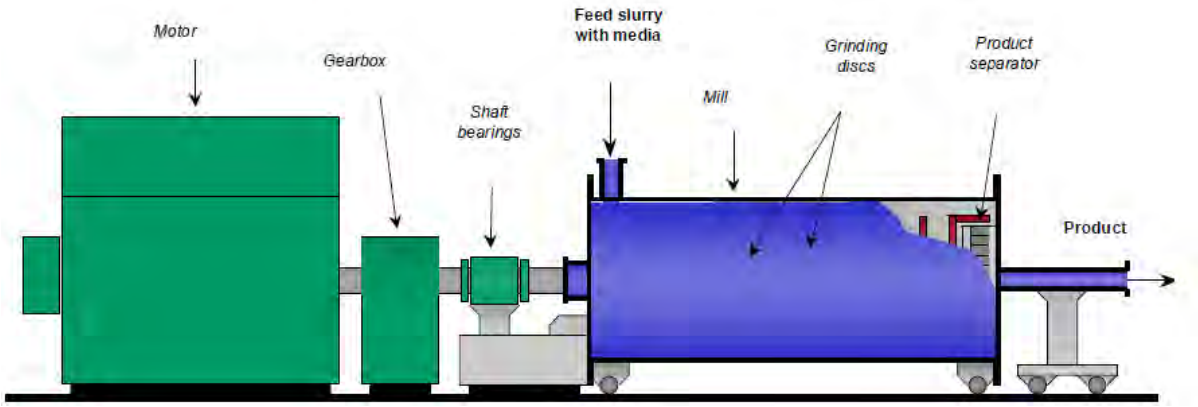

Figure 8: The Isamill system (Harbort *et al*., 1998).

The Isamill, unlike other stirred milling technologies, has a unique product separator which prevents grinding media from exiting the mill chamber with product material. This patented internal classifying technique is best described in Figure 9. Feed material introduced into the mill passes a number of stirrer discs with the region between the different discs described as a grinding stage. The spacing between the last disc and the rotor is much smaller than that between preceding discs. The small spacing between the last disc and the rotor creates high centrifugal forces which drive media back in the mill chamber (Pease *et al*., 2005).

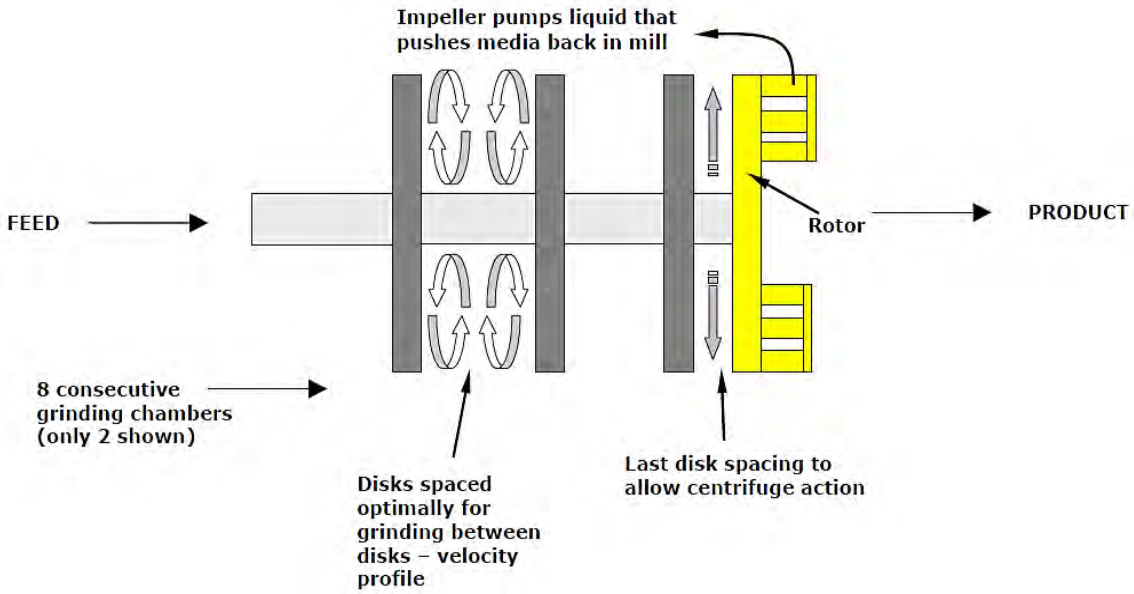

Figure 9: A schematic of the Isamill milling chamber (Pease *et al*., 2005).

2.2.2.4. Metso Minerals Stirred Media Detritor (SMD)

The SMD is a vertical stirred milling technology offered by Metso minerals. It consists of a vertical milling chamber with a concentric impeller with protruding horizontal pins. The main function of the impeller is to impart high energy motion on the charge increasing media-particle interactions and consequently improve grind efficiency (Metso, 2010). A schematic of the SMD is shown on Figure 10. Typical grinding media types used in the SMD are high-grade Alluvial Silica sand or ceramic beads with sizes in the range 1 – 3 mm (Litcher and Davey, 2006: 72). Fresh material is introduced into the mill via a feed pot located at the top cover of the mill and is directed to the bottom of the mill. The product material exits the mill via media retention screens situated around the top circumference of the vertical milling chamber (Metso, 2010). Some of the advantages of the SMD include (Metso):

- Low wear rates of mill components which mean low maintenance costs.
- Does not require the use of slurry seals or pressurized feeds.
- High power intensities but not high enough to necessitate a cooling system to deal with dissipated heat from the milling chamber.

Available SMD unit sizes range between 7.5 and 1100 kW. The SMD is able to treat feed material with a top size of ~250µm to a product size of sub 5µm (Metso, 2010). Laboratory units from 0.75kW unit sizes are also available. In continuous process, the difference in vertical stirred is often with the product discharge mechanism. In batch milling however, most vertical stirred mills utilizing pin stirrers are similar since product material is not discharged.

Figure 10: Schematic of the Stirred Media Detritor (Metso, 2010).

2.3. Breakage mechanisms in stirred mills

In breakage processes, the solid particle shape is altered beyond a certain limit as a result of external forces such as tension, compression, torsion, flexure, shear or attrition (Lowrison, 1974). The mode of particle fragmentation influences product quality. Downstream processes like froth flotation and leaching are significantly influenced by the quality of the product of comminution which is a function of particle shape, morphology and product size distribution (Varinot *et al*., 1997). The mode of fragmentation has an effect on the shape and product size distribution which are often very difficult to control. Knowledge of breakage mechanisms in fine grinding equipment like stirred mills is crucial in improving product quality.

The breakage mechanisms that have been identified in comminution are abrasion, cleavage and fracture/impact (Hennart *et al*., 2009; King, 2001; Kwade 1999a; Varinot *et al*., 1997; Kapur *et al*., 1997; Gao and Forssberg, 1995)

- **Abrasion** occurs when particles are subjected to low local shear stresses, resulting in a bimodal particle size distribution which includes fine progeny particles and particles similar in size to the parent particles.
- **Cleavage** occurs when particles are intensely compressed. This produces a distribution of progeny of sizes 50 – 80% (by volume) smaller than the parent particles.
- **Fracture/Impact** occurs by means of intense impact of particles. The resulting particle size distribution is wide and comprises of progeny much smaller compared to the parent particle size.

Figure 11 shows different fragmentation mechanisms and the resulting product size distributions. According to Gao and Forssberg (1995), impact breakage is linked to tumbling mills, and abrasion is more commonly related to ultrafine grinding machines. Production of fine particles from coarse particles is not a one-step breakage process. The coarse particles and their progeny undergo a number of transformations in size facilitated by the various breakage mechanisms which can occur either in series or parallel (Varinot *et al*., 1997; Gao and Forssberg, 1995). Therefore, all types of fragmentation modes are known to occur during the grinding process, with one normally being the dominant mechanism (Gao and Forssberg, 1995). This can only be postulated often due to unsatisfactory physical evidence of the main fragmentation mode at different stages of grinding.

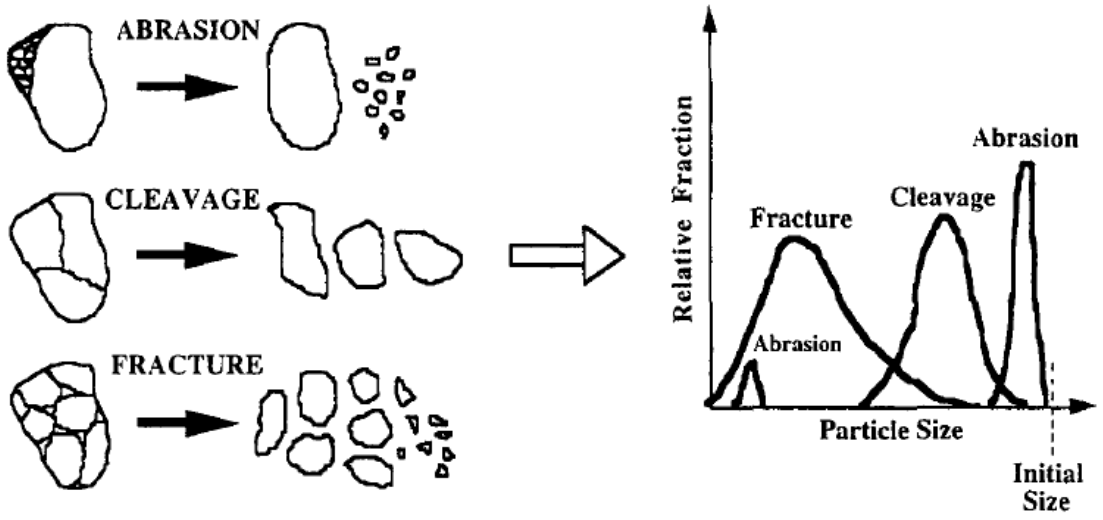

Figure 11: Different breakage mechanisms and the resulting product size distributions (adapted from Varinot *et al*., 1997)

2.4. Fine grinding models

Fine grinding is the realm of comminution that is not well understood in mineral processing. In the past, most mineral beneficiation process dealt with coarse grained ores due to their relative abundance. Therefore, the developments in comminution had focused more on the coarse end of the grinding spectrum neglecting the fine end. In recent years, depletion of high grade ores has forced the processing of challenging low grade ores characterized by fine grain sizes of the valuable metals. Models that had been frequently used to characterize product size in conventional milling devices have been extended to fine grinding applications with little success.

According to Napier-Munn *et al*. (1996), two basic types of models currently exist in comminution:

i. Fundamental models
ii. Black box models

2.4.1. Fundamental models

Fundamental models link process parameters with process outcome (Napier-Munn *et al*., 1996). This involves identifying a number of variables linked to the grinding machine and tying them to outputs like power draw, product size distribution and media motion. These models require immense computational power to develop. Examples of fundamental models include Discrete Element Modelling (DEM) and Computational Fluid Dynamics (CFD). These

models have been applied to stirred mills by Sinott *et al*. (2011), Jayasundara *et al*. (2009), Jayasundar *et al*. (2008) and Lane (1999).

2.4.2. Black box models

A black box model creates a link between the mill input and output with respect to particle size distribution. Essentially, the mill product size distribution is predicted from ore feed size and breakage characterisation (Napier-Munn *et al*., 1996). Two black box models are discussed in this section, the Population Balance Model and the Perfect Mixing Model.

2.4.2.1. Population Balance Model

The linear batch-grinding kinetic model also known as the population balance model (PBM) was developed in the early 1950s (Fuerstenau *et al*., 2004). The PBM is a black box model because it does not take into account the mineralogical structure of the ore or the fragmentation path involved in comminution (Weedon, 2001). This model has been successfully used to characterize product size in tumbling mills (Fuerstenau *et al*., 2004; Austin 1982). The PBM is a mass based model that describes the changes in material particle size distribution with time (Bilgili *et al*., 2004; Varinot *et al*., 1999). The batch grinding process can be described by the breakage distribution function and the selection or specific breakage rate function (Varinot *et al*., 1997; Bilgili *et al*., 2004; Tuzun *et al*., 1995). The selection function describes the fractional breakage rate of particles in each size class whereas the breakage function gives the mean size distribution of progeny fragments as a result of primary breakage events (Tuzun *et al*., 1995). The linear batch grinding model is shown in Equation 1.

$$\frac{\mathbf{dm_i(t)}}{\mathbf{dt}} = -\mathbf{S_i}\ \mathbf{m_i(t)} + \sum_{\mathbf{j=1,i>1}}^{\mathbf{i-1}} \mathbf{b_{ij} S_j m_j(t)} \qquad \textbf{Equation 1}$$

(Adopted from Tüzün *et al*, 1995)

$\mathbf{m_i}$: mass fraction of material in the mill in size class i at time t

$\mathbf{S_i}$: size-discretized selection function which gives the fraction of material broken down from i^{th} size class per unit time

$\mathbf{b_{ij}}$: size-discretized breakage distribution function for material appearing in size class i from size class j.

A conceptual perspective of the PBM is shown in Figure 12.

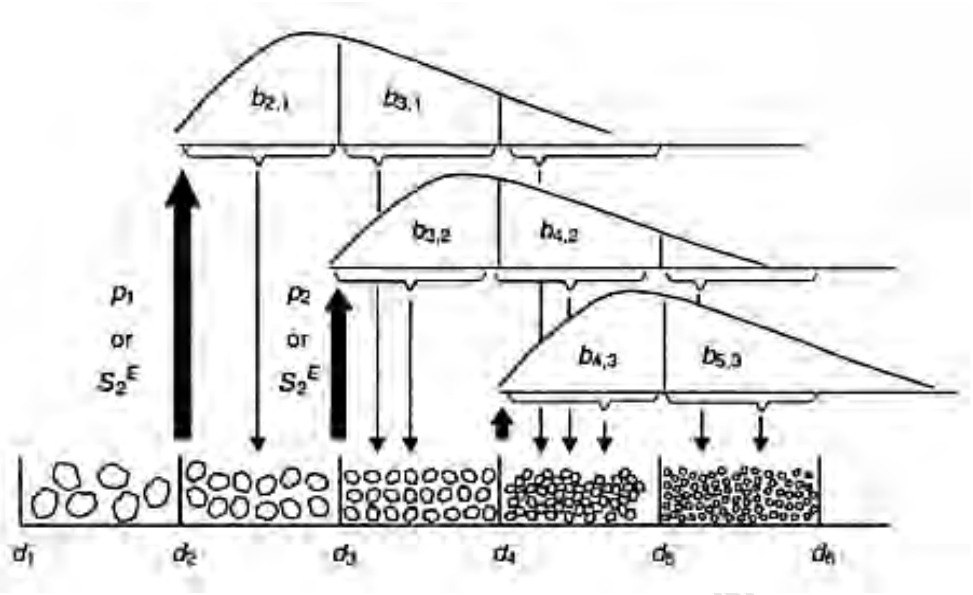

Figure 12: Conceptual view of the population balance model (adopted from Herbst *et al*., 2003: 76).

The use of the population balance model has been extended to stirred mills by a number of researchers (Samanli *et al*., 2011; Bilgili *et al*., 2004; Ma *et al*., 1998; Varinot *et al*., 1997; Tüzün *et al*, 1995). The grinding process is analogous to a chemical reaction. The breakage process can be assessed by fragmentation kinetics of particles inside the mill at specific conditions under which grinding takes place (Frances, 2004). An assumption that has previously been made is that the rate of disappearance of top size material is constant resulting in linear breakage kinetics (Samanli *et al*., 2011). This means that breakage rate of certain particles and size distributions from primary fragmentation is not affected by mill conditions (Samanli *et al*., 2011).

There are a number of problems arising from the use of the PBM for determining product size distribution. There is lack of *a priori* knowledge of the selection and breakage distribution function values (Varinot *et al*., 1999; Kwade, 1999a). The selection and distribution functions can be obtained from batch milling experiments. The material size range of interest is milled for a short period of time, the resulting product is sampled and a size analysis is performed (Austin and Luckie, 1971). However, currently, the experimental methods for obtaining these functions do not suffice in the case of fine and ultra-fine grinding (Varinot *et al.*, 1997). This is due to lack of practical methods for preparing monosize samples (Varinot et al., 1999; Orumwense, 1992). In addition, current particle size analysis techniques lack adequate resolution (Varinot *et al*., 1999).

$$\frac{dm_1(t)}{dt} = -S_1\, m_1(t) \qquad \textbf{Equation 2}$$

By separation of variables and integration, the solution for Equation 2 is Equation 3.

$$m_1(t) = m_1(0)e^{-S_1 t} \qquad \textbf{Equation 3}$$

Where m_1 is the top size fraction and S_1 describes the specific breakage rate for the top size class. The specific breakage rate can be obtained from the gradient of the residual top size versus grinding time semi-log graph (Orumwense, 1992).

The general belief is that fine and ultra-fine grinding regimes are characterized by non-linear breakage behaviour (Orumwense, 1992). This is due to various reasons which include (Orumwense, 1992):

- Changes in the average particle strength during grinding process.
- Cushioning effect of fines or shielding effect of coarse particles.
- Changes in the kinematic behaviour of the grinding media due to changes in the pulp characteristics e.g. rheology and spatial distribution of particles in the mill.

In the production of pigment nano-particles using a stirred mill, Bilgili *et al*., (2004) observed that the first order breakage law does not apply in the nano region of the grinding spectrum. The specific selection function in the first order hypothesis is assumed to be time invariant. However, according to Tüzün *et al*. (1995), the selection function is affected by operating variables. In addition, the specific breakage rate varies with top size as shown in Figure 13. It can be seen that the specific breakage rate decreases steadily with decrease in top size in the region of particle size less than 800µm possibly due to cushioning effect of fine particles as explained by Orumwense (1992). Similarly, above 800µm, the specific breakage rate decreases which can be attributed to shielding effect of the extremely coarse particles. In addition, if the feed particles are too large relative to the grinding media size, the breakage rates decrease due to the grinding beads being too small to trap the particles and cause breakage (Mankosa *et al*., 1986).

In general, the use of the population balance model poses numerous challenges. This are mostly related to the difficulty in solving the selection and distribution functions due to lack of adequate information on breakage progression within the milling chamber.

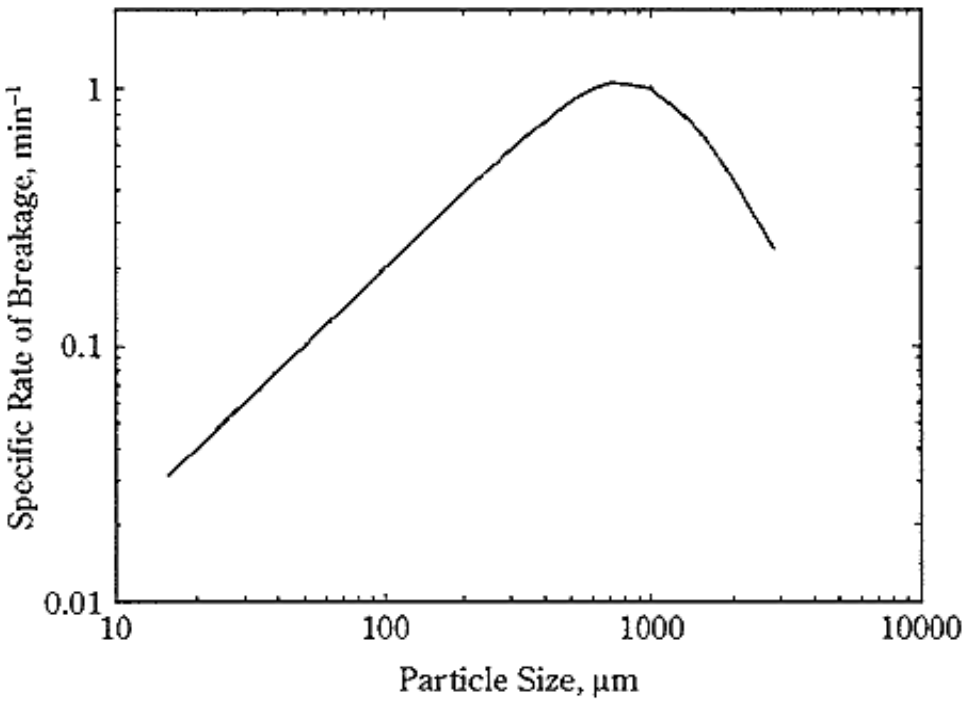

Figure 13: Typical variation of specific rate of breakage with particle size (adopted from Hogg and Cho, 2000).

2.4.2.2. Perfect Mixing Model

The perfect mixing model assumes the mill contents are perfectly mixed (Weedon, 2001). Figure 14 shows a conceptual representation of the model used to develop the mass balance expression shown in Equation 4 (Weedon, 2001).

$$f_i - p_i + \sum_{j=1}^{i-1}(a_{ij}S_j m_j) - S_i m_i = 0 \qquad \textbf{Equation 4}$$

Where:

S_i: Rate of breakage of material in size class i.

a_{ij} : Appearance function.

m_i: Mass of material in size class of interest.

Assuming the mill contents are perfectly mixed, the size fractions of interest in the mill can be related to their respective discharge rates, d_i as shown in Equation 5 (Weedon, 2001).

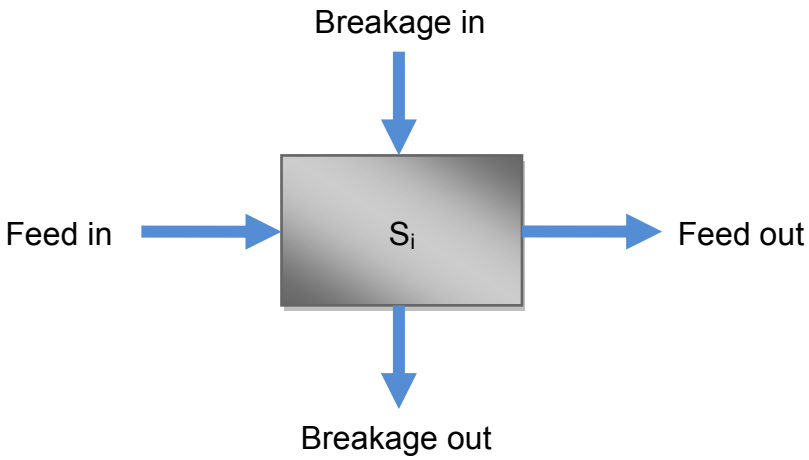

Figure 14: Conceptual representation of perfect mill mixing approach (after Napier-Munn *et al*, 1996).

$$s_i = \frac{p_i}{d_i}$$ **Equation 5**

Equation 5 can therefore be modified to Equation 6.

$$f_i - p_i + \sum_{j=1}^{i-1}\left(a_{ij} r_j \frac{p_j}{d_j}\right) - r_i \frac{p_i}{d_i} = 0$$ **Equation 6**

If the appearance function is known, then the breakage rates for each size class of interest can be calculated using Equation 6 given the feed and product of the respective size classes.

2.5. Factors Affecting Fine Grinding in Stirred mills

The quality of the product of stirred milling is influenced by a number of factors which include feed rate, media size and density, media load, slurry density and rotor speed. A number of these factors have been studied by He and Forssberg (2006), Jankovic (2003), Weller and Gao (1999), Tüzün *et al*, (1995) and Zheng *et al.* (1995). These factors have a direct impact on product quality and energy consumption in fine and ultra-fine grinding.

2.5.1. Impeller speed

The impeller speed has been shown to significantly affect the energy and grind efficiency in operations of both horizontal and vertical stirred mills. The impeller is responsible for charge motion in the mill. It has been established that the main breakage mechanism in stirred mills is attrition (Jankovic, 2001) which is caused by high shear rates. High shear rates in these

mills result from a differential velocity that exists between adjacent grinding beads which stress particles trapped between them causing breakage (Lane, 1999). The mill stirrer speed is, therefore, crucial in ensuring high shear rates in the milling chamber.

In the case of vertical stirred mills, the range of impeller speeds studied is from 300 – 500 rpm by Toraman and Katircioglu (2010), 50 – 150 rpm by Jankovic (2003), 260 – 1000 rpm by Zheng *et al*. (1996) and 200 – 765 rpm by Mankosa *et al*. (1989). Typical impeller speed ranges studied in horizontal stirred mills include, 400 – 1000 rpm (Jayasundara *et al*., 2010), 1204 – 2255 rpm (He and Forssberg, 2007), 2130 – 4370 rpm (Fadhel and Francis, 2001) and 805 – 2253 rpm (Gao *et al*., 1996). The range of impeller speeds studied in the case of horizontal stirred mill is much higher than vertical stirred.

In milling of limestone with a high speed Netzch mill, Jankovic (2003) observed that a higher speed had a positive effect on the grinding efficiency. However, for the tests done using a pilot tower mill, Jankovic (2003) observed that the energy efficiency actually decreased with increase in stirrer speed. In agreement with Jankovic (2003), Chaponda (2011) showed that the energy efficiency decreases with increase in impeller speed when operating the Isamill between 1500 and 2100 rpm. The decrease in energy efficiency with increase in stirrer speed is also supported by Zheng *et al*. (1996). The conflicting observations on the effect of stirrer speed on energy efficiency could suggest that that an optimum stirrer speed exists. The existence of an optimum stirrer speed for a specific slurry density has been observed by He and Forssberg (2007) when milling quartzite in a horizontal stirred mill. It is said that below the optimum stirrer speed, the stress intensities of the grinding media are insufficient to cause breakage whereas above the optimum, excess stressing results in energy wastage (He and Forssberg, 2007; Fadhel and Frances, 2001).

The influence of stirrer speed varies with the type of mill used. For instance, in low speed vertical mills, lower stirrer speeds favour improved energy efficiency and vice versa (Jankovic, 2003; Jankovic, 2001; Zheng *et al*., 1996).

High speed horizontal stirred mills like the Isamill are often operated at much higher stirrer speeds than the tower mill and the SMD. Studies conducted by Blecher and Schwedes (1996) on the energy distribution and particle trajectories in stirred ball mill at low and high Reynolds number revealed different energy density zones in the two cases. The energy density was taken as the ratio of the local specific energy to the mean specific energy in the milling chamber. The mean specific energy was taken as the ratio of the total dissipated energy to the net volume of the grinding chamber (Blecher and Schwedes, 1996). Energy density isolines were identified and plotted for the radial-axial directions at a Reynolds

number of 10 as shown in Figure 15. The highest velocity gradients were observed at the disk. Only one zone of high energy density was observed indicated by isolines with values greater than 1 on Figure 15. At a high Reynolds number, cyclic flow of material in the mill chamber was observed in the radial-axial directions due to the centrifugal effects. Two regions of high velocities were observed which were close to the stirrer speed and mill chamber wall. The isolines of energy density are shown on Figure 16. It was also observed that the higher the Reynolds number, the lower the total area with high energy density. These high energy density areas constitute only about 10% of the grinding chamber volume but a significant amount of the total energy is converted in these areas (Kwade 1999b; Blecher and Schwedes, 1996).

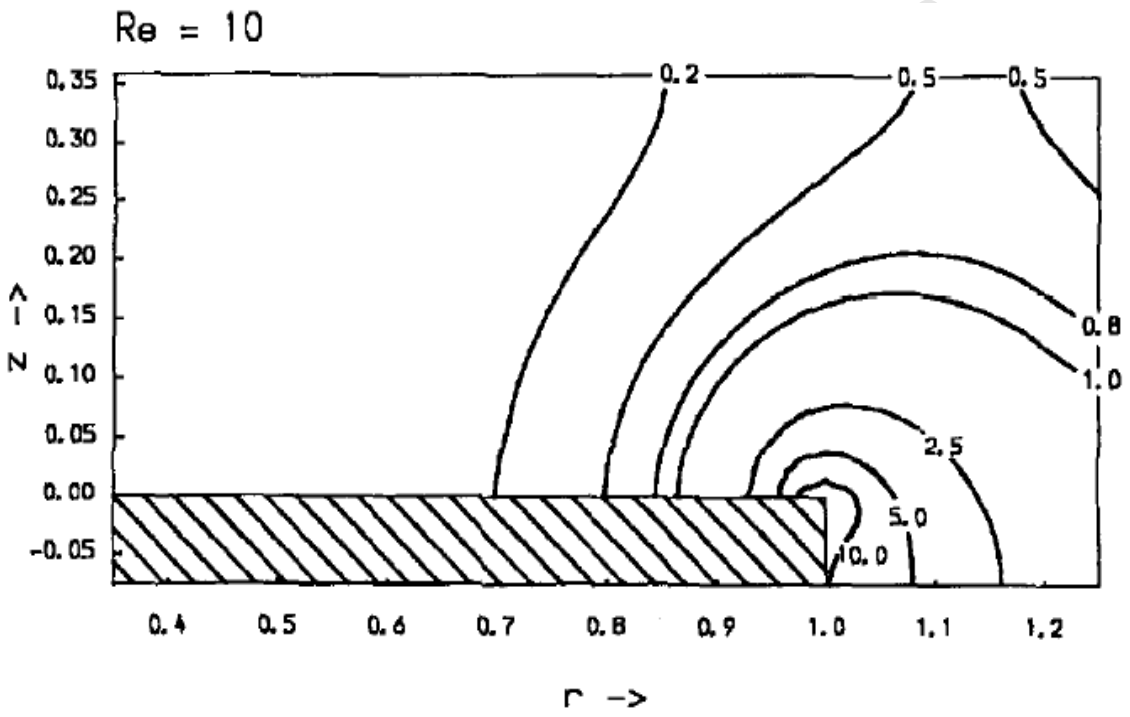

Figure 15: Isolines of energy density at Re=10 (Blecher and Schwedes, 1996).

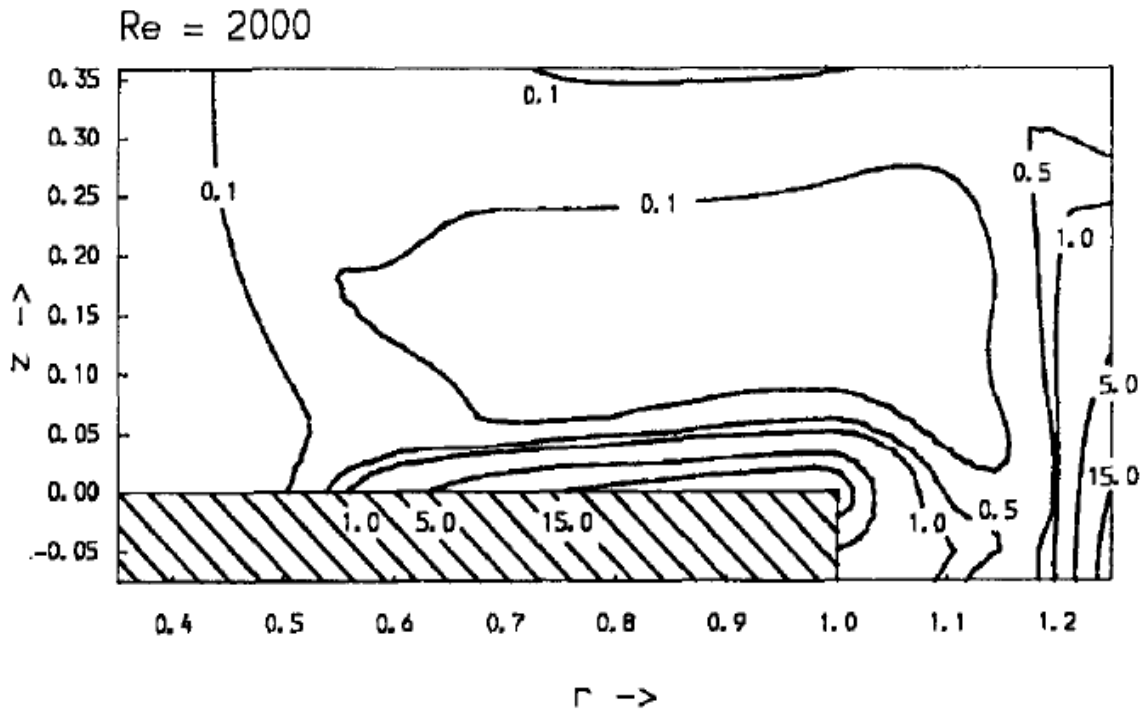

Figure 16: Isolines of energy density, Re=2000 (Blecher and Schwedes, 1996).

r→: Dimensionless distance from the shaft

z→: Dimensionless distance from the disk stirrer

2.5.2. Feed rate

The feed rate refers to the mass of slurry fed into the mill per unit time. This variable is crucial in that it determines several aspects of mill operations which include:

- The throughput of the milling equipment
- The rate at which the required product is obtained
- The residence time of feed material in the mill

The desire to obtain high production in concentrators often encourages metallurgists to push for high tonnage through the mills. Due to the high energy requirements for fine grinding, stirred mills often process low tonnages (10 – 100t/h) compared to the main stream grinding circuits (Jankovic, 2008). The SMD and Isamill have been widely used for regrinding floatation concentrates to improve concentrate grade. In other instances flotation tailings have been processed in these mills in an effort to improve the grade and recovery of valuable minerals (Rule *et al.*, 2008)

Low feed rates are matched by high residence times of material in the mill (Weller *et al.*, 2000) which potentially improves the grind. However such feed rates result in low production

rates and a high net energy input and consequently poor energy efficiency. In contrast, high feed rates may potentially result in low residence times of material which can lead to poor grind efficiency. High throughputs in horizontal stirred mills influence media flow dynamics leading to uneven media distribution across the mill length (Jankovic, 2008). In some vertical stirred mills, high feed rates can result in discharge of fine grinding media, an observation not seen when coarse grinding media are in use (Jankovic, 2008). When milling Calcite in a vertical stirred mill, Weller and Gao (1999) observed that the grinding efficiency was not sensitive to the flow rate. However, when milling Dolomite in a horizontal stirred mill, Weller and Gao (1999) observed that the energy consumption decreased with increase in flow rate. This was attributed to increase in pressure in the mill which possibly altered particle breakage. Chaponda (2011), when milling UG2 tailings, also observed a decrease in the specific energy consumption with increase in feed rate. The effect of feed rate therefore, appears to differ for vertical stirred mills compared to horizontal stirred.

2.5.3. Grinding media size

The size of grinding media has been considered to be a very important variable affecting fine grinding of minerals in stirred mills (Jayasundara *et al*., 2008; Kwade and Schwedes, 2002). The grinding media size determines the probability of particle breakage from shear stress (He and Forssberg, 2006). It has been observed that, generally, grinding efficiency increases with decrease in media size (He and Forssberg, 2006; Jankovic, 2003). However, for a specific feed size, an optimum media size is believed to exist above which the grinding efficiency decreases as a result of an increase in the spacing between grinding media which causes a decrease in the shear stress. Below the optimum grinding media size, the transfer of momentum from the stirrer to the media charge decreases which could result in the media charge being stationary (at a specific stirrer speed) when the grinding beads are too small (Jankovic, 2003). Figure 17 shows the effect of specific energy on product P_{80} from tests of 1mm and 2mm media (Lichter and Davey, 2006). It appears like at low specific energies, the grind is better from the 2mm media than the 1mm media. This can be attributed to the finer media being too small to assert sufficient stress on particles to cause breakage. However at higher specific energies, it appears like the P_{80} value converges. This shows that a grinding limit exists at high specific energy values.

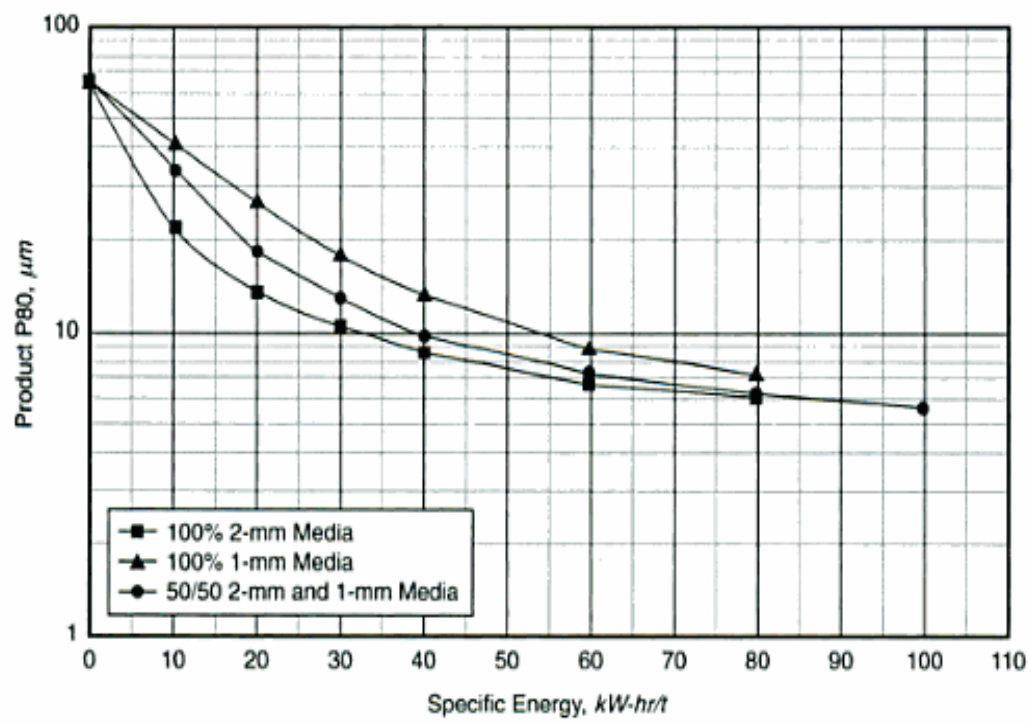

Figure 17: Effect of media size on mill efficiency for a typical SMD operation (From Lichter and Davey, 2006).

2.5.4. Grinding media density

The density of grinding media significantly affects comminution results. It has been observed that the higher the grinding bead density, the finer the comminution product (He and Forssberg, 2007; Zheng *et al*., 1996). Zheng et al. (1996) studied the use of steel and glass beads in milling limestone. Their results showed that the tests with steel beads gave a finer grind compared to glass beads. However, Zheng *et al*., (1996) observed that the glass media consumed less energy and ultimately reached a conclusion that the glass beads were more energy efficient than steel beads in milling of limestone. Contrary to the conclusions made by Zheng *et al*. (1996), Mankosa *et al*. (1986), when milling coal in a stirred mill, concluded that the steel beads were more energy efficient than glass beads. Mankosa *et al*. (1986) attributed their observations to the fact that the glass beads took longer to achieve the same energy input than the steel beads. When the grinding media density is too high then the energy consumption is significantly high and can potentially result in low energy efficiency (Zheng *et al*., 1996). According to Mankosa *et al*. (1986), the torque required to achieve the same energy input is lower when using low density media compared to high density media. The low input energy associated with low density media possibly results in poor grind, assuming the residence time is constant. Some of the issues associated with poor selection of grinding media type are (Becker and Schwedes, 1999):

- possibility of product contamination resulting from abraded wear
- high specific energy consumption as a result of grinding media wear

There is a significant variation in media economics between different types of grinding media. Steel media have been used in tower mills. However, the use of steel media in high energy mills has been discouraged as a result of diminishing energy efficiency and pulp contamination which is detrimental to downstream processes. Current grinding media research is focused on both structural and mechanical properties such as (Graves and Boehm, 2007):

- high fracture toughness
- low friction coefficient
- fine grain structure with high surface stability.

Currently, existing natural materials fall far short of these criteria which has been the driving force for establishing zirconia-based engineered ceramics and other types of grinding media suitable for fine grinding. Ceramic grinding media have been used in the Isamill and SMD operations with satisfactory results.

2.5.5. Grinding media load

The grinding media load refers to the volume fraction of grinding beads present in the mill at a particular time of operation. This fraction is often reported as a percent volume filling. Weller and Gao (1999) observed that a higher media load significantly decreased the specific energy in horizontal stirred mills but had little effect on the specific energy in vertical stirred mills to produce a specific P_{80} size. Weller and Gao (1999) explained that for the vertical stirred mill, as long as the media covers a minimum number of stirrer pins, then increasing the amount of media will only increase the mill effective volume without changing grind efficiency. In the horizontal stirred mill, reducing media load reduces interaction of media with impeller disks resulting in low mill capacities and poor grind efficiency (Weller and Gao, 1999).

The competing effects of high and low media loading on grind and energy efficiency imply that an optimum media load exists for a specific throughput at constant operating conditions like stirrer speed and slurry density. When milling UG2 slurry in an Isamill, Chaponda (2011) observed that the specific energy consumption decreased with increase in media load from 50% to 65% but increased when the media load was further increased to 80%. Chaponda (2011) then concluded that an optimum media load for which the specific energy consumption is a minimum exists at about 65% media loading. Media load in stirred mills is

known to decrease with time as a result of media wear. A decrease in the media load is matched with a decrease in power draw which diminishes energy efficiency. The media load is often the control variable used to maintain a constant power draw for consistent product quality. Isamill media filling is in the range of 70-80% by volume (Pease, 2007).

2.5.6. Solids concentration

The solids concentration refers to the fraction of solids by mass in the slurry fed to the mill. This is usually controlled by the amount of grinding additives used in the milling process. Water is a widely used additive in both conventional and modern milling processes. For breakage to occur in a grinding process, particles must be trapped between grinding media and sufficiently stressed. The trapping of particles between juxta-positioned grinding media happens by chance. The likelihood of it happening at low solids concentrations is low. At higher solids concentration the mean inter-particle distance is reduced and consequently the probability that a particle will be trapped between grinding media and sufficiently stressed to breakage is increased (Kwade, 1999). Therefore an increase in the slurry density will result in an increase in grinding efficiency. However, when the solids population is too high, charge mobility is hindered leading to poor grind efficiency (Jankovic, 2003). It has been reported that the solids concentration has an effect on the slurry rheology, otherwise known as slurry flowability (Ding *et al*., 2007; Bernhardt *et al*., 1999).

Figure 18 shows the effect of solids concentration on the apparent viscosity at various shear rates (courtesy of He and Forssberg, 2007). It can be seen that above 65wt% solids, there seems to be an exponential increase in the slurry apparent viscosity with increase in solids concentration. The effect is greatest at low shear rates. In ultra-fine grinding of powders such as limestone, material target sizes can be as low as <10μm, a range with significant rheological effects on slurry (Bernhardt *et al*., 1999). In such instances, chemical additives are employed to manipulate slurry viscosity so as to improve flowability (Ding *et al*., 2007; Bernhardt *et al*., 1999). In the platinum industry, particularly in treating Merensky ore, the use of chemical additives is not common. Water is therefore the only chemical used to adjust the solids concentration to the desired levels. For a specific stirrer speed, the fineness of grind has been observed to increase with an increase in solids concentration to a certain point beyond which the grinding efficiency decreases (Jankovic, 2003; Zheng *et al*., 1996). At higher solids concentration, flow problems due to high viscosities are expected, resulting in a decrease in grinding efficiency (Jankovic, 2003; Mankosa *et al*., 1989).

In conclusion, if the slurry volume is constant, an increase in the solids concentration (wt%) will result in an increase in the grind efficiency due to an increase in the particle population in

the mill which consequently leads to an increase in the particle breakage probability. However, beyond a certain solids concentration, the particle population in the mill becomes too high making it difficult to induce motion on the charge. This possibly leads to an increase in the power draw resulting in a decrease in the grind and energy efficiency. A number of researchers (He and Forssberg, 2007; Ding *et al*., 2007; Bernhardt *et al*., 1999; Jankovic, 2003; Zheng *et al*., 1996) have alluded to viscosity problems above a certain critical solids concentration. However, this critical solids concentration point differed depending on the material being milled.

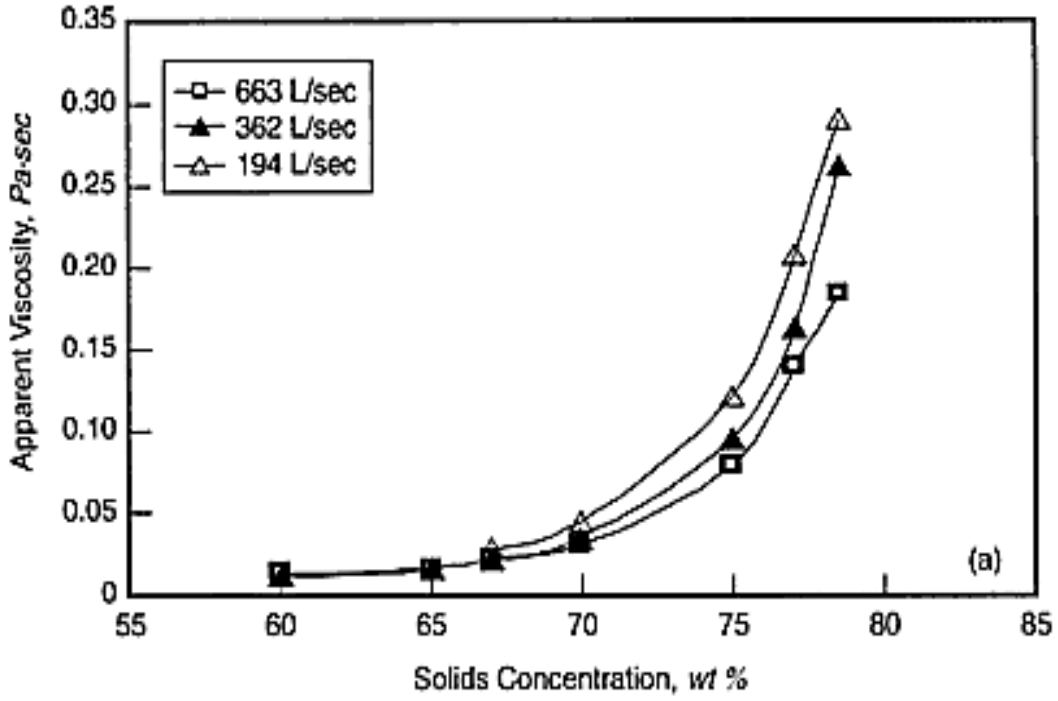

Figure 18: Effect of solids concentration on the apparent viscosity (From He and Forssberg, 2007).

2.5.7. Stress Intensity

Conflicting evidence of the effect of different variables affecting fine grinding in stirred mills has rendered any trends observed for any of the variables inconclusive with respect to grind and energy efficiency. It has been observed from studies by He and Forssberg (2006), Jankovic (2003) and Weller and Gao (1999) that higher stirrer speeds improve the grinding efficiency in some cases but the opposite effect was observed for others. Larger grinding media have been observed to be suitable for grinding coarser particles and smaller grinding media for fine particles (He and Forssberg, 2006); Jankovic, 2003; Weller and Gao, 1999). These observations imply that there exist interactions between the different variables making

the optimization process of stirred milling circuits non-trivial. The concept of stress intensity was, therefore, introduced in an effort to combine the different variables so as to establish a comprehensive variable (Jankovic, 2003). The stress intensity is an indication of the specific energy required for breakage at a specific stress event (Kwade, 1999a). An optimum stress intensity is believed to exist for all stirred mills (Kwade *et al*., 1996) beyond which the energy for breakage is too high, hence wasted and below which the comminution energy is insufficient for breakage, resulting in a reduction in the breakage rate (Jankovic 2003). According to Kwade (1999a), the process of particle breakage in stirred mills is mainly influenced by:

- how frequently feed particles are subjected to stress (Number of stress events)
- the magnitude of the stress intensity present at each stress event.

Kwade (1999a) revealed that the number of stress events can be related to the product fineness. The product of the stress intensity and the stress number can be measured by the specific energy. This indicates that the specific input energy is proportional to the stress intensity and the stress number. If the expressions for the stress number and stress intensity are known, then it is possible to obtain optimum operating conditions, provided the optimal stress intensity is maintained (Kwade, 1999a). The approach for a batch mill is given in the Appendix, Section 7.3. However, the general form of the stress intensity model is shown in Equation 7 (Kwade and Schwedes, 2002).

$$SI_{GM} = d_{GM}^3 \rho_{GM} v_t^2 \qquad \textbf{Equation 7}$$

(after Kwade and Schwedes, 2002)

A modified expression of the stress model has also been in use. This was developed by Kwade et al. (1996) and takes into account the effect of slurry density on the stress intensity. The expression for modified stress intensity is shown in Equation 8.

$$SI_M = d_{GM}^3 (\rho_{GM} - \rho_{sl}) v_t^2 \qquad \textbf{Equation 8}$$

(after Kwade *et al*., 1996)

Methods of measuring bead velocities *in situ* have been studied using Positron Emission Particle Trackin (PEPT). Van Der Westhuizen *et al*. (2011) and Jayasundara *et. al*. (2011) studied the motion of media inside an Isamill™ using PETP. Their finding showed that the media velocities at the disc tip were proportional to the disc tip speed. The highest bead

velocities occurred at the radius of holes inside the disk (Van Der Westhuizen *et al*., 2011). Studies by Conway-Baker *et al*. (2002) and Blecher and Schwedes (1996) showed that velocity gradients exist in the milling chamber and that the highest energy intensities are experienced in two zones. The existence of velocity gradients suggests that the different grinding media move at different velocities and that the stress intensities are different at different stress events. The stress intensity model suggested by Kwade (1999a) represents the maximum mean stress intensity at a given stress event hence representing the actual intensities by a distribution is a more realistic approach (Kwade, 1999a).

In conclusion, stress models are increasingly being applied in optimising energy efficiency in stirred mills. Most of the studies applying stress models have been done at constant energy input. The application of the media stress model at constant residence time has not been fully explored. If found applicable, the stress model can be used to optimise continuous mills when operating at constant feed rates.

2.6. Effect of stirred milling on product size distribution

The mode of fragmentation of material has a direct impact on the product size distribution. A grinding event involves a combination of attrition/abrasion and impact modes of breakage. However the predominant breakage mode in stirred mills is attrition (Jankovic, 2001). Attrition/abrasion modes of breakage result in a narrow size distribution which is beneficial to downstream processes such as flotation. A number of studies have been done on product size distribution in stirred mills to varying extents (Jankovic and Sinclair, 2006; Wang and Forssberg, 2000; Gao and Forssberg, 1995). The general consensus in fine grinding is the narrowing of particle size distribution in this domain. The resistance to breakage increases several fold with decrease in particle size. It is expected that breakage-resistant particles will tend to produce a coarser progeny, hence the narrowing of the product size distribution at finer particle sizes (Jankovic and Sinclair, 2006). According to Jankovic and Sinclair (2006), the narrowing of size distribution in fine grinding is independent of the stirred milling technology used. Variation in product size distribution width has been attributed to (Jankovic and Sinclair, 2006):

- alterations in material breakage properties.
- variations in the grinding environment which has an effect on the mode of fragmentation.

In tower mill operations, classifiers are used to steepen the size distribution of the product and enhance the overall performance. However, over-grinding of material is one of the

ramifications of a classifying stage in a tower mill operation. The tower mill has been observed to produce a wider particle size distribution compared to the Isamill (Gao *et al*., 2002). The SMD and the Isamill are often operated in open circuit minimizing problems of over-grinding of material especially gangue minerals.

2.7. Effect of residence time on fine grinding in stirred mills

The concept of residence has often been used in various scenarios to investigate the mixing properties and flow dynamics of fluids. The residence time describes the average life time of material flowing through a vessel or piece of equipment.

Tracer studies for horizontal and vertical mills have been conducted by Weller *et al* (2000). The outcome of the study highlighted the difference in flow characteristics in the two categories of stirred mills. In addition, for the horizontal stirred mill, the liquid residence time was observed to be highly influenced by the flow rate but unaffected by stirrer speeds.

2.8. Application of fine grinding technology

Fine grinding technologies such as stirred mills have been applied in various capacities in the mining industry. However, since they cannot handle the large throughputs in the primary milling circuit, stirred mills have been confined to the secondary and tertiary circuits. Isamills have been utilized for regrinding of Lead-Zinc concentrates at Mount Isa Mines in Australia (Pease *et al*., 2005). In the platinum industry in South Africa, Isamills have been installed at Lonmin and Anglo Platinum for coarser grinding applications owing to the flotation benefits of inert grinding media (Pease *et al*., 2005). The use of steel media in conventional milling technologies and some stirred mills like tower mills results in pulp contamination which is detrimental to the flotation chemistry of sulphide minerals (Bruckard *et al*., 2011; Peng and Grano, 2010; Grano, 2009). The SMD and the Isamill are, therefore, the preferred stirred milling technologies for regrinding in flotation circuits due to their ability to utilise inert grinding media such as ceramics. The open circuit mode of operation of the SMD and Isamill lowers chances of over-grinding of material, producing a steep product size distribution which minimizes entrainment of very fine gangue mineral particles that could compromise mineral grade and recovery. The SMD has proven to be economically viable for treating rougher concentrates in the platinum group minerals (PGM) industry (Rule *et al*., 2008). Figure 19 shows the application of an SMD in treating Merensky rougher concentrates at the Platinum Mile plant in South Africa (Rule *et al*., 2008). Stirred mills have found wide acceptance in the platinum industry in South Africa as shown in Table 2 (Rule, 2011).

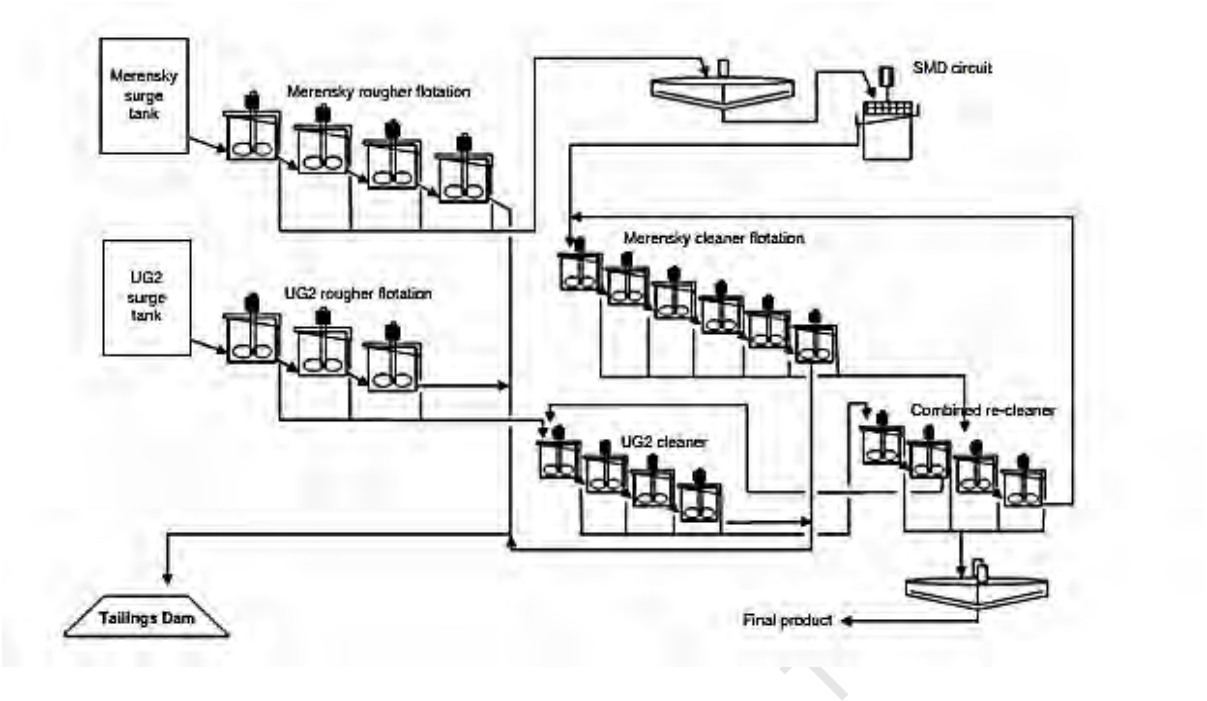

Figure 19: Application of the SMD to the Platinum Mile plant circuit (Rule *et al*., 2008).

Table 2: Total installed base of stirred mills in South Africa, PGMs and PGMs from chromite operations (Rule, 2011).

Operator	Operation	Number of stirred mills	Type	Installed power kW	Application
PGM concentrators					
Anglo Platinum/JVs	WLTR	1	IsaMill™M10000	2600	UFG/MIG
	Waterval UG2	2	IsaMill™M10000	6000	MIG
	Mogalakwena South	3	IsaMill™M10000	9000	MIG
	Mogalakwena North	4	IsaMill™M10000	12000	MIG
	Waterval	4	IsaMill™M10000	12000	MIG
	Amandelbult	4	IsaMill™M10000	12000	MIG
	Amandelbult	1	IsaMill™M3000	1500	UFG
	Mogalkwena North	1	IsaMill™M10000	3000	UFG
	Waterval	1	IsaMill™M10000	3000	UFG
	Mototolo	1	Metso SMD™355	355	UFG
RBR	BRPM	1	IsaMill™M10000	3000	MIG
Lonmin	Eastern Platinum C	1	IsaMill™M3000	1000	UFG
	Eastern Platinum A/B	1	Metso SMD™355	355	UFG
Platmin	Boynton	1	IsaMill™M3000	1500	MIG
PGM tailings retreatment					
Impala	Rustenburg TRP	2	Metso SMD™355	710	UFG
Platinum Mile	Paardekraal TRP	2	Metso SMD™355	710	UFG
	Paardekraal TRP	2	Deswik-2000 litre	1065	UFG/MIG
Chromite tailings retreatment					
Aquarius/JV	RK1 chromite tails	1	Deswik-1000 litre	500	MIG
Sylvania	Steelpoort	2	Metso SMD™185/18.5	203.5	UFG/MIG
	Lannex	1	Metso SMD™185/18.5	185	UFG/MIG
	Lannex	1	Kings	75	MIG
	Milsell	2	Metso SMD™185/18.5	203.5	UFG/MIG
Tharisa	Brits Chrome TRP	1	Deswik-500 Litre	220	MIG

Stirred mills have also been considered a viable option to enhance exposure of gold surfaces for improved leaching kinetics. Studies conducted by Ellis (2003) revealed that the leaching performance obtained after fine grinding using an Isamill and a vertical stirred mill was similar for the two mills. Improved leaching kinetics was observed when material was finely ground using the Isamill prior to leaching. Studies on the effect of iron contaminants on thiosuphate leaching of gold have been conducted by Feng and Van Deventer (2010). Iron contamination of pulp often from grinding bead debris was found to be detrimental to leaching of gold. The ability of the Isamill and SMD to utilise inert grinding media like ceramics makes them the preferred choice for fine grinding prior to leaching processes. High energy efficiencies of these stirred mills coupled with low capital and operating costs make them an economically viable choice for improved leaching processes.

2.9. Summary of literature review

Design and operating variables such as the residence time, impeller speed, solids concentration, media density and size, stress intensity have been shown to affect the energy consumption and grind in stirred mills. Evidence of the effects of these variables on mill energy and grind efficiency is conflicting. There is a suggestion that these variables interact making it difficult to decipher the effects of individual variables. Currently there exists no recipe of these variables that give optimal performance with respect to energy consumption and grind efficiency.

Kwade et al. (1996) proposed a model that uses major operating variables such as media properties, media tangential velocity and slurry density to estimate a comprehensive variable, the stress intensity. The stress intensity describes the energy at each breakage event. However, most of the studies applying the stress intensity model in stirred mills (Jankovic, 2003; Kwade and Schwedes, 2002; Jankovic, 2001; Kwade, 1999a; Kwade et al., 1996) have been done at constant specific energy input. Stress models applied to stirred mills at constant residence time have not been extensively studied.

The product from stirred mills is known to be of a narrow size distribution which is advantageous to downstream processes such as flotation. The narrow size distribution has been attributed to the dominant attrition breakage mechanism in stirred mills. Research on the integration of stirred mills into existing comminution circuits for fine grinding is not wide. Therefore, this creates an opportunistic setting to assess the limitation of stirred mills in order to establish the range and performance.

CHAPTER THREE: EXPERIMENTAL PROGRAMME

3.1. Introduction

This chapter gives a description of the equipment and experimental procedure used in the test work performed for the thesis. The milling tests were conducted at Mintek in Randburg, Johannesburg. The test work involved using a 5 litre batch vertical stirred mill to perform grinding tests on a platinum ore obtained from Lonmin. The tests were performed to understand the influence of various design and operating variables on the performance of the vertical stirred mills.

3.2. Batch Vertical Stirred Mill (VSM)

The batch vertical stirred mill used in the experimental work is manufactured by Metso. Figure 20 shows a picture of the batch VSM and all the major components of the equipment are labelled.

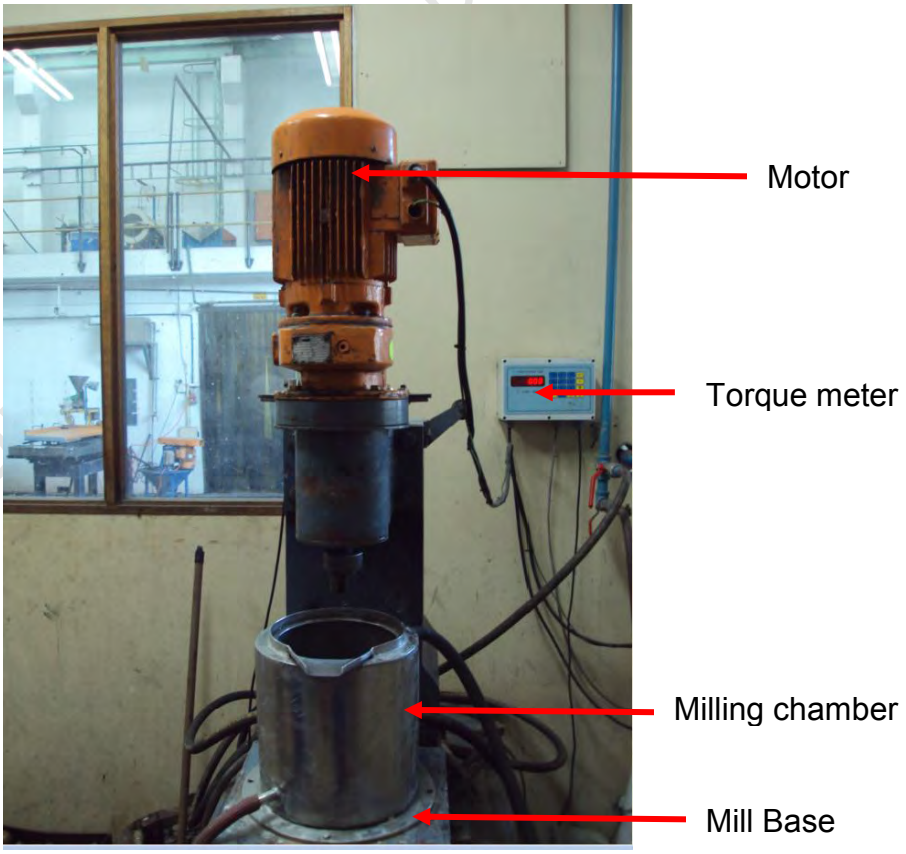

Figure 20: A picture of the batch vertical stirred mill used.

The stirred mill used in the test work can be operated with different stirrer types, the major categories being the pin and disk stirrers. Schematics of these stirrers are shown in Figure 21 and Figure 22 respectively. The illustrations displayed in Figure 21 and Figure 22 are not drawn to scale.

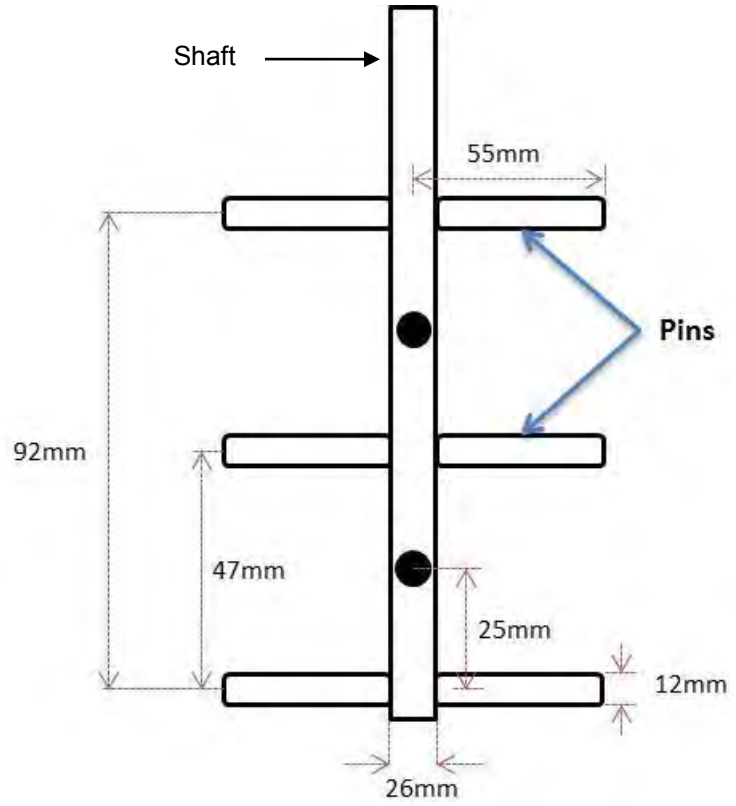

Figure 21: A schematic of the pin stirrer used (illustration not to scale).

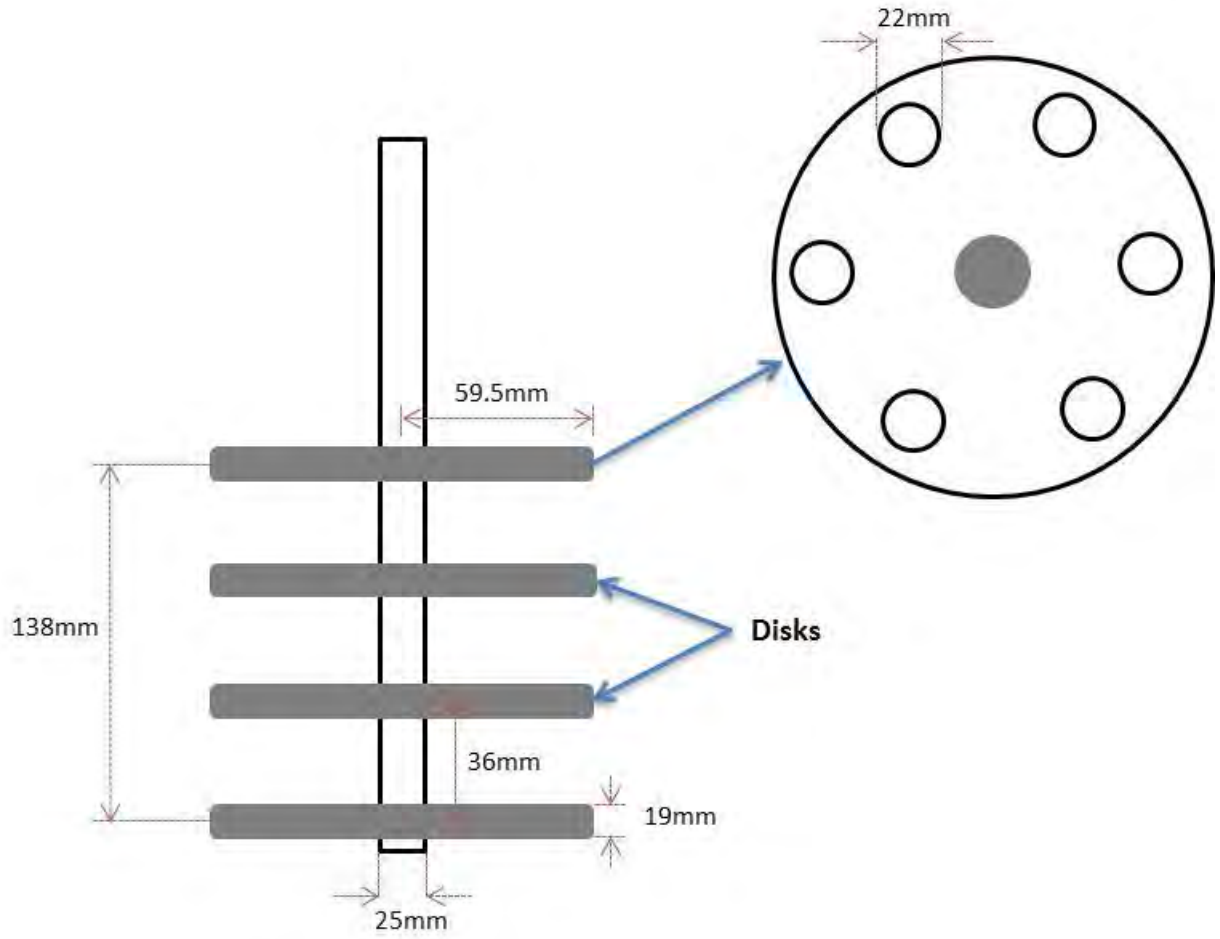

Figure 22: A schematic of the disk stirrer used (illustration not to scale).

3.2.1. Description of the major components of the batch VSM used

The VSM used had a number of components, mainly the motor, shaft and stirrer, milling chamber and torque meter. The setup also included a computer connection which had a software that capture and displayed values of the torque, power and the calculated specific energy.

Motor

The function of the electric motor is to convert electrical energy into mechanical energy which essentially facilitates the movement of the shaft that in turn moves charge within the mill.

Gear box

The purpose of the gear box is to transform the input provided by the motor into an output of desired rotational speed and torque.

Shaft

The shaft is attached to the gearbox. It holds either the protruding impeller arms or concentric disks and facilitates the transfer of kinetic energy onto the charge.

Impeller arms/ disks

The purpose of the impeller arms or disks (shown on Figure 21 and Figure 22) is to facilitate violent motion of charge which improves the grinding activity within the mill.

Table 3 shows the specifications for the equipment used in the test work for this thesis.

Table 3: A summary of the equipment specifications.

Motor max. power (kW)	1.1
Max. stirrer speed (rpm)	586
Milling chamber volume (litres)	5
Grinding media type	Ceramics
Grinding media size	Various

3.2.2. Batch VSM preparation

Prior to the start of the test work, a calibration curve for converting impeller frequency to rotational speed was established using a laser tachometer. The reason for this was that only the impeller frequency in Hertz (Hz) was displayed on the VSM set-up.

The shaft and impeller were initially mounted on the mill motor. At this point the milling chamber was empty. A reflective surface was placed on the mill shaft serving as a laser light reflector for the tachometer. The mill was then switched on and the frequency controller set to 20 Hz. Once the mill shaft had reached the operating frequency set-point (20 Hz), a laser light from the tachometer was pointed horizontally towards the reflective surface on the rotating shaft as described in Figure 23. The tachometer measured the rate at which the light was reflected back and displayed this as revolutions per minute (rpm). The procedure was repeated for frequencies of 30, 40 and 50 Hz and the respective impeller speeds in rpm recorded.

The impeller speeds in rpm recorded were then plotted against their respective frequencies on a Cartesian plane as seen in Figure 24. Figure 24 was used to convert the rpm values to frequency (Hz) which was the unit of measure by the machine. The impeller frequency controller was then adjusted to the desired frequency before loading the mill.

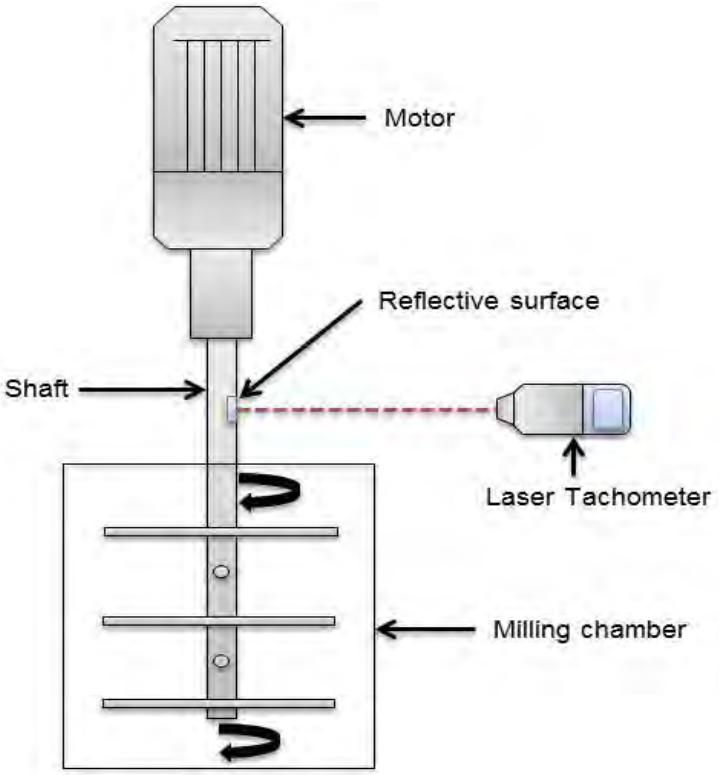

Figure 23: Schematic illustrating impeller speed measurements using a laser tachometer.

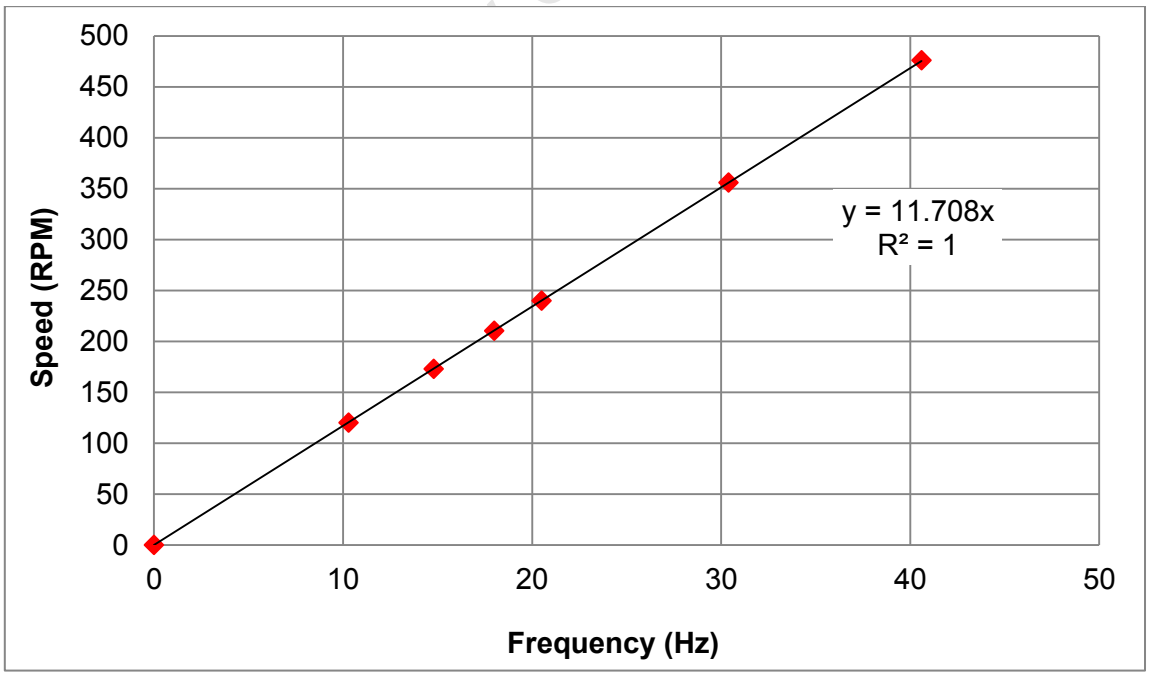

Figure 24: Relationship between impeller frequency (Hz) and speed (rpm).

3.2.3. Determination of the no load power

The no load power is the energy required to move the stirrer when the mill is empty. This is required in order to calculate the net energy from the gross energy consumed which is a more accurate description of the energy supplied to the charge. The stirrer was put in place when the mill was empty. For the pin impeller, the stirrer frequency was then set to 20Hz and the mill turned on. After 5 minutes, the power drawn was recorded. Two more power readings were recorded at 10 minutes and 15 minutes after the start of the mill. An average value of the three recorded data was used as the no load power for the pin impeller at 20Hz. The same procedure was repeated for stirrer frequencies of 30, 40 and 50 Hz. In the case of the disk impeller, the same procedure done for the pin impeller was followed. However in this case, the tests were done for impeller speeds 30, 40 and 50Hz. Results of the no load power tests for the pin and disk impellers at different stirrer frequencies are shown in Table 4 and Table 5.

Table 4: No load power values for pin stirrer at different stirrer frequencies.

Stirrer type	Pin stirrer			
	Power (W)			
Frequency (Hz)	at 5mins	at 10mins	at 15mins	Pavg (W)
20	0.4	0.4	0.4	0.4
30	4.4	2.9	2.9	3.4
40	7.5	7.3	7.3	7.4
50	33.5	32.5	32.5	32.8

Table 5: No load power values for disk stirrer at different stirrer frequencies.

Stirrer type	Disk stirrer			
	Power (W)			
Frequency (Hz)	at 5mins	at 10mins	at 15mins	Pavg (W)
30	2.9	4.4	4.5	3.9
40	11.9	9.4	10.2	10.5
50	36.6	41.0	32.5	36.7

3.2.4. Grinding media load

The grinding media load in terms of volume was kept constant at 70%. This was based on the mill volume. The mass of the grinding media required to make up 70% mill volume was calculated from the density of the media assuming the mill voidage was 0.4 which is a widely acceptable estimate.

3.2.5. Milling test matrices

In this section, each primary variable test matrix is presented on a separate table. The choices of variable range were carefully selected and these were designed to match the capacity of the equipment and laboratory conditions found at Mintek.

Table 6 to Table 11show the matrices of the different types of tests undertaken in this study. The aim of these tests was to assess the influence of selected operating variables on the specific energy and grind efficiency. This would assist in understanding energy consumption in vertical stirred mills in the milling of Merensky, a platinum bearing ore. The net specific energy, SE_{net}, referred to as just the specific energy in this thesis, was calculated using the difference between the gross power (energy required to move stirrer and charge) and the no load power (energy required to move on stirrer), residence time, T_r and mass of dry solids. This is shown in Equation 9.

$$SE_{net}\left(\frac{kWh}{t}\right) = \frac{Gross\ power(kW) - No\ load\ power(kWh)}{Mass_{\ solids}\,(tons)} \times T_r \qquad \textbf{Equation 9}$$

3.2.5.1. Variation in the specific energy input

Table 6 shows the test matrix for the grind curve study. The specific energy input was varied from 5 kWh/t to 25 kWh/t at increments of 5 kWh/t whilst all other variables remaining constant. Initial tests on the same ore type with a similar size distribution was done by Little and Van De Ruit (2012). They found that an increase in the specific energy input by about 5 kWh/t gave more distinctive changes in the size distributions which could easily demonstrate significant differences in the trends as shown in Figure 25. In this test work, the specific energy input range was increased to 25kWh/t to see if a limit is reached in terms of size reduction.

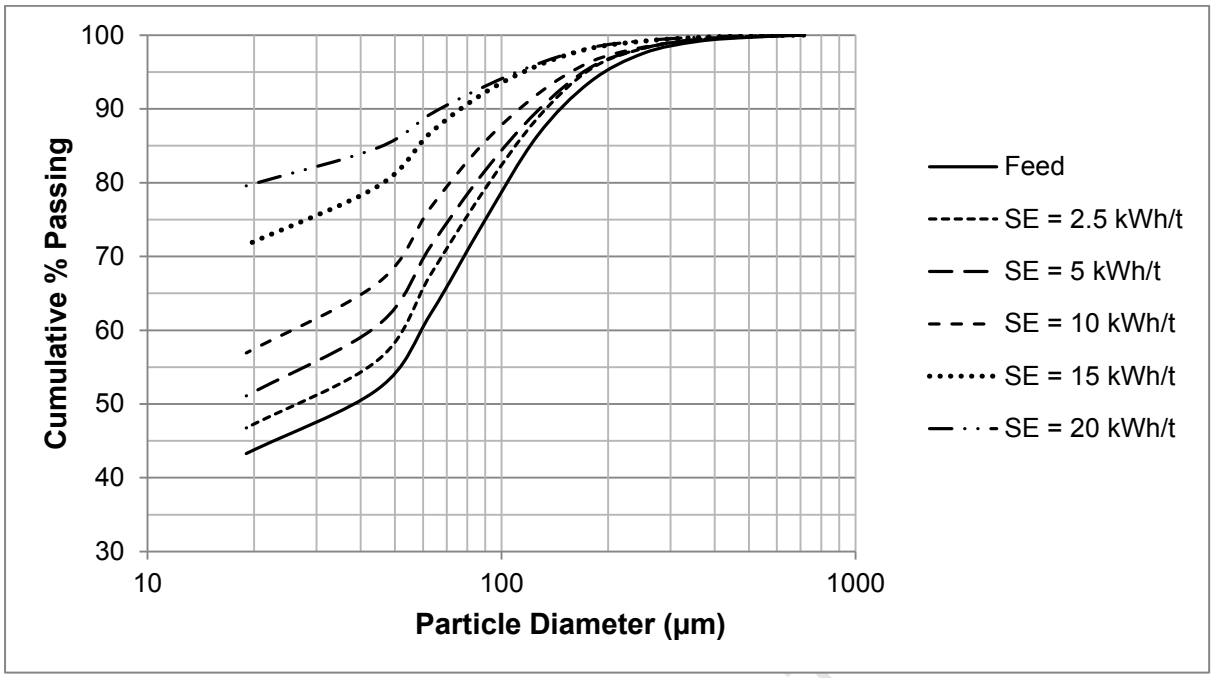

Figure 25: The relationship between specific energy input and product size distribution for selection of specific energy input levels. Media density = 2600 kg/m3, short-pin impeller, 235 rpm (after Little and Van De Ruit, 2012).

Table 6: Grind curve test matrix.

Test	Grind curve tests							
						Repeat tests		
Specific Energy (kWh/t)	**5**	**10**	**15**	**20**	**25**	**10**	**15**	**20**
Media size (mm)	-8+6.7	-8+6.7	-8+6.7	-8+6.7	-8+6.7	-8+6.7	-8+6.7	-8+6.7
Media SG	6.1	6.1	6.1	6.1	6.1	6.1	6.1	6.1
% Solids	40	40	40	40	40	40	40	40
Impeller speed (RPM)	586	586	586	586	586	586	586	586

3.2.5.2. Variation in the media size and density

Table 7 and Table 8 show the test matrices for high and low density ceramic media tests, respectively. The range of grinding media size in both tests was not wide. This was because the grinding media size test was no the main output of the study but was required to complete the evaluation of operating variables. Figure 26 and Figure 27 show a picture of the high and low density media used in the study, respectively.

Table 7: High density media size tests matrix.

Variable	High density media size			
			Repeat test	Repeat test
Media size (mm)	-8 + 6.7	-13.2+11.2	-8 + 6.7	-13.2+11.2
Media SG	6.1	6.1	6.1	6.1
% Solids	40	40	40	40
Impeller speed (RPM)	586	586	586	586

Figure 26: A picture showing a sample of the high density ceramic media used.

Table 8: Low density media size test matrix

Variable	Low density media size					
				Repeat	Repeat	Repeat
Media size (mm)	-4.75 + 2.8	-6.7+5.6	-8+6.7	-4.75 + 2.8	-6.7+5.6	-8 + 6.7
Media SG	2.6	2.6	2.6	2.6	2.6	2.6
% Solids	40	40	40	40	40	40
Impeller speed (RPM)	586	586	586	586	586	586

Figure 27: A picture showing a sample of the low density ceramic media used.

3.2.5.3. Variation in the solids concentration

Table 9 shows the matrix for the solids concentration test. The range of solids concentrations selected ranged from 30% to 80% solids. This range is sufficiently wide and offers adequate data points to map the influence of solids concentrations size reduction and specific energy. In industrial cases, the recommended operating range of SMDs is 30-60% solids by weight (Metso, 2010). This stringent range preference has been attributed to operational difficulties at high solids concentration. Chocking of pipes at solids concentration above 60% is of great concern to metallurgists as this can result in unplanned down times with severe financial consequences. In this particular test, the batch mill could not handle solids concentrations of less than 30% as the mill was too small for the excessive water requirements.

Table 9: Solids concentration test matrix

Variable	% Solids							
						Repeat tests		
% Solids	30	50	60	70	80	30	50	60
Media size (mm)	-8+6.7	-8+6.7	-8+6.7	-8+6.7	-8+6.7	-8+6.7	-8+6.7	-8+6.7
Media SG	6.1	6.1	6.1	6.1	6.1	6.1	6.1	6.1
Impeller speed (RPM)	586	586	586	586	586	586	586	586

3.2.5.4. Variation in the impeller speed

Table 10 shows the matrix for impeller speed tests. The maximum impeller frequency was 50 Hz. Four impeller speed levels were selected which were between 20 and 50 Hz at 10 Hz increments. This translates to an impeller speed of 235 to 586rpm. The impeller speed ranges used by other researchers utilising a vertical stirred media mill include, 300 – 500 rpm (Toraman and Katircioglu, 2010), 50 – 150 rpm (Jankovic, 2003), 260 – 1000 rpm (Zheng *et al*., 1996) and 200 – 765 rpm (Mankosa *et al*., 1989). For the case of horizontal stirred mills, impeller speed ranges already tested include, 400 – 1000 rpm (Jayasundara *et al*., 2010), 1204 – 2255 rpm (He and Forssberg, 2007), 2130 – 4370 rpm (Fadhel and Francis, 2001) and 805 – 2253 rpm (Gao *et al*., 1996). It can be observed that the horizontal stirred media mills are operated at much higher impeller speeds than vertical stirred media mills. The selected range of impeller speeds used in this test work is within the range of those used by other researchers (Toraman and Katircioglu, 2010; Zheng *et al*., 1996; Mankosa *et al*., 1989) who worked on the vertical stirred media mill.

Table 10: Impeller speed test matrix.

Variable	Impeller speed					
				Repeat	Repeat	Repeat
Impleller speed (RPM	235	351	471	235	351	471
% Solids	40	40	40	40	40	40
Media size (mm)	-8 + 6.7	-8 + 6.7	-8 + 6.7	-8 + 6.7	-8 + 6.7	-8 + 6.7
Media SG	6.1	6.1	6.1	6.1	6.1	6.1

3.2.5.5. Disk impeller tests

Table 11 shows the disk impeller test matrix. These tests were done merely to compare the performance of the disk and pin stirrer. The tests were done at selected impeller speeds and solids concentration. Other variables such as media size and media density were kept constant throughout for disk stirrer tests.

Table 11: Disk impeller test matrix.

Variable	% Solids				Impeller speed		
				Repeat			Repeat
% Solids	30	40	50	30	40	40	40
Impeller speed (RPM)	586	586	586	586	351	471	586
Media size (mm)	-8+6.7	-8+6.7	-8+6.7	-8+6.7	-8+6.7	-8+6.7	-8+6.7
Media SG	6.1	6.1	6.1	6.1	6.1	6.1	6.1

3.3. Sample preparation and pre-test planning

3.3.1. Test work ore type

Merensky ore with a bulk density of 3118 kg/m^3 from Lonmin was used in this thesis project. Sulphide and PGM mineralogy of Merensky have already been discussed in Section 2.1.1 and 2.1.2, respectively. PGMs in Merensky are typically associated with base metal sulphides. In previous years, the PGM grain size in Merensky has been reported as about 236µm (±45µm) by Liddell *et al*. (1986). However over the years, the PGM grain size has declined significantly. Liberation of minerals of value requires fine grind hence the increase in the demand for a fine product.

Merensky has been widely mined in the Bushveld Igneous Complex, North West of South Africa. This was the main reason for selecting the ore for this test work. In addition, the mineralogy of Merensky is not as complex as other major platinum bearing ores such as UG2 and Platreef.

3.3.2. Feed sample preparation

Initial preparation of bulk Merenksy sample was done by grinding a large sample taken from the mine in a RoM pilot plant ball mill at the Magotteaux pilot station, Frank concentrator. The specifications and conditions under which the pilot ball mill was operated are shown in Table 12.

Table 12: RoM mill specifications and operating conditions.

Rom mill length (m)	2.20
Rom mill diameter (m)	1.23
Rom mill speed (% Critical speed)	75
Rom mill ball filling (% mill volume)	24
Feed rate (kg/hr)	1400
Solids concentration (wt%)	75

The ball mill product was screened on an 850µm sieve to remove the grits. Since the bulk sub 850µm was too large, manageable amounts were obtained by mixing thoroughly and splitting using the “cone-and-quarter” method as described by Schumacher *et al*. (1990) and Hogg (2003:32). A random portion from the initial bulk sample, obtained through cone and quartering, was then split into 1 kg sub samples using a 10 cup rotary splitter shown in Figure 28. Keeping the feed consistent for all the tests was important in this study and

random sub sample portions from the rotary splitter were obtained and screened to assess if the particle size distributions were similar. The feed size distribution for the feed sample used is shown in Figure 29. The error bars presented in Figure 29 represent the standard error based on the standard deviation from two measurements of size distribution. The feed was fairly consistent for all the tests and the author of this thesis is confident that the results are not biased due to differences in the feed particle size distributions.

Figure 28: A 10 cup rotary splitter used for batch sample preparation.

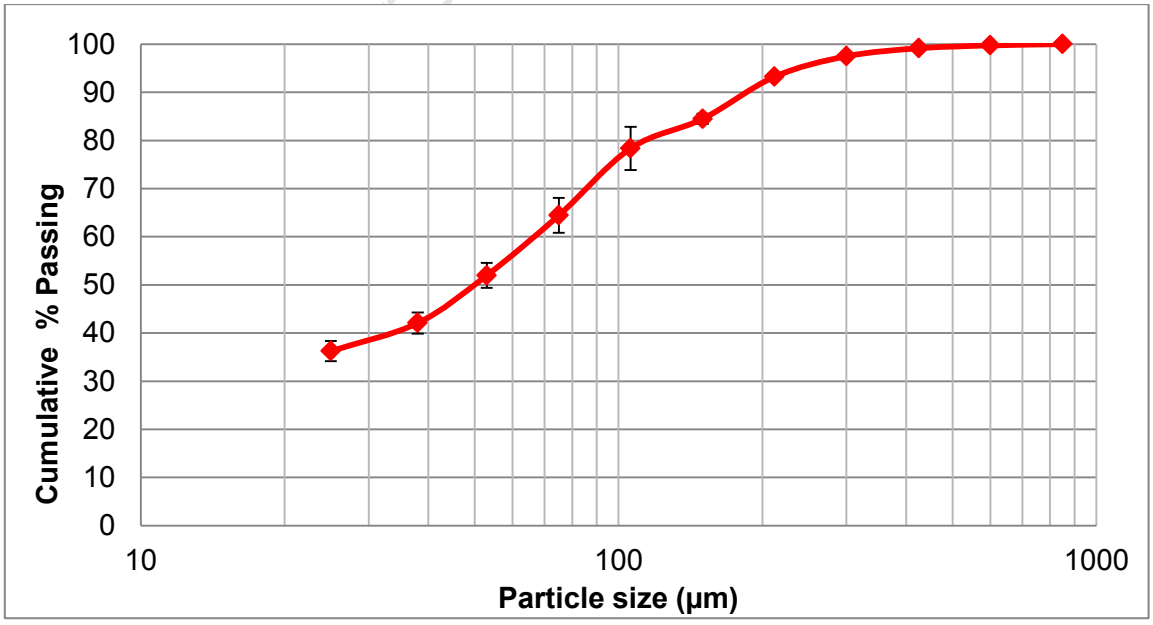

Figure 29: Feed size distribution for the Merensky ore used in the test work.

3.3.3. Test procedure

3.3.3.1. Pre-test preparation

Only 1kg sub-sample was used for each batch milling test. Prior to loading the sample into the mill, the sample was weighed and then the amount of water to give the desired per-cent solids was calculated. The appropriate mass of water was then weighed using a 5 litre beaker. The 1kg sample was mixed with the pre-weighed water. This was done to ensure rapid homogeneity of the slurry during milling since the batch milling times were quite short. Half of the required media was placed into the mill initially and the remainder was loaded after adding the slurry and inserting the stirrer. The reason for pre-mixing the sample and water and then loading only part of the media was twofold:

i. To avoid large quantities of slurry settling in the dead volume of the mill (bottom).
ii. To ease mounting of the shaft onto the machine. If all the charge is loaded prior to installing the shaft, then it becomes difficult to mount it.

The rest of the media is then loaded once the impeller shaft has been appropriately installed on the machine. The milling chamber is then covered with a lid to prevent charge from splashing out whilst in operation.

3.3.3.2. Batch runs

The VSM setup is connected to a computer which requires the dry mass of the sample being milled as an input. At this point, all equipment variables have been selected and the machine is switched on to run for a desired batch time. Once the machine is switched on (refer to Figure 30), the timer on a stop watch is started simultaneously. The mill was allowed to run for the desired period of time. Once complete the equipment was stopped (see display on Figure 30). The specific energy displayed on the computer screen was recorded at the time the mill at the time the mill was stopped.

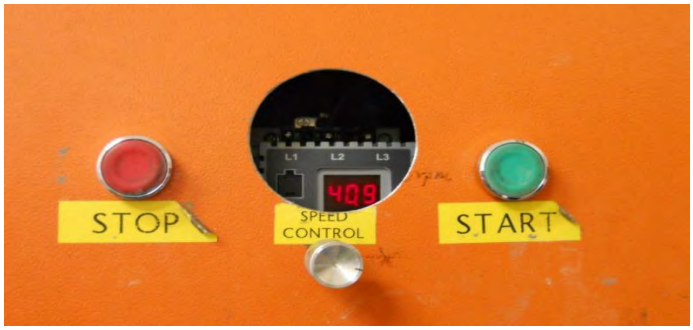

Figure 30: Vertical stirred mill power switch and speed controller (courtesy of Little and Van De Ruit, 2012).

3.3.3.3. Removal of charge from mill

After completion of each batch test, the impeller shaft was uninstalled and the mill tilted strategically, pouring the contents into a bucket with a media retention screen at the top. This ensured media was separated from the slurry prior to further processing. This process is illustrated in Figure 31. The mill and grinding media were then washed thoroughly, the wash water draining through the media retention screen and into the bucket. This was done to minimize material losses.

Figure 31: A picture showing charge removal from the mill.

3.4. Sample processing and data analysis

3.4.1. Product sample drying and splitting

The mill product samples collected in buckets were removed from the mill, filtered using an air filter press shown in Figure 32. The filter cake obtained was dried in an oven. The dry samples were weighed and their masses recorded. This was done for mass accounting. Ideally, the mass of dry sample after milling should equal the mass of dry sample before milling. If not then loss of solid mass during material processing can be identified, quantified and minimized. If the losses were too large, the samples were discarded and the test repeated.

The dry filter cake was screened over a 1mm screen to break lumps. A 1mm screen was used as opposed to a roller so as to avoid altering the size distribution of the product

samples. The 10 cup rotary splitter shown in Figure 28 was then used to split the dry samples to 300g sub-samples for screening.

The dry 300g sub-samples were transported to the Centre for Minerals Research (CMR) laboratories, at the University of Cape Town (UCT) for wet screening procedure and further analysis. The sub-samples were wet screened using the standard CMR wet screening procedure given in Section 3.4.2.

Figure 32: A photo showing an air filter press used to filter mill product samples.

3.4.2. Particle size analysis

Particle size analysis was performed using a combination of wet and dry screening. The procedures for wet and dry screening are discussed in Section 3.4.2.1 and 3.4.2.2, respectively.

3.4.2.1. Wet screening procedure

Wet screening was conducted to obtain the size distributions from the feed and product samples. The wet screening set up is shown in Figure 33. Wet screening is performed at screens of aperture sizes of 150, 106, 75, 53, 38 and 25µm. The sub-sample was initially weighed and wet screened on the finest screen (25µm). The screen was firmly placed on a

vibratory sieve shaker. An empty 20 litre bucket was placed underneath the screen. The vibratory sieve shaker is started up and the sub sample to be screened is then placed on the screen and water added to the sample. Water is added continuously during the process and the undersize is collected in the bucket underneath the screen.

The screening process is stopped when only clear water is discharged from the screen undersize. The undersize is removed, labelled and kept aside to be filtered later. The oversize is placed on a 150µm sieve which is firmly clamped onto the vibratory sieve shaker. An empty 20 litre bucket is placed underneath the sieve and wet screening proceeded as described for the 25µm sieve. The process is stopped when only clear water is discharged through the undersize. The 150µm screen oversize, if any, is placed on a pan and dried in the oven at 80°C. The dry material is then weighed and packed in clearly labelled plastic bags awaiting dry screening on sieve sizes above 150µm. The undersize is screened on a 106µm sieve using the same procedure described for the 150µm sieve. The oversize from the 106µm sieve is collected and dried while the undersize from the 106µm sieve is screened on the next sieve in the series and the process is repeated down to 25µm. The dried samples were weighed for size distribution purposes. The undersize from the 25µm sieve was combined with the original minus 25µm, filtered and then dried. The dried sub 25µm was weighed and the mass recorded.

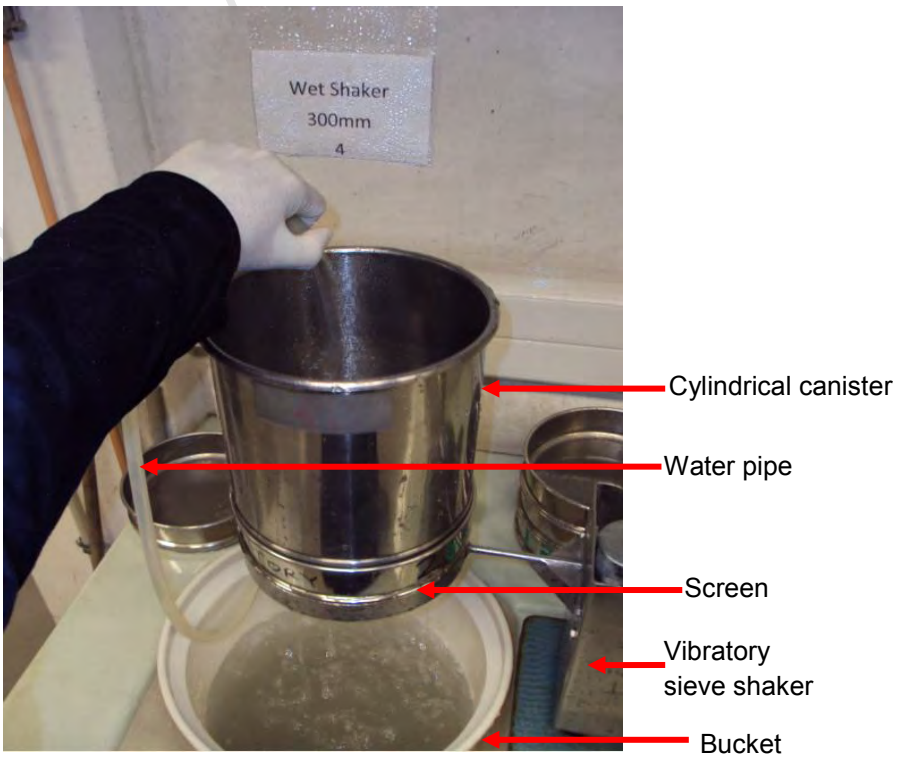

Figure 33: Wet screening set up.

3.4.2.2. Dry screening procedure

The 150µm oversize material was dry screened on 850, 600, 425, 300, 212, 150, 106, 75, 53, 38, and 25 µm screens. The screens are placed on a stack with the sieve with the largest aperture on top and the smallest at the bottom. The stack of screens is then placed on a sieve shaker. The shaker is started up and allowed to run for 20 minutes. After completion the stack of screens is removed from the shaker. The samples from each screen are removed and weighed. Masses of the oversize material on each screen are then recorded. A complete size distribution is then obtained by combining data from wet and dry screening processes.

CHAPTER FOUR: RESULTS AND DISCUSSION

4.1. Introduction

In the platinum industry, size reduction using stirred mills has been successfully implemented in many concentrators. This has been partly due to their ability to utilize less energy than ball mills for fine grinding application. However, what still remains of concern is optimisation of stirred mills with respect to energy consumption. The energy consumed in these mills is inevitably affected by both design and operating variables. Since energy is the key driver for size reduction, it is crucial to assess how the energy consumption can be reduced by selecting optimal operating conditions. In this thesis, variables tested were limited to residence time, solids concentration, impeller speed, impeller type, media density and media size. Test matrices detailing the experimental program are presented in Section 3.2.5. The ability to have the vertical stirred mill setup connected to a computer enabled the calculation and display of the specific energy while the machine was in operation. The specific energy was calculated using power draw (in Watts), mass of sample being milled and time. This information, collected by a software on the computer, was monitored and recorded for each test. This section focusses on evaluating the relationship between the key operating variables and the specific energy consumption.

4.2. Effect of operating and design variables on energy consumption

This section discusses the effect of operating and design variables on energy consumption. The variables include solids concentration, impeller speed and type, media size and media density.

4.2.1. Effect of solids concentration on energy consumption

The solids concentration was manipulated by varying the amount of water while keeping the mass of solids constant at 1 kg. This means the total volume of slurry differed depending on the solids concentration. Figure 34 shows that the specific energy increases with solids concentration over a range of 30 – 80% by mass and the relationship is not linear. For this work, a second order polynomial function was used to describe the relationship and an R^2 value of 0.972 suggests that it is a good fit.

The increase in the specific energy observed between 30wt% and 50wt% solids, appears to be steady. When the solids concentration is increased further (above 50wt %), there appears to be a reduction in the rate at which the specific energy increases. When milling calcite in a

vertical stirred mill for solids concentration 40 – 65wt%, Weller and Gao (1999) observed that the energy consumption was minimum at 65% solids contrary to what was observed in this thesis work. This could have been due to differences in ore properties and operating conditions. Weller and Gao (1999) operated a continuous system where as a batch vertical mill was used in this thesis. However, similar to the observation made in this test work, Jayasundara et al. (2009) observed that the power draw increases with increase in solids concentration from 1000 – 3000 kg/m^3 in an Isamill. The observations by other authors reveal the impact of other slurry effects related to variation in solids concentration, such as slurry viscosity (He and Forssberg, 2007; Fadhel and Frances, 2001). As the solids concentration increases, the average inter-particle distance shortens, increasing the number of stress events per particle. This however also leads to an increase in shear stress and consequently slurry viscosity. A high slurry viscosity hinders charge motion, forcing the impeller to work harder to move charge. This results in an increase in power draw and consequently an increase in the specific energy.

Figure 35 is a photo showing charge at 80wt% solids after milling for 102 seconds. It appears that at high solids concentration, the grinding media and mill wall are coated with slurry. A layer of media can be seen pasted on the mill wall. Work by He and Forssberg (2007) assessing the influence of slurry rheology on stirred milling of quartzite, revealed high solids concentration (70%) lead to viscosity issues. A high slurry viscosity hinders charge motion and consequently inhibits effective particle breakage.

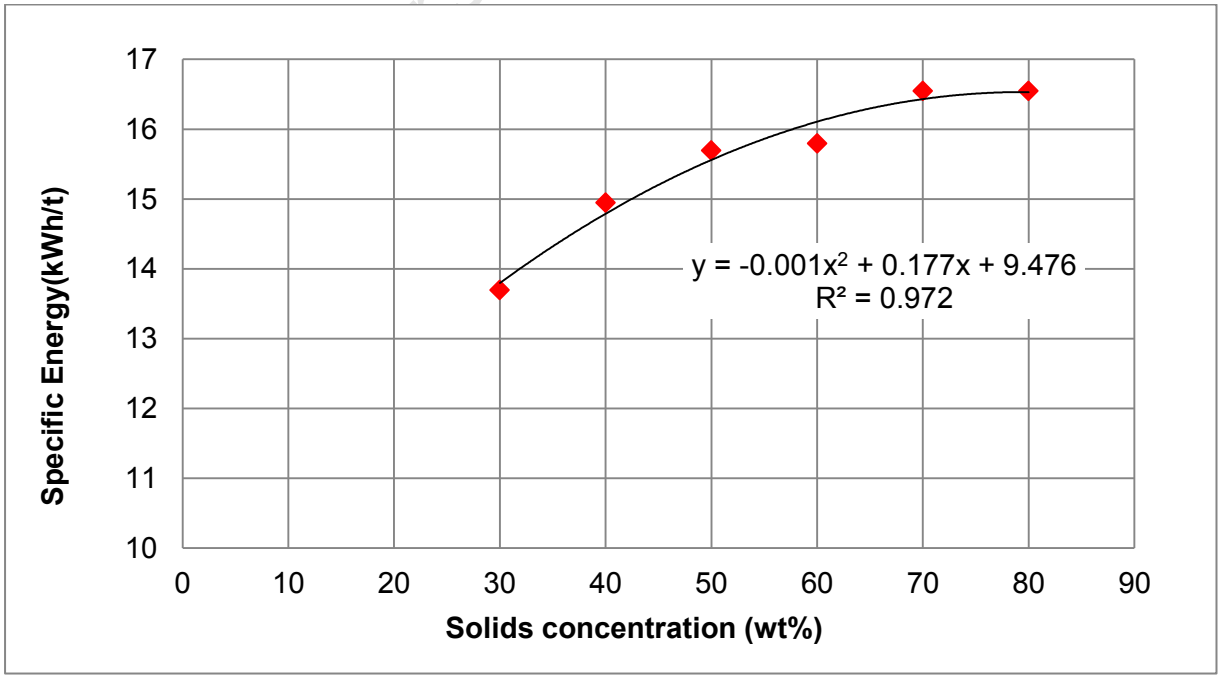

Figure 34: Effect of solids concentration on the specific energy input.

Figure 35: A photo showing charge after milling for 102 seconds at 80wt% solids.

The viscosity of slurry varies with solids concentration for a range of crystalline minerals which include Pyrite, Merensky, UG2, Calcium carbonate and Limestone to mention a few (Ding *et al*., 2007; Paterson, 2004; Jankovic, 2003; Bernhardt *et al*., 1999). For these minerals, an increase in the solids concentrations results in an increase in the slurry viscosity. Work on the flow behaviour of Merensky tailings by Paterson (2004) revealed that the slurry increasingly exhibited non-newtonian behaviour above 60% solids (by mass). Further increase in solids concentration above this point, the slurry becomes paste like to the detriment of processing and pumping (Paterson, 2004). Although Paterson (2004) made those conclusions based on slurry motion in a closed conduit, it is plausible that similar behaviour of Merensky slurry at high solids concentration occurs in stirred mills. When the viscosity is high, movement of charge is hindered. Particle shearing is diminished leading to poor breakage and decreased energy efficiency.

Figure 36 shows the effect of solids concentration on the size based specific energy. The energy efficiency was defined by the size based specific energy consumption (kWh/t of new sub 25 or 38μm). The size classes selected were sub 25μm and sub 38μm. These size classes gave the most distinct results in terms of energy efficiency. In addition, since the study is on fine grinding, the size classes selected are what is commonly used to represent grind results in fine grinding for mineral processing applications. The R^2 value for the sub

25µm and sub 38µm curves 0.90 and 0.92, respectively. This suggests that the proposed inverse fractional power equation is a good fit of the set of data obtained. The increase in solids concentration results in the gradual decrease in the size based specific energy over the range of solids concentration tested. The decrease in the size based specific energy can be attributed to an increase in the sub 25µm and 38µm product. In the grinding of coal in stirred ball mill, Mankosa *et al*. (1989) observed that an increase of solids concentration from 20 – 50wt%, had no effect on the energy efficiency. This observation is contrary to the observations in Figure 36. Since Mankosa *et al*. (1989) worked with coal, the reason for the conflicting observations could be due to the differences in ore properties which could have resulted in variation in the product quality. In addition, in the work by Mankosa *et al*. (1989), the specific input energy was kept constant. In this thesis test work, the residence time was instead kept constant while the specific energy input was dependent on the power drawn which varied with changes in solids concentration.

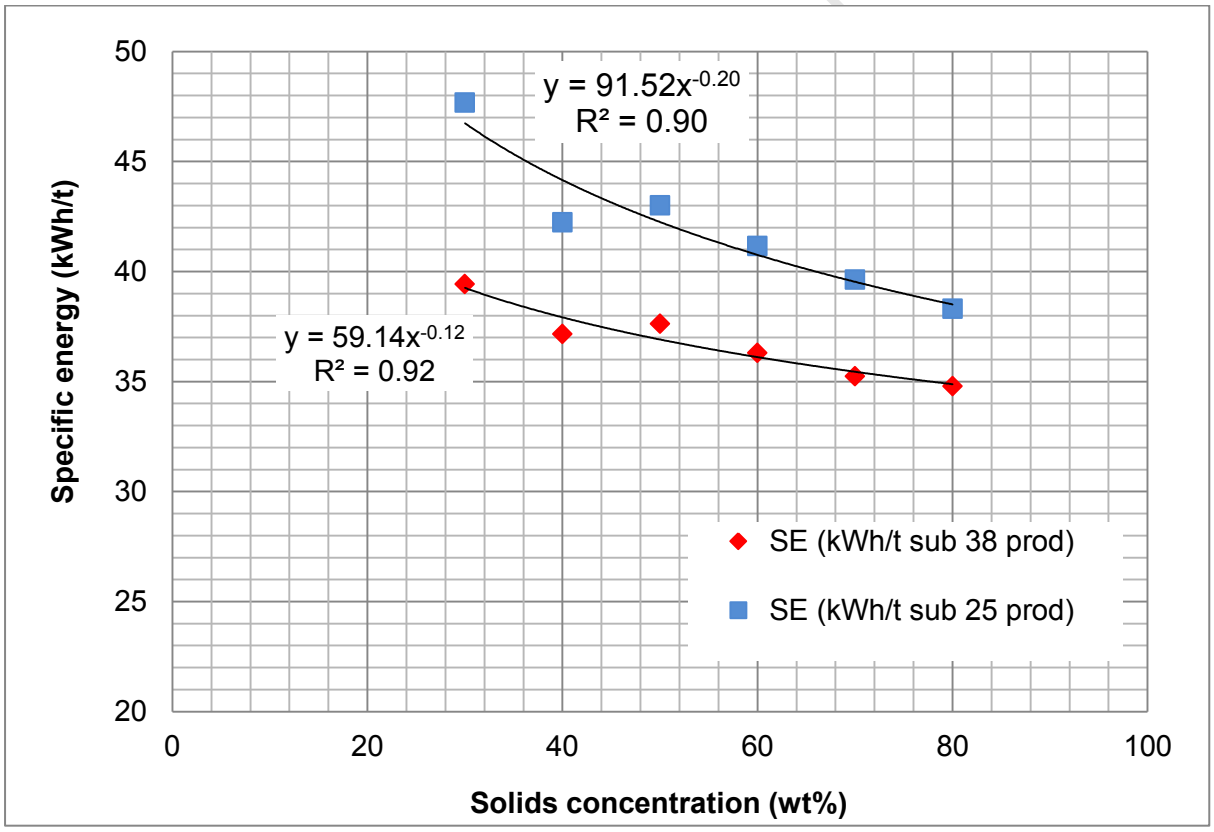

Figure 36: Effect of solids concentration on size based specific energy at 586 rpm.

4.2.2. Effect of impeller speed on energy consumption

The impeller speed was varied between 235 and 586rpm (20 – 50Hz). The impeller speed tests were done at 40wt% solids. The test matrix containing test work details is given in **section 3.2.5.4,** Table 10.

Figure 37 shows that an increase in the impeller speed results in an increase the specific energy over the range of impeller speeds tested. There appears to be a linear increase in the specific energy consumption with increase in impeller speed between 230 and 470 rpm. The increase in specific energy declines between 470 rpm and 586 rpm. The increase in specific energy consumption with increase in impeller speed is in agreement with Weller and Gao (1999) when milling calcite in a vertical stirred mill using impeller tips speeds of 2.5 to 3.9 m/s. Similarly, Zheng *et al*. (1996), Gao *et al*. (1996) and Jayasundara *et al*. (2010) observed that the energy consumption increases with increase in the impeller speed.

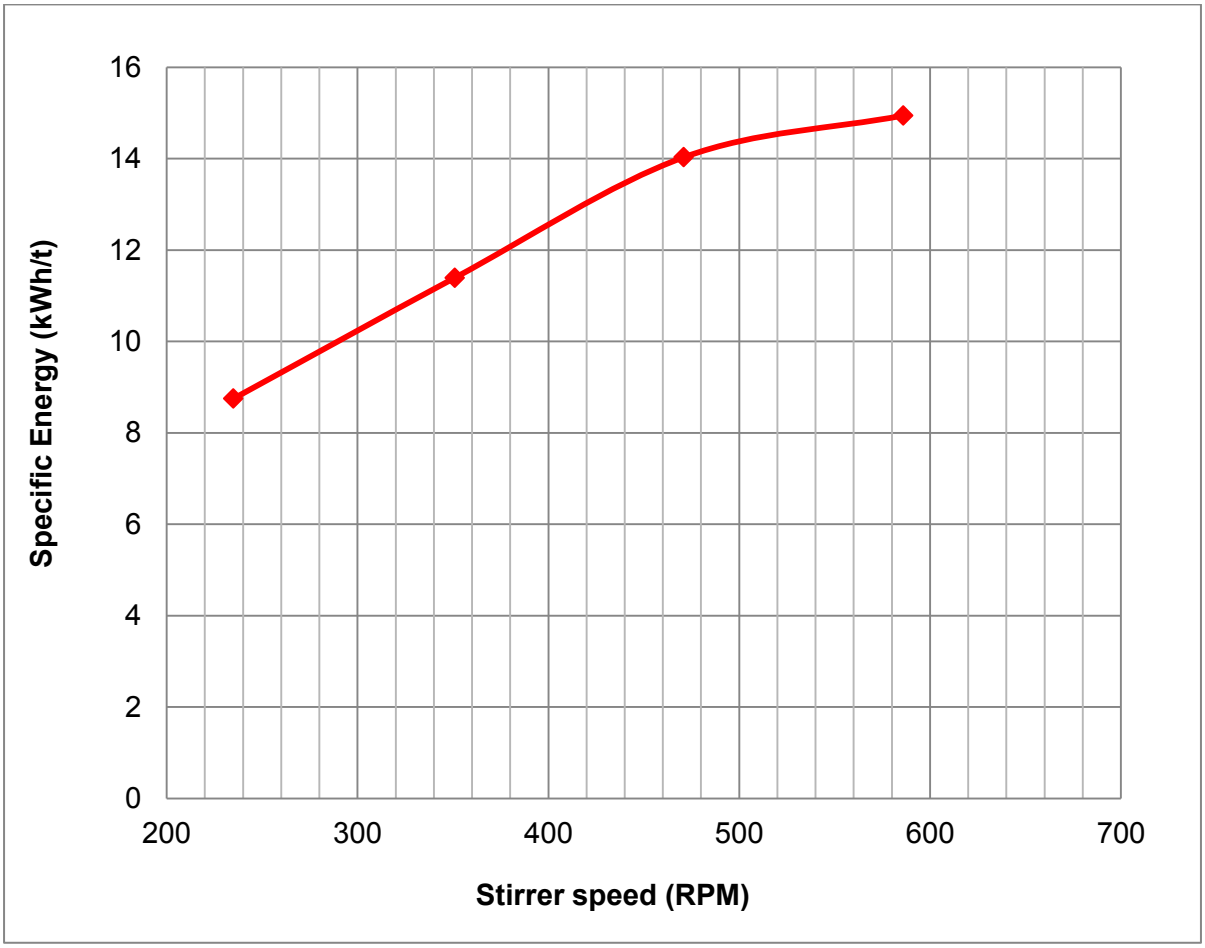

Figure 37: Effect of impeller speed on the specific energy input at 40% solids.

Figure 38 shows the effect of impeller speed on the energy efficiency. For both the sub 25µm and sub 38µm, an increase in the impeller speed from 235rpm to 351rpm results in a sharp decrease in the size based specific energy. The specific energy decreases sharply from impeller speeds of 235 to 351 rpm and then reduces gradually from 351 to 586 rpm. At this point, the rate of increase in the power is not matched by significant size reduction to sub 38µm and sub 25µm. This applies for both the sub 25µm and 38µm product size material. This therefore indicates decreasing energy efficiency at impeller speeds above

351rpm. It has been mentioned by various researchers (He and Forssberg 2007; Jankovic, 2003; Fadhel and Frances, 2001, Gao *et al*., 1996; Zheng *et al*., 1996), that the impeller speed has a significant effect on the energy efficiency. When milling dolomite in a horizontal stirred mill, Gao *et al*., (1996) observed that the power draft increased with increase in stirrer speed in the range 805 – 2253rpm. This led to an increase in the specific energy consumption with increase in stirrer speed, similar to what was observed in this thesis work. In the stirred milling of quartzite with impeller speeds in the range 1204 – 2255 rpm, He and Forssberg (2007) observed that the energy efficiency increased with increase in stirrer speed from 1204 to 1808 rpm but decreased thereafter. This alludes to the existence of an optimum stirrer speed which was not observed in this thesis work. Jankovic (2003) found that there is better energy utilisation when operating a vertical stirred mill at lower stirrer speeds (50 – 150 rpm). The decrease in energy efficiency with increase in impeller speed has also been reported by Zheng *et al*. (1996) and Mankosa *et al*. (1989). It is noteworthy that the observations made by Zheng *et al*. (1996) were for tests done using a pin mill at impeller speeds of 500 – 1500 rpm. The range of impeller speeds studied by Mankosa *et al*. (1989) was 200 – 1350 rpm (at 43wt% solids), covering the range of impeller speeds used in this study (235 – 586 rpm).

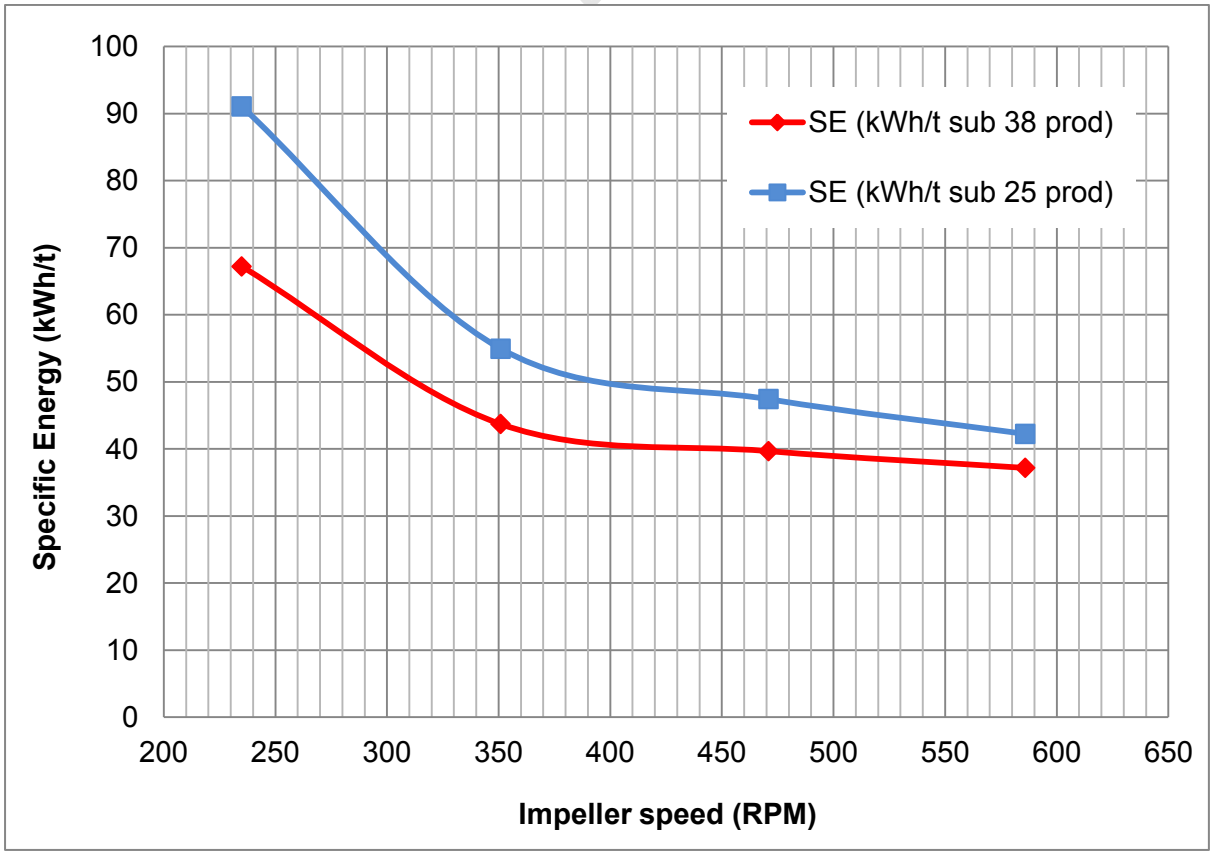

Figure 38: Effect of impeller speed on the energy efficiency.

Figure 39 shows the effect of impeller speed on energy efficiency (m^{-2}/Wh) and specific surface area (m^{-2}/m^{-3}) from Zheng *et al*. (1996). Figure 39 shows that the energy efficiency increases from 200 – 500 rpm and decreases thereafter. In this thesis work, the decrease in energy efficiency was observed at impeller speeds above 351 rpm. However, unlike Zheng *et al*. (1996), an optimum impeller speed was not observed in this work with respect to size based specific energy. This may have been due the use of much coarser media and different ore milled compared to the work by Zheng *et al*. (1996).

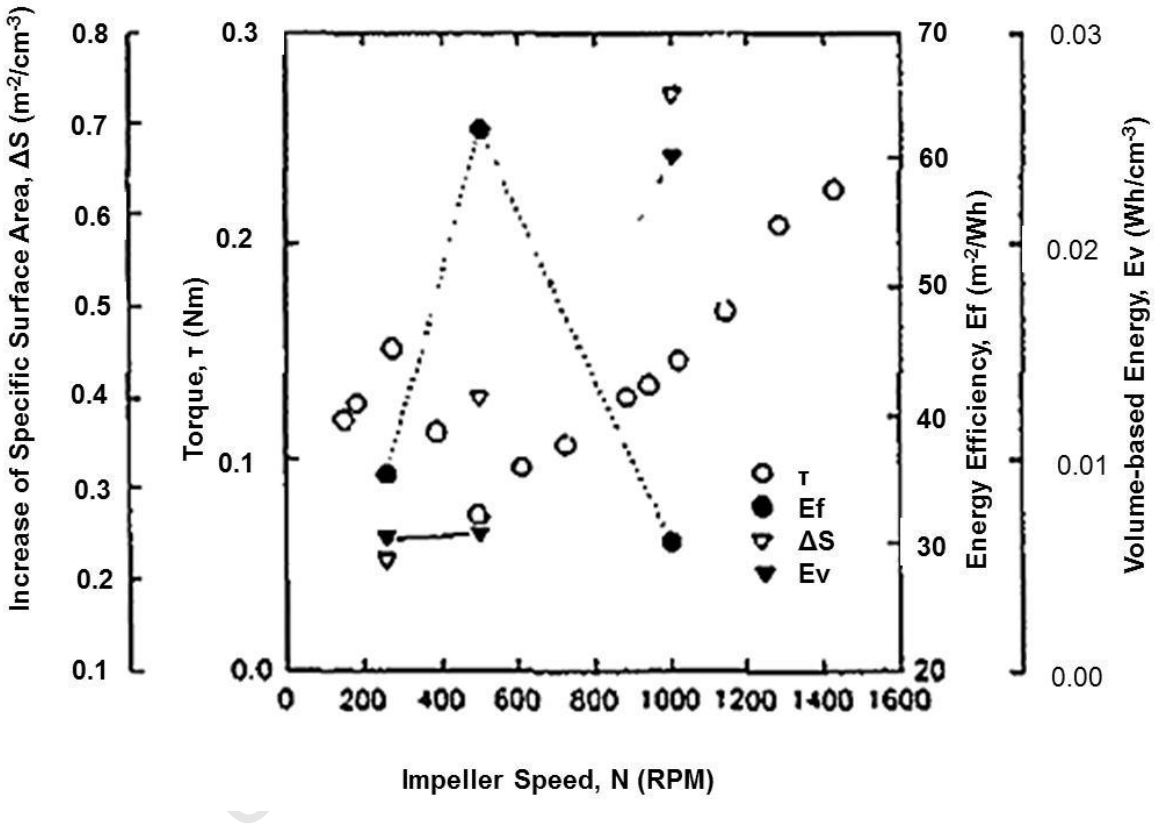

Figure 39: Effect of impeller speed. Conditions: D = 6.5 cm; T= 11.8 cm; t = 15min; c=60%; R=3; d=2.05mm; V=150cm3 (Zheng et al., 1996).

4.2.3. Effect of stirrer type on energy consumption

The stirrer type is one of the important design variables considered in stirred milling operations. It is responsible for imparting energy on to charge which essentially results in particle breakage. In this study, a number of tests were carried out using a disk and pin stirrer types. The aim was to compare the performance of the disk stirrer to that of the pin stirrer. Vertical stirred media mills are typically operated at 30 – 60wt% solids (Metso, 2010). The comparative tests for the disk stirrer were therefore carried out at 30wt%, 40wt% and

50wt% solids concentration which fall within the typical operating range. In addition, tests were done at 351rpm, 471rpm and 586rpm.

Figure 40 shows the specific energy at different solids concentration for both disk and pin stirrers. The specific energy for the disk stirrer is much lower than that of the pin stirrer. Since the mass of solids ground in the mill was 1 kg and the residence time 102 seconds for both tests, the pin stirrer's higher specific energy must have been as a result of a greater power draw. Jayasundara (2007) studied particle flow in an Isamill using the Discrete Element Method (DEM) modelling. The mill operating conditions used by Jayasundara (2007) were, a media filling of 80%, an impeller speed of 1000rpm and 3mm particles with a density of 2500kg/m^3. The flow patterns, mixing patterns and power draw for a pin stirrer and disk stirrers with no holes (0H), 3 holes (3H) and 5 holes (5H) were studied. Jayasundara (2007) reported that the power draw in stirred milling using a pin stirrer is significantly higher than when a disk stirrer is used (Figure 41). Jayasundara (2007) attributed the higher power draw when using a pin impeller to higher collision frequencies compared to when using disk impellers. The high collision frequencies result in high collision energies and hence a high power draw.

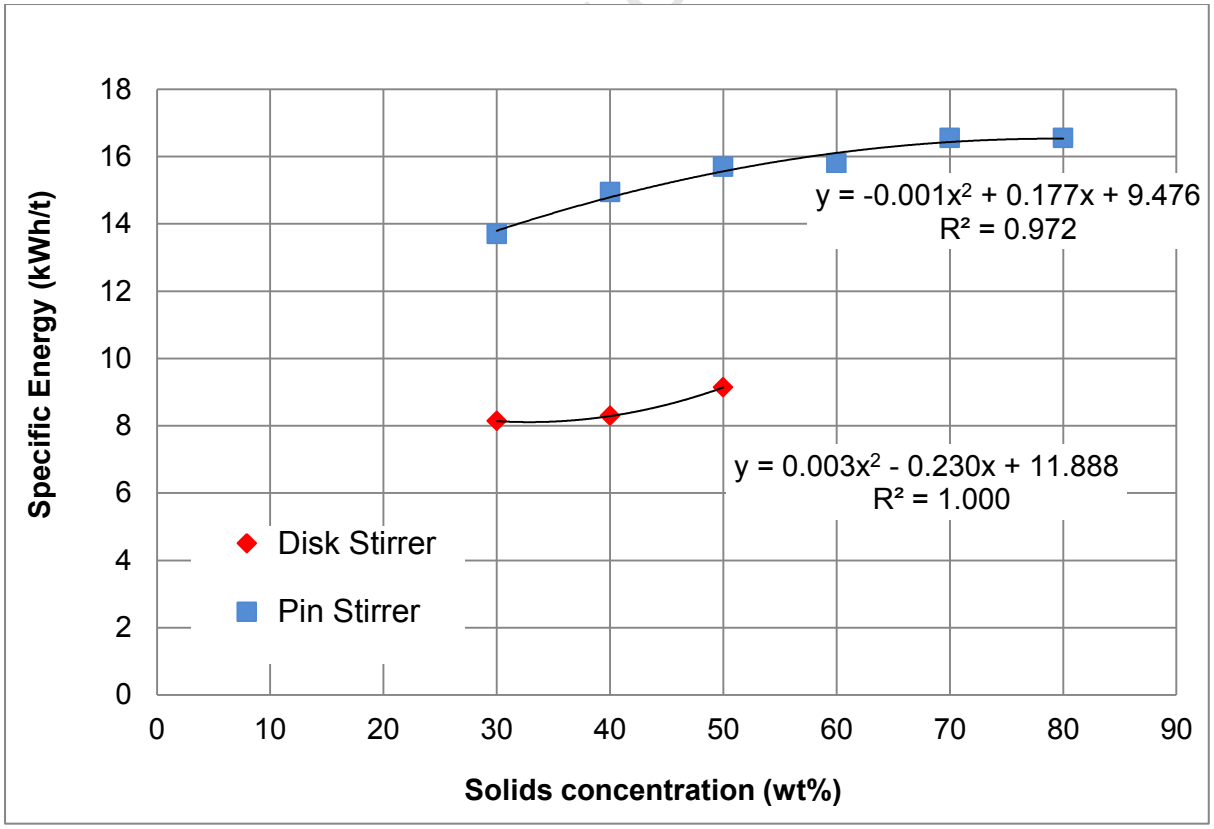

Figure 40: A comparison of the effect of solids concentration on the specific energy for disk and pin stirrers at 586 rpm impeller speed.

For the test work in this thesis, the pin stirrer occupied less space of the milling chamber than the disk stirrer. The greater volume available for charge motion possibly resulted in increased media-particle contacts through attrition and abrasion processes. The more violent the charge motion, the greater the energy consumed. This could explain why the milling with the pin impeller generally required more energy than when using a disk impeller at similar conditions.

Furthermore, Theurkauf and Schwedes (1999) explored particle and fluid motion in stirred mills comparing the disk and pin stirrers. Theurkauf and Schwedes (1999) used the light-sheet technique to visualize tracer grinding bead (coloured glass beads) velocities in a transparent grinding chamber. Polystyrol tracer particles (x_{50}=350μm) were used with silicon oil as the fluid. Tracer particle and fluid velocities were analysed using Particle Image Velocimetry (PIV). Figure 42 (Theurkauf and Schwedes, 1999) shows how the flow fields differ for a disk (a) and pin (b) stirrer when the stirrer tip speed is similar. The findings of Theurkauf and Schwedes (1999) revealed that pin stirrers showed higher and more unstable circumferential fluid velocities than disk stirrers.

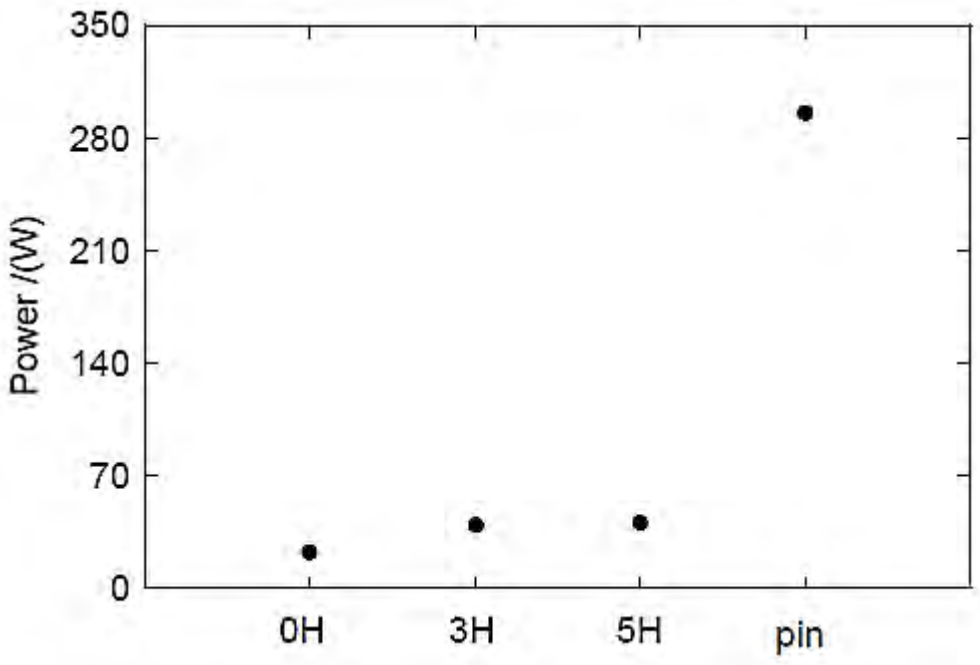

Figure 41: Effect of stirrer type on power draw (adopted from Jayasundara, 2007 Phd thesis).

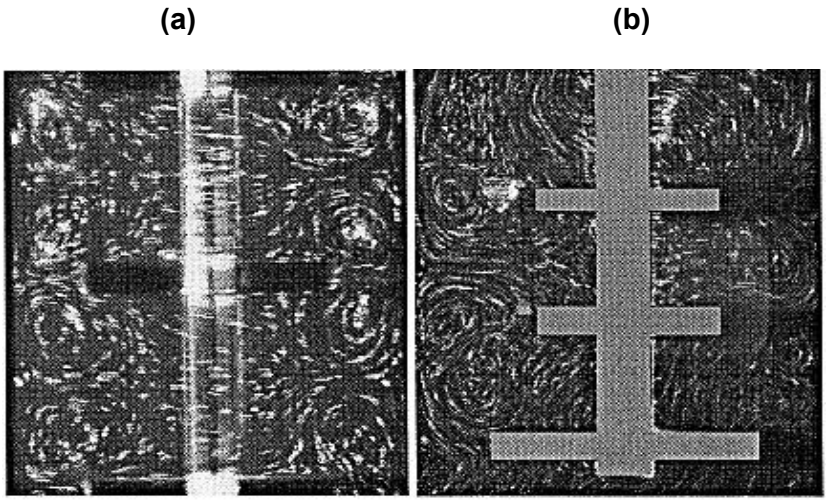

Figure 42: Tracer streak lines of the flow field at stirrer tip velocity of 1.3 ms^{-1} using vertical light-sheet: (a) disk stirrer; (b) pin stirrer (Theurkauf and Schwedes, 1999).

Figure 43 shows a comparison of the specific energy based on the sub 25µm product for the disk and pin stirrers. The disk stirrer size based specific energy is greater than that for the pin stirrer. In reference to Figure 40, since the specific energy consumption is higher for the pin stirrer compared to the disk stirrer, this can only happen if the amount of sub 25µm obtained for the pin stirrer is significantly higher than that of a disk stirrer. From this, a conclusion can be drawn that for the range of solids concentration tested, the pin stirrer is more energy efficient than the disk stirrer.

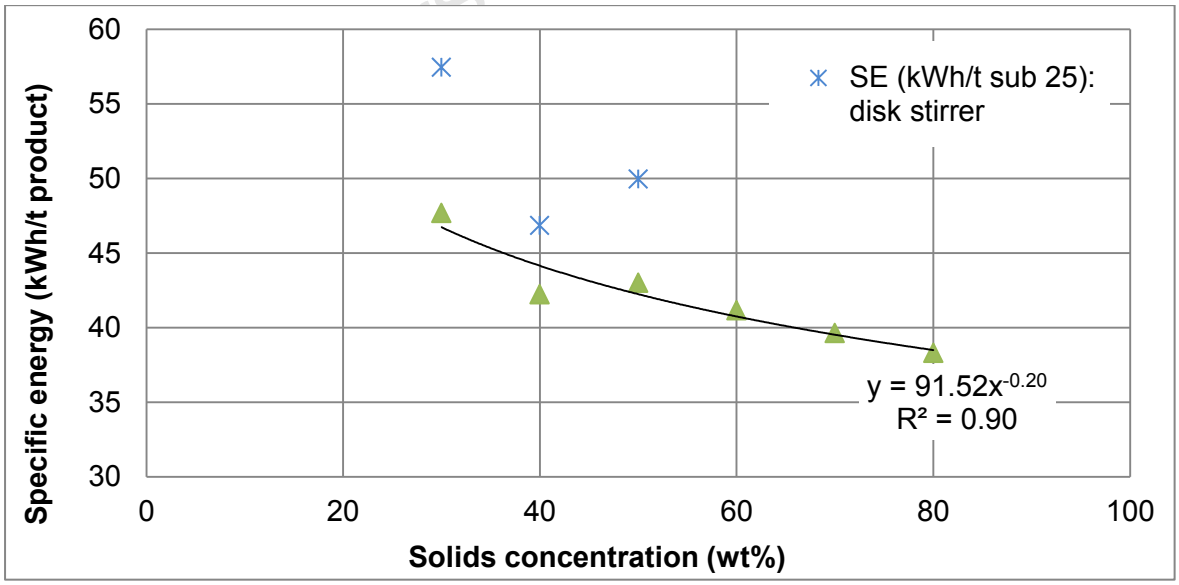

Figure 43: A comparison of effect of solids concentration on the size based specific energy input for the disk and pin stirrers at 586rpm impeller speed.

The effect of impeller speed on the specific energy for the disk and pin stirrers are shown in Figure 44. The effects of impeller speed on specific energy were more pronounced for the pin stirrer compared to the disk stirrer. From Theuerkauf and Schwedes (1999), this can be attributed to pin stirrers exhibiting higher and more fluctuating circumferential fluid velocities than disc stirrers. When the impeller speed was increased from 351rpm to 471rpm, the specific energy consumption increased slightly for the disk stirrer test. However the specific energy consumption dropped when the impeller speed was further increased to 586rpm. The drop in specific energy consumption at 586rpm impeller speed can be attributed to fluidization of charge which possibly resulted in a decrease in the torque and consequently the power draw.

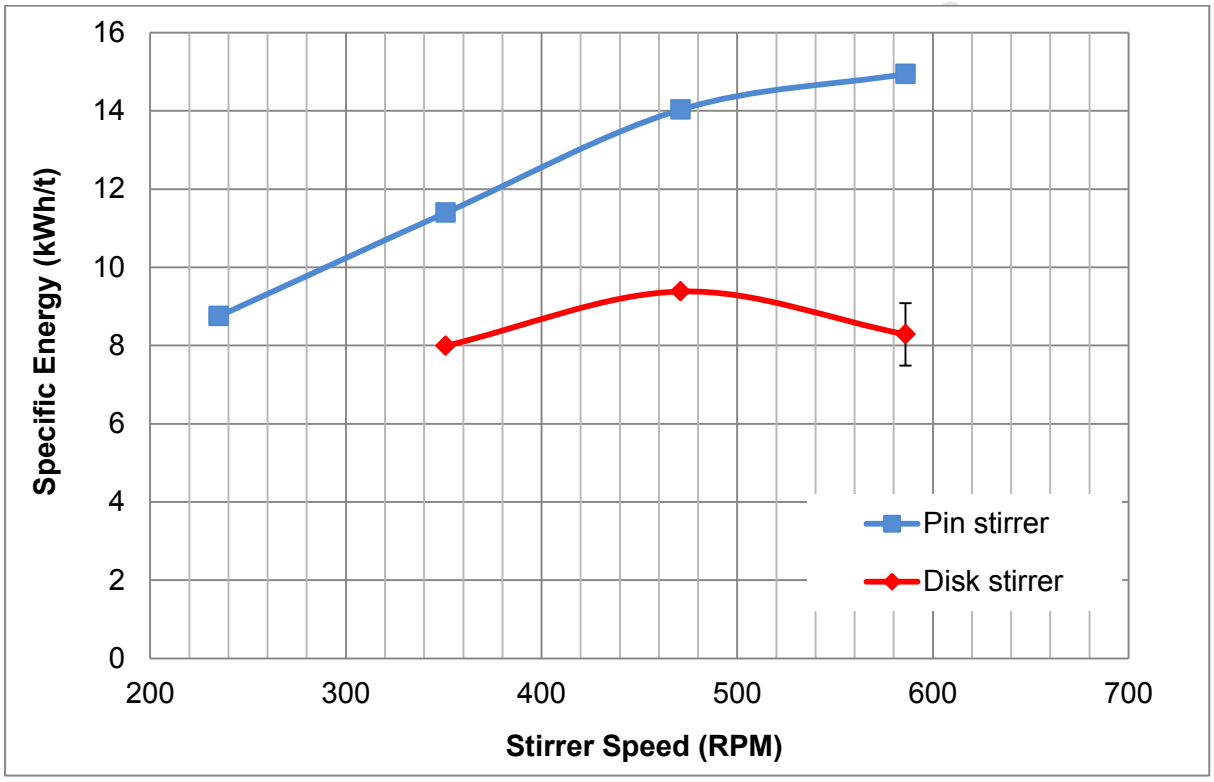

Figure 44: Effect of impeller speed on the specific energy input for the disk and pin stirrers at 40% solids.

Figure 45 shows the effect of impeller speed on size based specific energy. The specific energy based on the sub 25µm product was selected as a basis for comparison. This was defined as the specific energy required to produce a sub 25µm product. The size based specific energy is greater for disk stirrer compared to the pin stirrer. This can be attributed to lower amount of sub 25µm product obtained for the disk stirrer compared to the pin stirrer (refer to Figure 46) possibly due to a lower overall specific energy consumption which resulted in poor grinds.

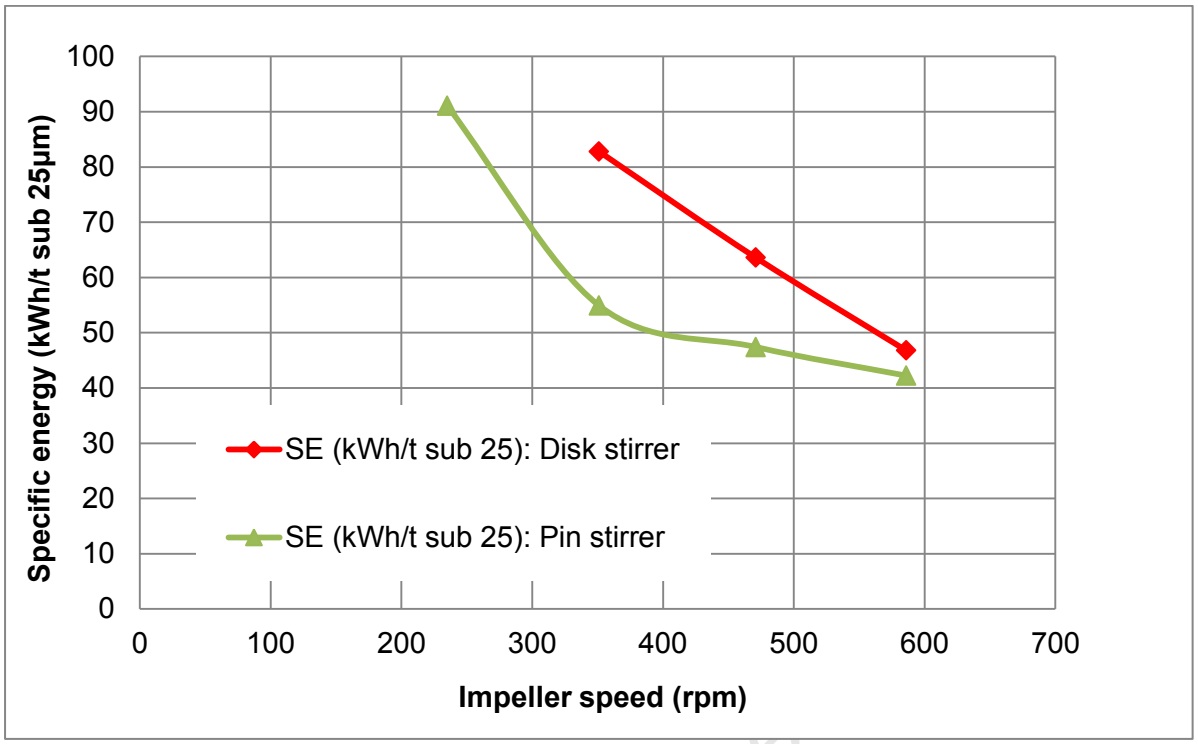

Figure 45: A comparison of effect of impeller speed on the size based specific energy input for the disk and pin stirrers.

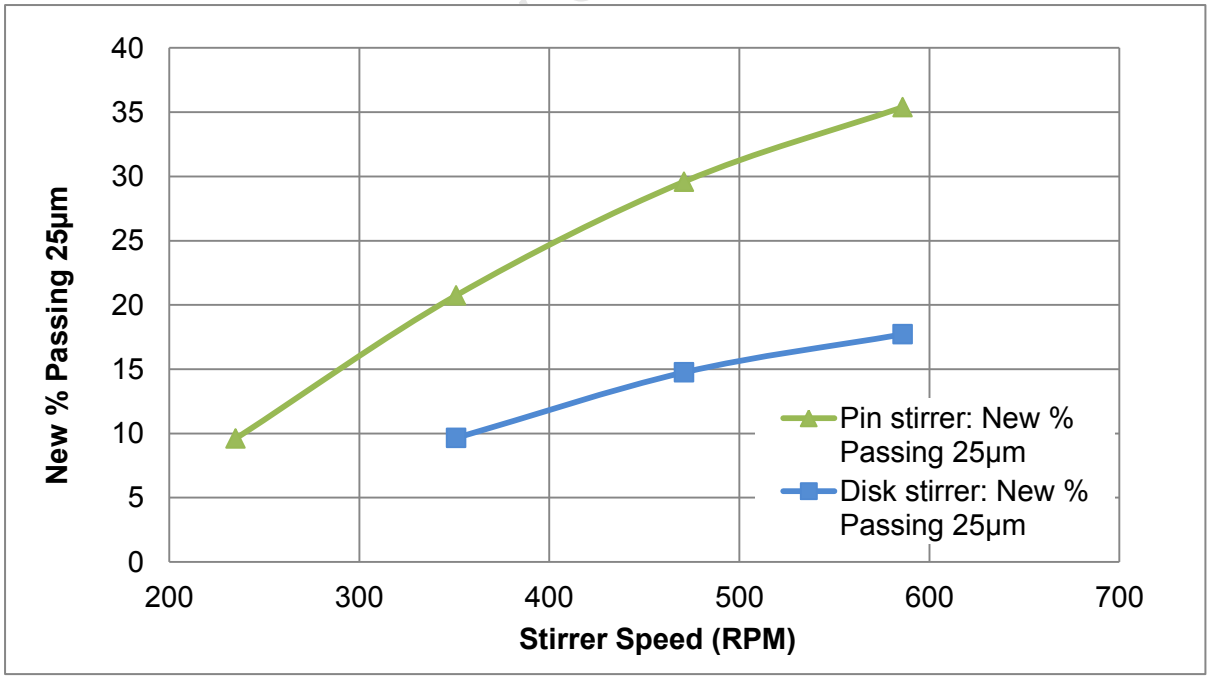

Figure 46: Effect of stirrer speed on the % passing 25µm for pin and disk stirrers.

Figure 47 (courtesy of Little and Van De Ruit, 2012) shows the product size distribution of merensky ore when different impeller types were used. It is important to note that the ore used in the test work done by Little and Van De Ruit (2012) was of a similar size distribution to that used in this thesis. It can be seen that the product size distribution when different impeller types are used vary. The pin impellers give a finer product than the disk impeller.

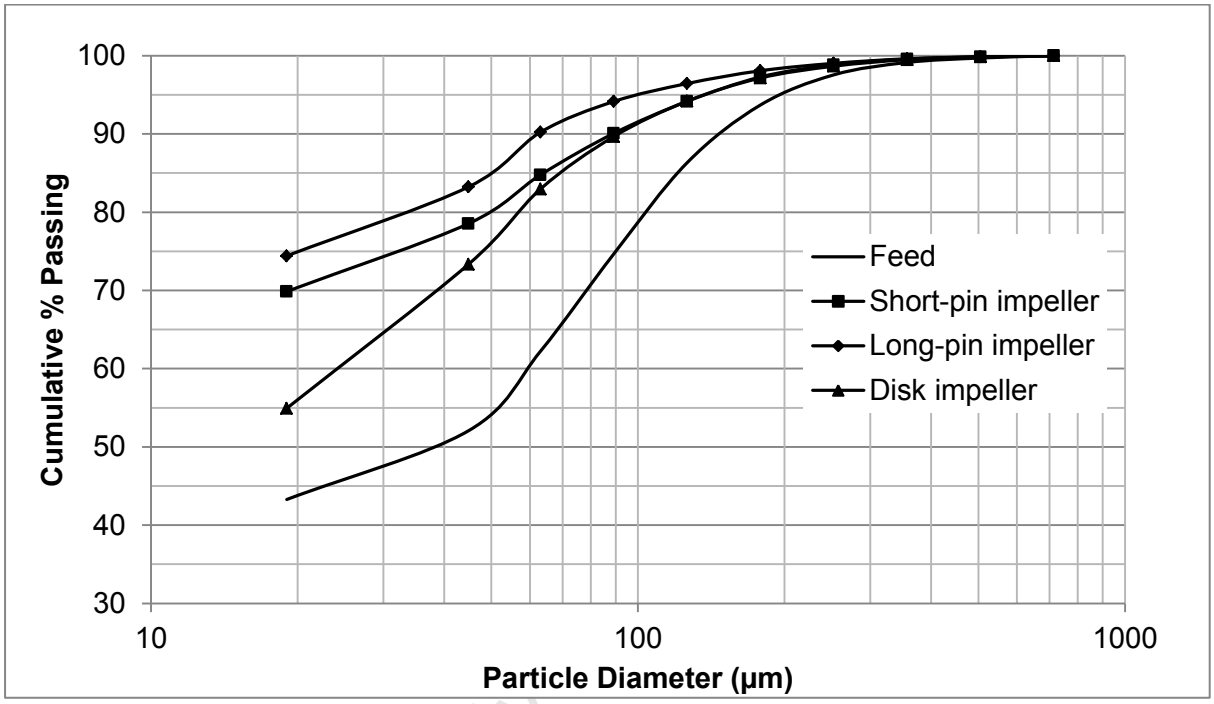

Figure 47: Cumulative particle size distributions showing the effect of impeller type on mill product size, with a specific energy input of 10 kWh/t. Impeller speed = 470 rpm, Media density = 4400 kg/m^3 (Little and van de Ruit, 2012).

Figure 48 (Little and Van De Ruit, 2012) shows a signature plot for tests done using a long pin, short pin and disk impeller types. The range of specific energy inputs was 4 – 15 kWh/t. The specific energy required to obtain a certain P_{80} size is lower for the pin impellers as compared to the disk impeller. This further supports the conclusion made in this thesis that the pin impeller requires less energy to achieve a specific product size compared to the disk impeller. This is mainly due to higher collision frequencies experienced as a result of more violent charge motion when pin impellers are used.

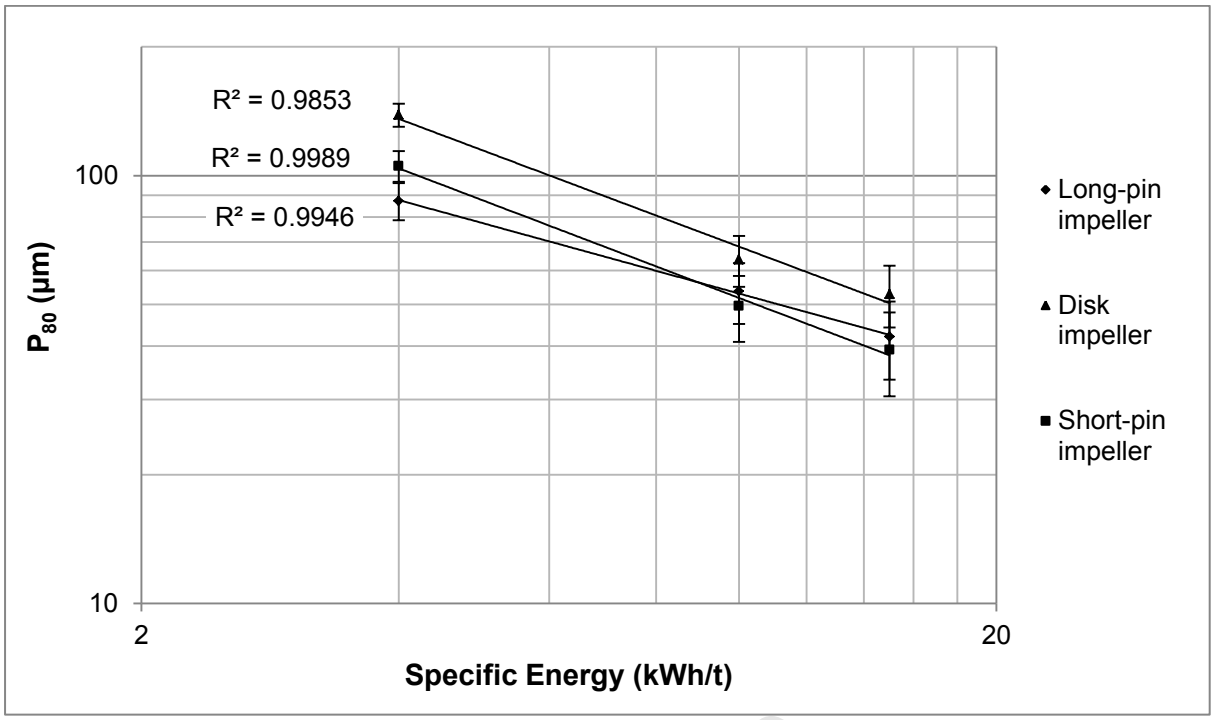

Figure 48: The signature plots obtained for different impeller types. Error bars show 95% confidence limits. Impeller speed = 470 rpm, Media density = 4400 kg/m^3 (Little and van de Ruit, 2012).

4.2.4. Effect of grinding media properties on energy consumption

Grinding media properties such as size and density are crucial in fine grinding using stirred mills. Poor choice of grinding media can have a negative effect on the grind and energy efficiency. Tests on the effect of media density and size on the grind and specific energy conducted on low density (SG of 2.6) and high density (SG of 6.1). The results and discussions are presented in this section.

4.2.4.1. Effect of media size on the specific energy at constant residence time

Batch milling tests were conducted at 102 seconds using high and low density ceramic media of different sizes. Table 13 shows the variation in specific energy with media size for both high and low density media. For the same media type, the specific energy consumption is less by 33% for the test where fine grinding media was used compared to that where coarse media was employed. This means that power draw for the coarse media is greater than that of fine media. This was observed for both low and high density media types. For the high density media, the specific energy required to produce a sub 25µm product is less when fine media is used compared to coarse media. This could be due to fine media having a greater surface area which improves media-particle interaction and consequently particle breakage. This leads to production of more sub 25µm material with fine media compared to

coarse media. In addition, less energy is consumed by the fine media compared to the coarse media resulting in a lower specific energy required to produce a sub 25µm product.

For the low density media, the specific energy required to produce a sub 25µm product is less when fine media is used compared to coarse media. The reason for this is similar to the one already explained for the high density media. The results are in agreement with those reported by Altun *et al*. (2013). When comparing the performance of 4mm and 6mm media in milling cement in a horizontal stirred, they observed that the 4mm media produced a finer product by consuming 24% less specific energy compared to the 6mm media. This meant that the fine media was more energy efficient than the coarse media for fine grinding. In the work by Jankovic (2003), it was observed that for a relatively coarse feed (F_{80} ~ 20 - 46µm), the specific energy input was higher for the fine media test compared to the coarse media test. However for a fine feed (F_{80} < 10 µm), the specific energy input for the fine media test was observed to be lower than that of the coarse media test. From this conflicting evidence, a conclusion that fine media is suited for grinding fine feeds was drawn. In the fine grinding of limestone using a vertical stirred mill, Zheng *et al*., (1996) observed reduced energy consumption with finer media and this was attributed to increase in fluidity of bulk media. A similar observation has previously been reported by Yue and Klein (2006) for quartz milling tests using grinding media size in the range – 3mm + 0.5mm. The increase in specific energy with increase in media size appears not to be exclusive to high density media.

The findings in this thesis that finer media are more energy efficient for fine grinding are supported by Altun et al. (2013), Yue and Klein (2006), Jankovic (2003) and Zheng et al. (1996). However, it is important to note that when selecting the appropriate media size for fine grinding application, the feed top size should not be ignored.

Table 13: Variation of specific energy with media size and density

Media size (mm)	Media density (g/cm^3)	Media filling (%)	Grind time (s)	Specific energy (kWh/t)	Specific energy (kWh/t new sub 25µm)
-8+6.7	6.1	70	102	15.0	42.2
-13.2+11.2	6.1	70	102	22.4	89.9
-4.75+2.8	2.6	70	102	4.5	32.1
-8+6.7	2.6	70	102	5.8	41.6

4.2.4.2. Effect of media density on the specific energy at constant residence time

Comparison of media density was done basing on media size range of -8mm + 6.7mm. This comparison was done for tests carried out at similar residence times. In reference to Table 13, the high density media is seen to consume a significantly larger amount of energy compared to the low density media. This can be explained based on the difference in media loading with respect to media mass. The media load for all the tests conducted for this thesis was 70% by volume. Since the media densities were different, the low density media mass required to make up 70% mill volume was significantly lower than that of high density media. Therefore, the mill would require more energy to move the heavier (high density) media resulting in a higher power draft. This explains the higher specific energy input recorded for the high density media test. According to Mankosa *et al*., (1986), lower energy consumption is expected if density of media is reduced without significantly compromising grind performance. In this thesis, the media density test range was limited to two levels. It is possible for a different conclusion to be reached with a wider range of media densities. For instance, Durant (2012) observed that there was no relationship between media density and power draw as seen in Figure 49. In his work, the media surface properties such as the media surface friction coefficient was identified as having a better linear correlation with power draw than media density.

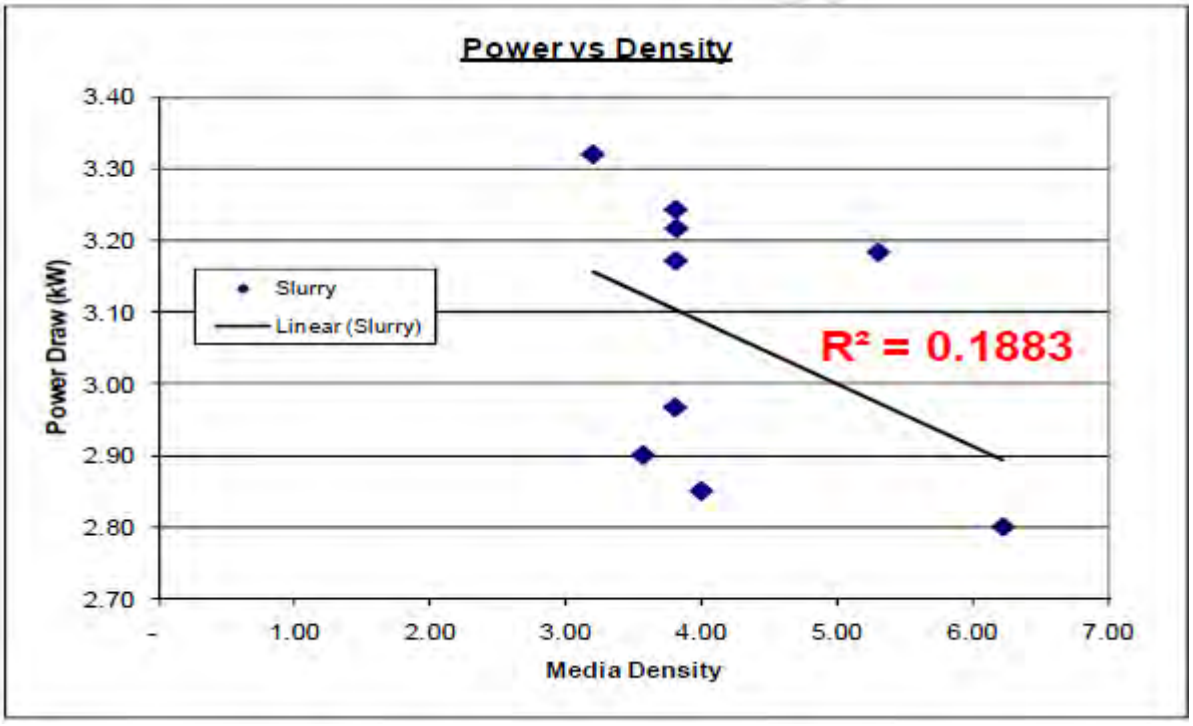

Figure 49: Relationship between media density and power draw as measured in slurry (Durant, 2012).

4.3. Effect of energy input on grind

Operating and design variables influence energy consumption in stirred mills. This energy is responsible for size reduction. Results and discussions of the effect of energy consumption on grind are presented in this section.

Energy is the major driver for size reduction. For this reason, in order to maintain a desired product size, it is necessary to maintain a constant energy input. According to Yue and Klein (2006), it is preferable to operate mills near the upper power limit in industrial practice. As discussed in section 4.2, a number of operating and design variables affect the power draw and ultimately the specific energy consumption. However, it is crucial to assess how energy input into stirred milling machines influences particle breakage. The product size distribution is often used as a proxy for assessing material breakage. Various techniques for determining size distributions exist. In this thesis, the sieving technique was employed to obtain size distributions for all samples collected. This chapter focuses on assessing the relationship between specific energy and grind. The size at which 80% of material passes (P_{80}) was used to characterize size distribution. The feed size, F_{80}, was kept constant for all tests (Refer to Section 3.3.2).

4.3.1. Effect of specific energy on product size at various conditions

It has already been established that various conditions such as residence time, solids concentration and impeller speed have an effect on the specific energy input in stirred mills. The energy input results in breakage of particles within the mill. It is worth noting that the variation of specific energy was due to variation in selected operating variables. The P_{80} values used were obtained from tests involving variation of solids concentration, impeller speed and residence time. The particle size distributions from which the P_{80} values were extracted are shown in Figure 50, Figure 51 and Figure 52. The P_{80} values from the different tests were then plotted against the specific energy input. It can be seen that the size distributions obtained from varying specific energy, solids concentration and impeller speed are different. Variation in the residence time appears to have the greatest influence on the changes in the product size distribution whereas solids concentration has the least.

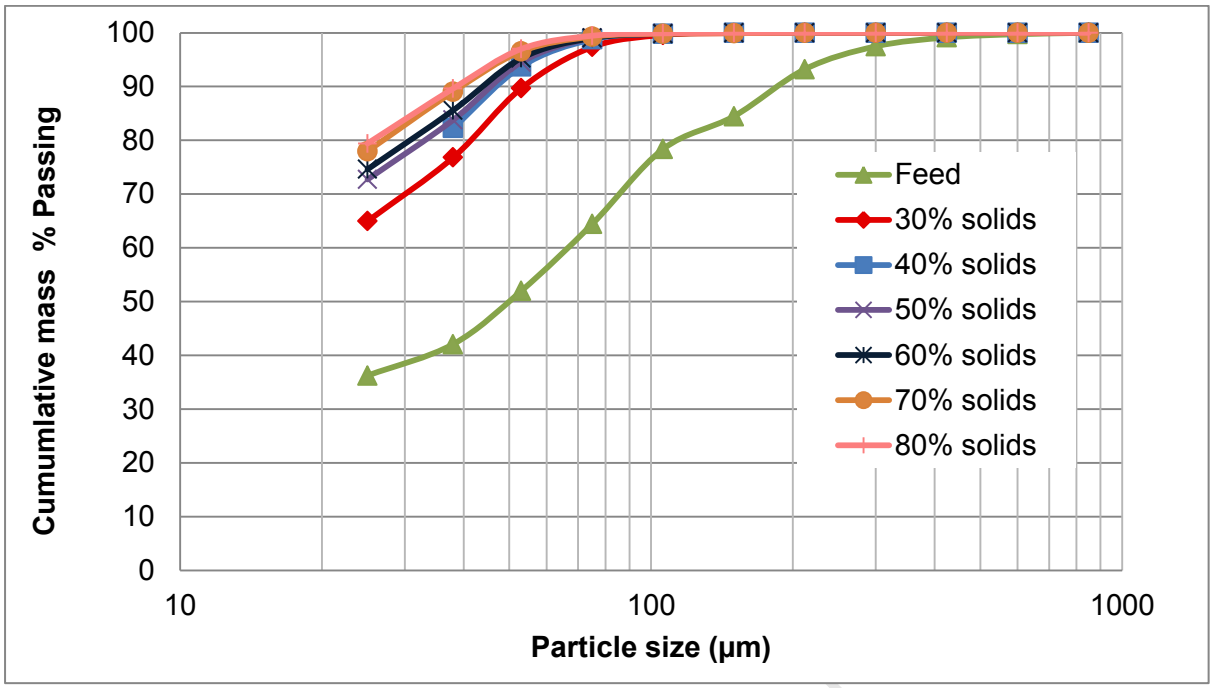

Figure 50: Laboratory vertical stirred mill product size distributions due to variation of solids concentration for a feed with an F_{80} of 118µm.

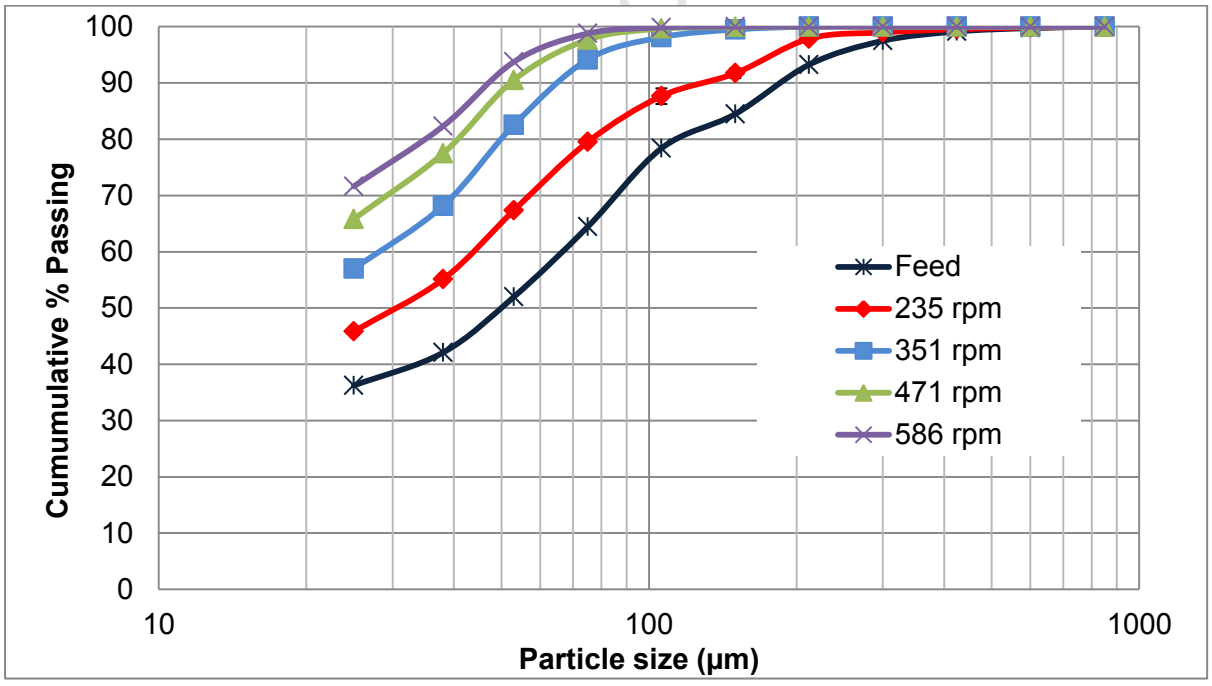

Figure 51: Laboratory vertical stirred mill product size distributions due to variation of impeller speed for a feed with an F_{80} of 118µm.

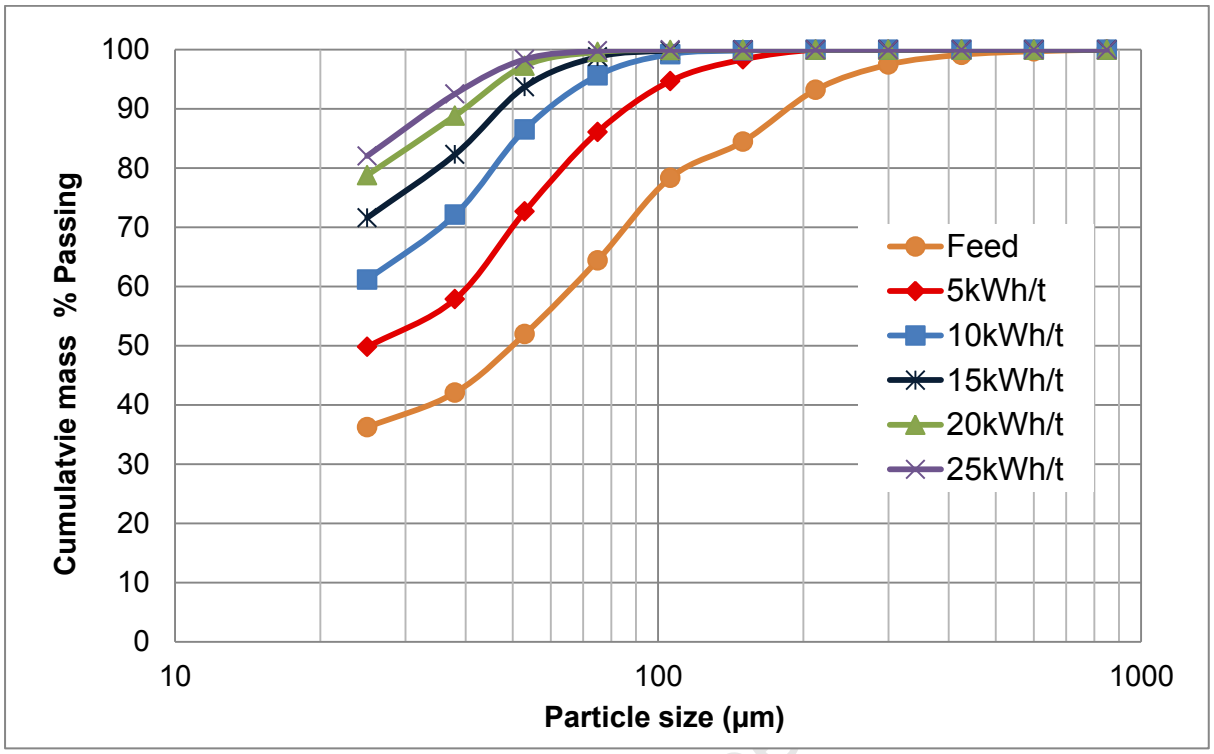

Figure 52: Laboratory vertical stirred mill product size distributions due to variation of specific energy for a feed with an F_{80} of 118µm.

A relationship between specific energy and grind altered using the three variables is given in Figure 53. For all the cases presented, an increase in the specific energy resulted in an exponential decrease in the P_{80}. The decrease in the P_{80} is due to more energy available for particle breakage. The exponential decrease in the P_{80} however indicates that the rate at which it decreases declines with increase in specific energy. In studying single particle fraction under impact loading, Tavares and King (1998) revealed that the particle fracture energy increased with decrease in particle size for various minerals and is shown in Figure 54. Since the size of the largest micro-cracks within the particle must decrease when the particle size is reduced, the particle strength increases, if fracture toughness of the material remains constant (Tavares and King, 1998). This could explain the increase in energy consumption with decrease in product particle size (P_{80}) as observed in Figure 53.

Specific energy variations due to variation in solids concentration has been discussed in section 4.2.1. Since water was used to manipulate solids concentration, an increase in the solids concentration leads to a decrease in the slurry suspension volume. This leads to compacting of slurry, increasing the probability of media-particle contact. When the probability of media-particle contact is increased, the likelihood of particle fragmentation is increased. This results in a finer product. This has been supported by He and Forssberg

(2007) who concluded that an increase in the solids concentration leads to an improvement in the grind performance. However, caution must be taken when increasing solids concentration in fine grinding using stirred mill. Very high solids concentrations are discouraged as viscosity effects tend to hinder charge motion resulting in poor grinds.

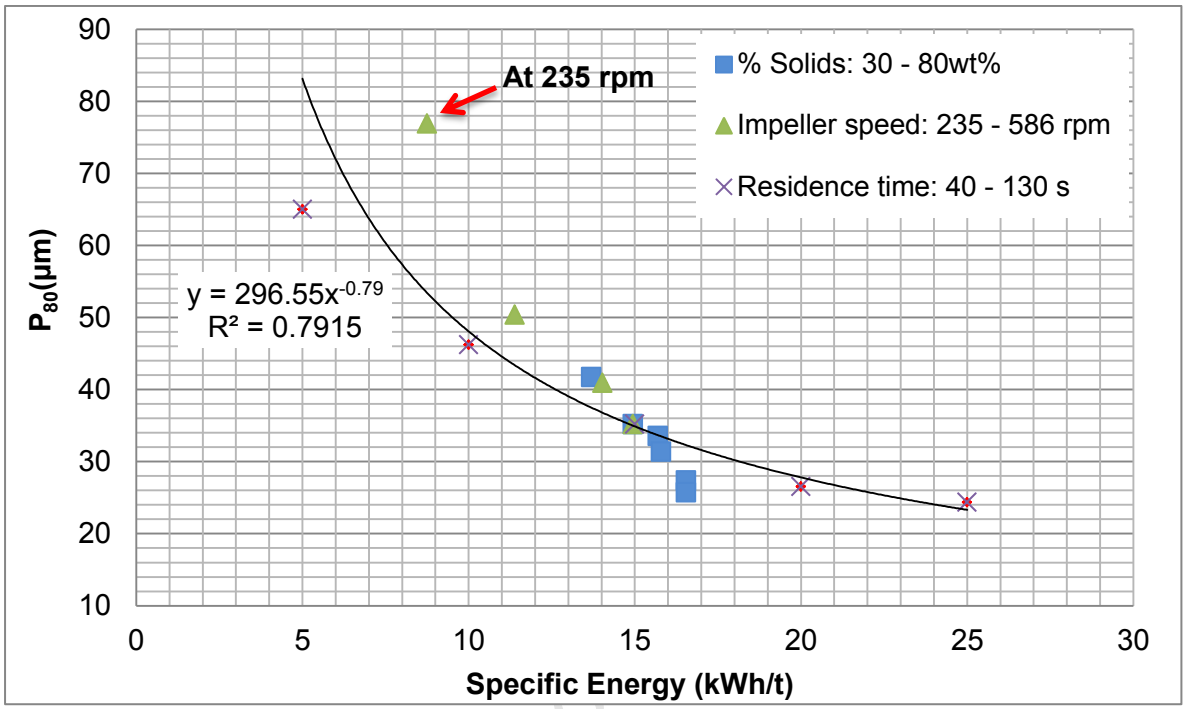

Figure 53: Variation of P_{80} with specific energy input.

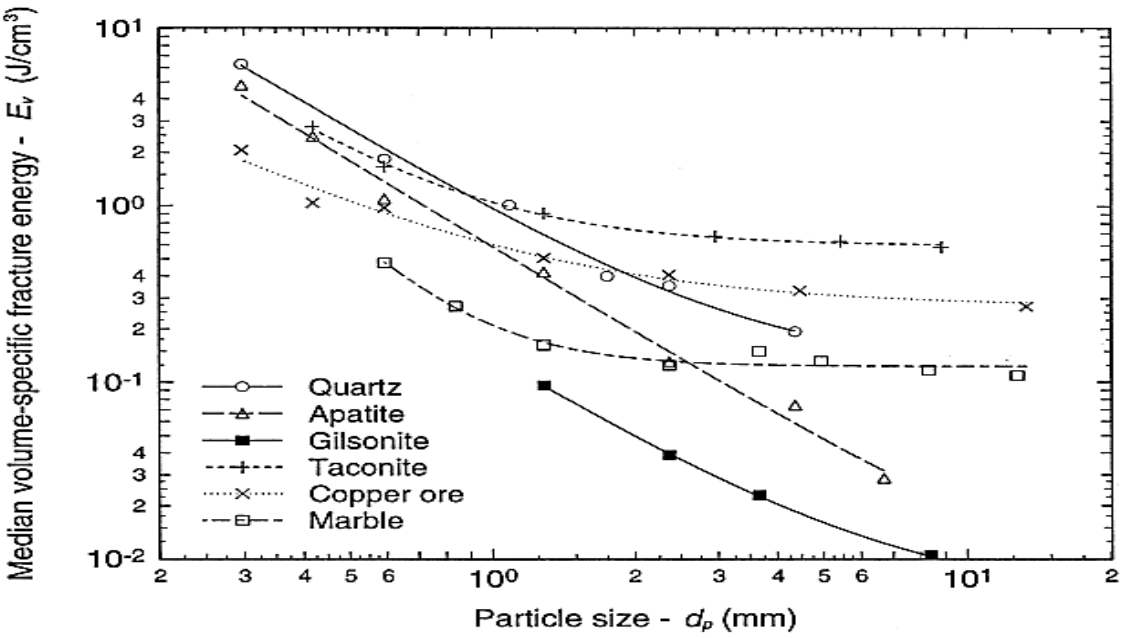

Figure 54: Variation of mean volume-specific particle fracture energy with particle size for various materials (Tavares and King, 1998).

It has been shown in section 4.2.2 that an increase in the impeller speed results in an increase in the specific energy input over the range of impeller speeds tested. In this thesis work, the increase in specific energy input results in an increase in the energy available for particle breakage causing a reduction in the P_{80}. The exponential decrease in the P_{80} with increase in the specific energy has been observed by various researchers (Ntsele and Allen, 2012; Jankovic, 2003; Samanli *et al*., 2011). Jankovic (2003) recorded a positive effect on grinding efficiency with increase in stirrer speed when treating zinc concentrates. When milling limestone using a stirred mill, Zheng *et al*., (1996) observed that an increase in impeller speed resulted in an increase in energy consumption and improvement in grind. However, the energy efficiency decreased with increase in impeller speed, similar to what Mankosa *et al*., (1989), Fadhel and Frances (2001) and He and Forssberg (2007) observed in grinding coal, alumina hydrate and quartzite respectively. From Figure 53, the test done at impeller speed of 235 rpm appears to be an outlier. Figure 55 shows a photo taken when discharging the mill after the 235 rpm impeller speed test. It appears that there is some charge crusted at the bottom of the mill. It is possible that some of the charge was not actively involved in the grinding processes leading to poor grinds. This could explain the outlier in Figure 53.

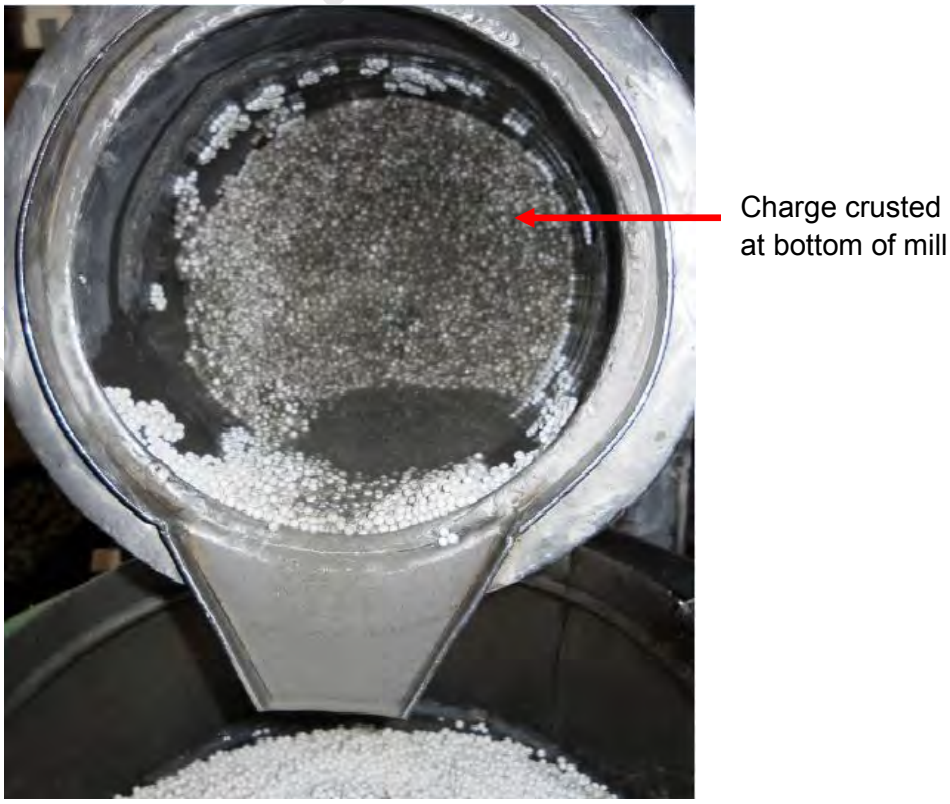

Figure 55: A photo showing charge crusted at the bottom of the mill after operating at 235 rpm and 40wt% solids.

The grinding time also influences the energy and grind efficiency. An increase in the batch milling time results in an increase in the specific energy input and consequently an exponential decrease in the P_{80}. These results agree with those of Gao and Forssberg (1995) from milling of Dolomite in a stirred ball mill. Similarly in the milling of calcium carbonate, Jankovic (2003) reported an exponential decrease in the P_{80} size with increase in the specific energy. When the residence time is increased, material in the mill is subjected to the available energy for a longer period of time increasing the likelihood of particle fragmentation.

Figure 56 (courtesy of Little and Van De Ruit, 2012) shows the product size distribution obtained when milling at different stirrer speeds (235 – 590 rpm) at a constant specific energy input of 10kWh/t. It can be observed from Figure 56 that the fineness of product material increases with increase in impeller speed.

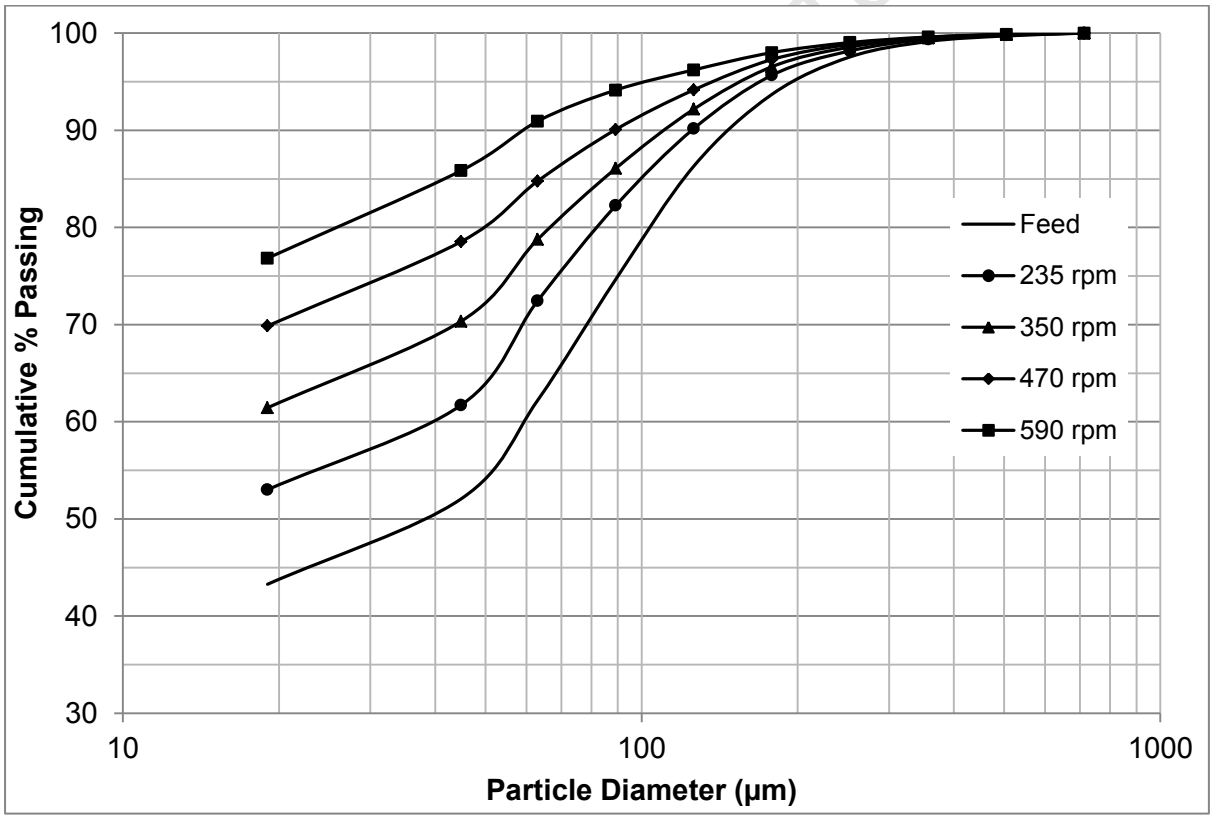

Figure 56: Cumulative particle size distributions showing the effect of increasing impeller speed on mill product size, with a specific energy input of 10 kWh/t. Media density = 4400 kg/m^3, short-pin impeller used (Little and Van De Ruit, 2012).

Figure 57 (courtesy of Little and van de Ruit, 2012) shows signature plots for tests done at impeller speeds ranging from 235 to 590 rpm**.** It can be seen from Figure 57 that at a constant specific energy input, an increase in the impeller speed results in a finer grind. This can be attributed to increase in stressing of particles as the impeller speed increases.

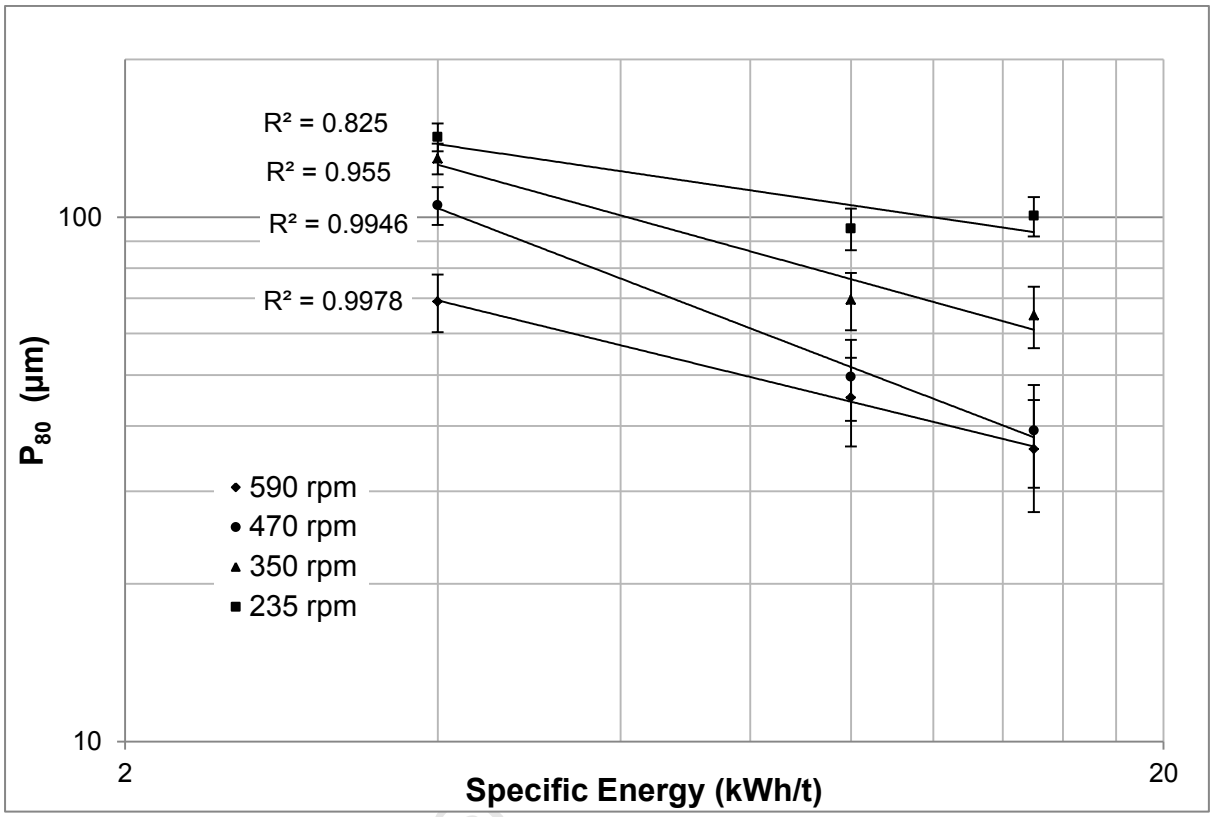

Figure 57: Signature plots illustrating the effect of impeller speed on P_{80}. Media density = 4400 kg/m^3, short-pin impeller used. Error bars show 95% confidence limits (Little and Van De Ruit, 2012).

4.3.2. Effect of media properties on product size

In this section, the effect of media properties which are media size and density, are discussed based on tests performed under constant residence time and constant specific energy input conditions given in Table 14.

4.3.2.1. Effect of media size and density on product size at constant residence time

Media properties play a key role in the performance of stirred mills. From Table 14, it can be seen that at constant residence time (102 seconds), the high density fine media (+6.7-8.0mm) gave a finer product and a lower specific energy than the high density coarse media (+11.2-13.2mm). In these high density media tests performed at the same residence time, the specific energy input for the run with coarse media is greater than that for the fine media.

The general perception would be that higher specific energy input would result in a lower P_{80} value as more energy would be available for size reduction. This shows that the high density fine media is better suited for fine grinding for the feed used in the test. The use of coarse media results in poor media-particle contact. This is because for a constant media filling volume, the number of coarse grinding media is less than that of fine media. This reduces the likelihood that a particle is trapped between grinding media resulting in poor breakage (Mankosa *et al*., 1986). This results in a relatively coarser grind for the large media compared to the fine media. In the case of fine media, the surface area of contact with particles is large. This improves media-particle interaction and consequently results in a finer grind. The lower specific energy associated with the fine media can be attributed to the fluidization of charge with decrease in media size which reduces the power draw and hence the specific energy. In agreement with these results, Jankovic (2003) found that a decrease in the grinding media size at constant speed, significantly improved size reduction in grinding of zinc concentrate using a vertical stirred mill. Similar observations have been reported by He and Forssberg (2007) and Zheng et al., (1996) when grinding quartzite and limestone, respectively. The range of media sizes used in this thesis project was not large enough to observe an optimum bead size. There is a belief that an optimum bead size exists for a given impeller speed (He and Forssberg, 2007; Jankovic, 2003). Various researchers have reported the existence of an optimum ratio of grinding media to feed size which has been quoted as 20:1 by Mankosa *et al*., (1986) and 12:1 by Zheng *et al*., (1996). According to Zheng *et al*., the optimum ratio varies with media and mineral type.

Table 14: Effect of grinding media properties on grind

Media size (mm)	Media density (g/cm^3)	Grind time (s)	Specific energy (kWh/t)	P_{80} (µm)
+6.7-8.0	6.1	102	15.0	27
+11.2-13.2	6.1	102	22.4	41
+11.2-13.2	6.1	83	15.0	45
+5.6-6.7	2.6	314	15.0	24

4.3.2.2. Effect of media size and density on product size at constant specific energy input

Media property effects on product size were also compared at 15kWh/t as shown on Table 14. At 15kWh/t, the high density fine media (+6.7 - 8.0mm) gave a product with a significantly lower P_{80} compared to the high density coarse media (+11.2 - 13.2mm). The reason for this is that the surface area for contact with particles is much larger for the fine

media compared to the coarse media. This means that increased media-particle interactions for the fine media contributed to the fine product obtained in comparison to the product when coarse media is used.

This brings to the fore the importance of media selection in fine grinding using stirred mills. Information is not available to allow the comparison of low and high density media of the same size range. However comparing the P_{80} values of low density media (+5.6 – 6.7mm) and high density media of adjacent size range (6.7 – 8mm) at 15kWh/t specific energy input, the low density media test gave a finer product. The grind time for the low density media was greater than that for high density. This was because for the same media filling, the low density media weighed less than the high density media. The power draw for the low density media was hence lower meaning it required a longer residence time to achieve 15kWh/t compared to high density media. It appears that size reduction is not significantly affected by media density. However, it is possible that a different observation could be made outside the range of media densities and sizes tested. The disadvantage with low density media is the high wear rates associated with it. However, it should be mentioned that Farber *et al*. (2011) have reported that choosing high density media of optimum size can improve milling efficiency by about 30%.

4.4. ASSESSING BREAKAGE RATES IN STIRRED MILLS

4.4.1. Introduction

The breakage rates at various operating conditions were calculated using the perfect mixing model approach. The breakage rates were calculated at varying specific energy input, solids concentration and impeller speed. The breakage distribution function for fine particle breakage by Eksi *et al*. (2011) was used to solve the perfect mixing model mass balance.

4.4.1.1. Effect of specific energy input on breakage rates

The effect of specific energy input on breakage rates was evaluated by calculating the ratio of breakage rate to discharge rate (R/D) for various size classes at different specific energies. The specific energy input ranged from 5kWh/t to 25kWh/t at 5kWh/t intervals. Figure 58 shows that for all specific energy inputs, R/D decreases with decrease in particle size. This is partly due to the increase in particle strength with decrease in size (Tavares and King, 1998; Gao and Forssber, 1995).

R/D increases with increase in the specific energy input. This is because as the specific energy input increases, the energy available for particle breakage increases which leads to an increase in the breakage rates. It can therefore be concluded that high specific energy input leads to high breakage rates.

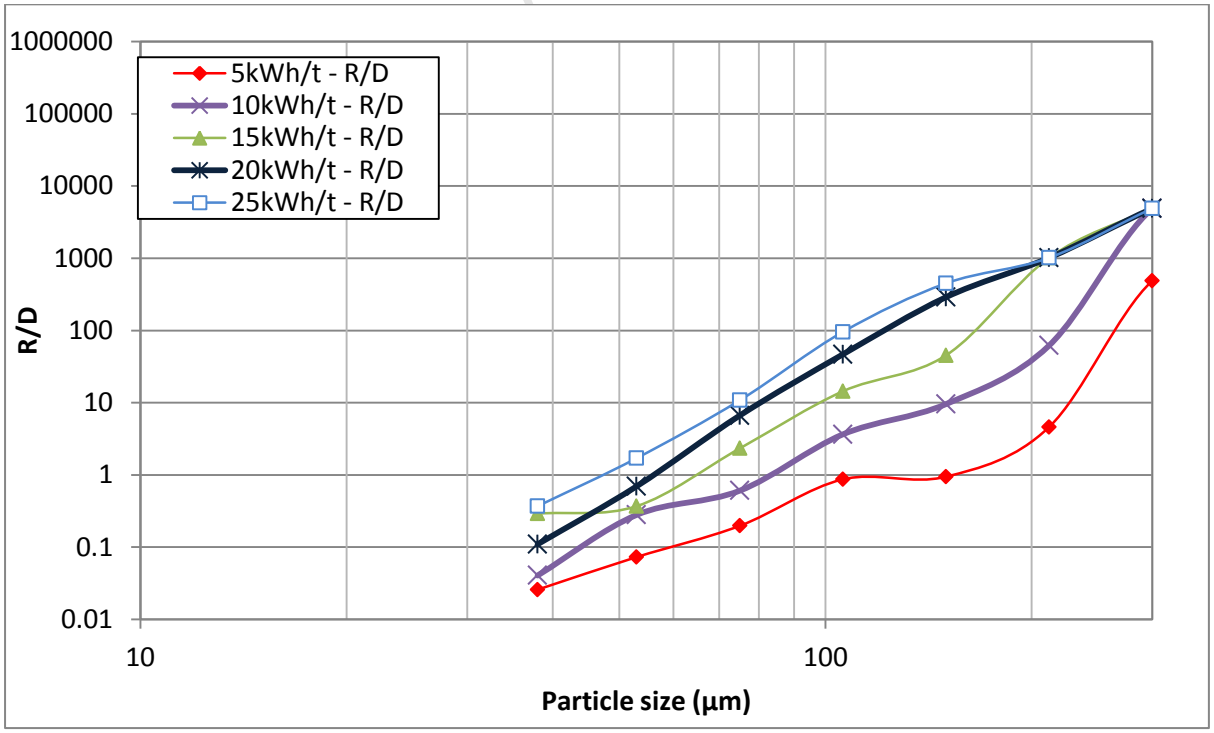

Figure 58: Effect of specific energy input on breakage rates in a vertical stirred mill at 40wt% solids and 586rpm impeller speed.

4.4.1.2. Effect of solids concentration on breakage rates

The effect of solids concentration on breakage rates in a vertical stirred mill was also studied. The range of solids concentration considered was between 30 and 80wt% solids at 10wt% intervals. R/D was plotted versus particle size at different solds concentration conditions and shown in Figure 59. Figure 59 shows lower breakage rates at finer particles sizes and these increase with size which is in agreement with Hogg and Cho (2000). The test carried out at 30wt% solids generally shows lower values of breakage rates compared to the other solids concentration conditions. At low solids concentration, the ratio of mass of solids to the mass of fluid is low. The likelihood of particles being trapped between grinding media and sufficiently stressed to breakage is low due to poor media-particle interactions. It can be concluded that the influence of solids concentration on breakage rates in a batch vertical stirred mills is less compared to that of specific energy input.

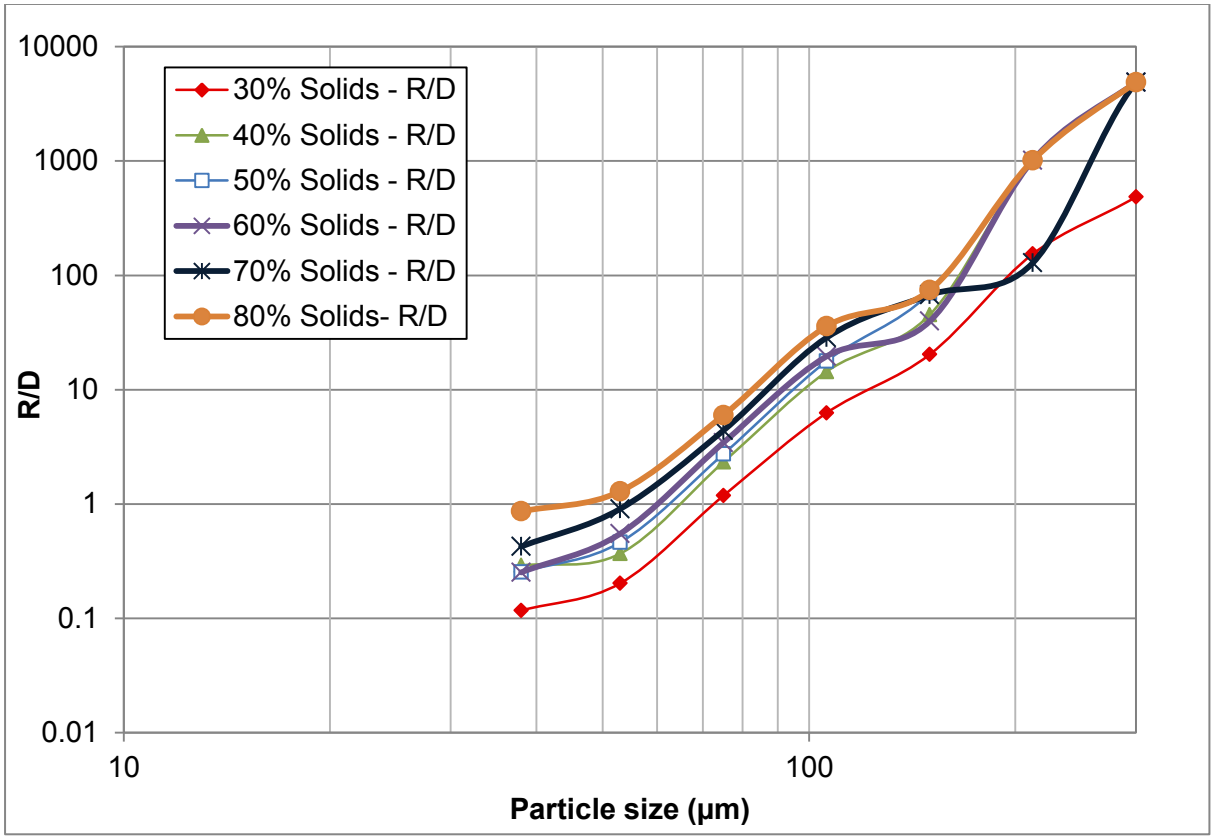

Figure 59: Effect of solids concentration on breakage rates in a vertical stirred mill at 586 rpm impeller speed.

4.4.1.3. Effect of impeller speed on breakage rates

The effect of impeller speed on breakage rates was evaluated at impeller speeds of 235, 351, 471 and 586 rpm. Figure 60 shows how breakage rates for various particle sizes vary with varying impeller speeds. The breakage rates increase with increase in the impeller speeds in the range 235 - 586 rpm. Since the kinetic energy is proportional to the square of the rotational speed, when the impeller speed is increased, so does the kinetic energy transferred from the impeller to the charge. This increase in energy in the mill results in high breakage rates. The breakage rates were generally observed to decrease with decrease in particle size for all impeller speeds tested. It can be concluded that the impeller speed has a significant influence on breakage rates with higher speeds resulting in high breakage rates.

It can be concluded that the breakage rates in a batch vertical stirred mill can be enhance by using higher impeller speed and high input energies induced by long residence times.

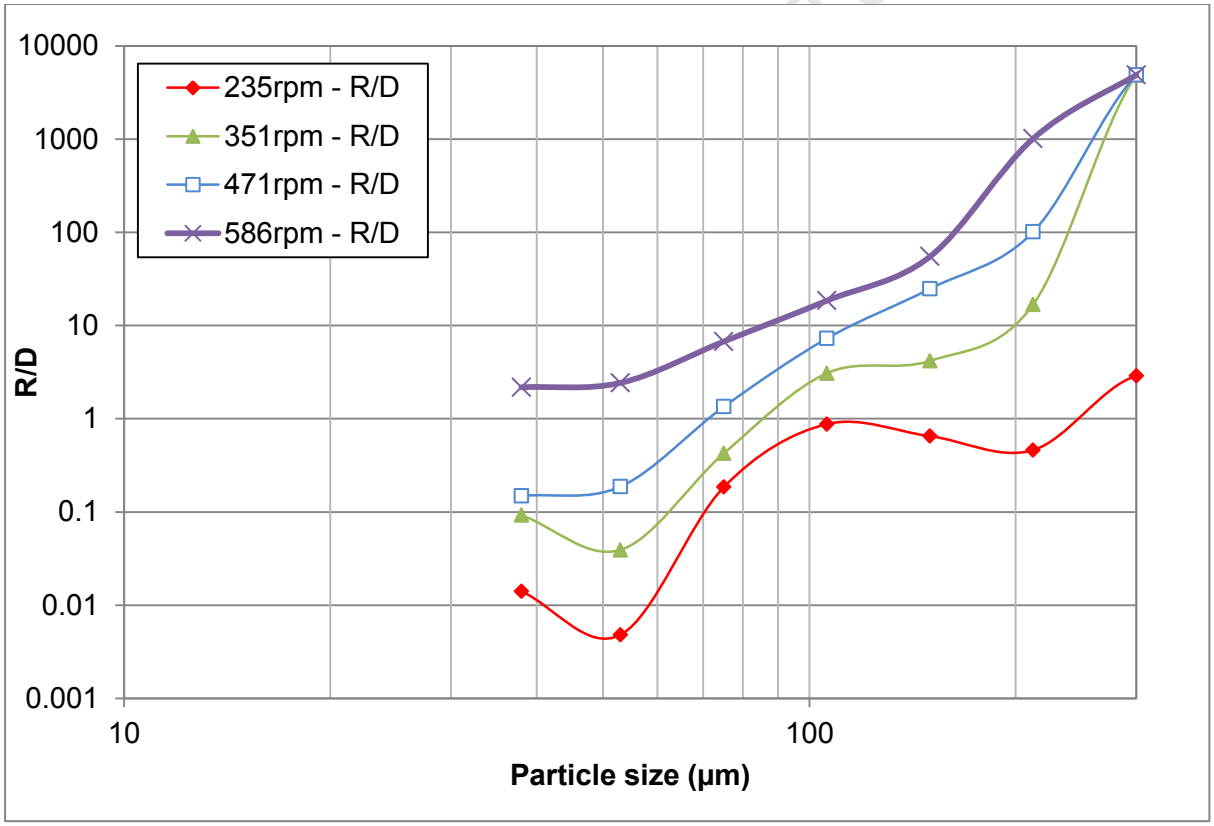

Figure 60: Effect of impeller speed on breakage rates in a vertical stirred mill at 40wt% solids.

4.5. EFFECT OF STRESS INTENSITY ON PRODUCT SIZE AND ENERGY EFFICIENCY

4.5.1. Introduction

The intention of this section is to discuss the effect of stress intensity on product size and the energy efficiency. The concept of stress intensity has already been discussed in Section 2.5.7. The media stress intensity was calculated with the media size, media density, solids concentration and impeller tip speed using Equation 7 and 8 shown in Section 2.5.7. The concept of stress intensity provides a link between these variables and grind allowing the selection of the most suitable operating conditions for optimal results. The stress intensity approach of optimizing energy efficiency in stirred mills has been studied by Kwade (1999), Kwade and Schwedes (2002) and Jankovic (2003).

4.5.2. Effect of media stress intensity on the product size (P_{80})

The stress intensity in this case was calculated using Equation 7 in Section 2.5.7. The effect of media stress intensity on the P_{80} is shown in Figure 61. Figure 61 shows that the P_{80} decreases with increase in the media stress intensity. The P_{80} decreases sharply from 77μm to 50μm when the media stress intensity increases from 4.41×10^{-3}Nm to 9.83×10^{-3}Nm. Thereafter, the P_{80} decreases steadily from 50μm to 35μm when the media stress intensity is increased from 9.83×10^{-3}Nm to 27.41×10^{-3}Nm. The decrease in product size with increase in media stress intensity is in agreement with Jankovic (2003) when milling zinc concentrate using a pin mill. However, Jankovic (2003) observed that there is an optimum stress intensity beyond which the product becomes coarse. In this thesis work, the range of media stress intensities was not large enough to observe the optimum stress intensity point. In addition, the variation in media stress intensity was only as a result of variation in impeller tip speed hence it is unlikely to obtained a coarser product at higher stress intensities if the media size is kept constant.

It can therefore be concluded that the media stress intensity has an influence on the merensky product size in a batch vertical stirred mill operated at constant residence time.

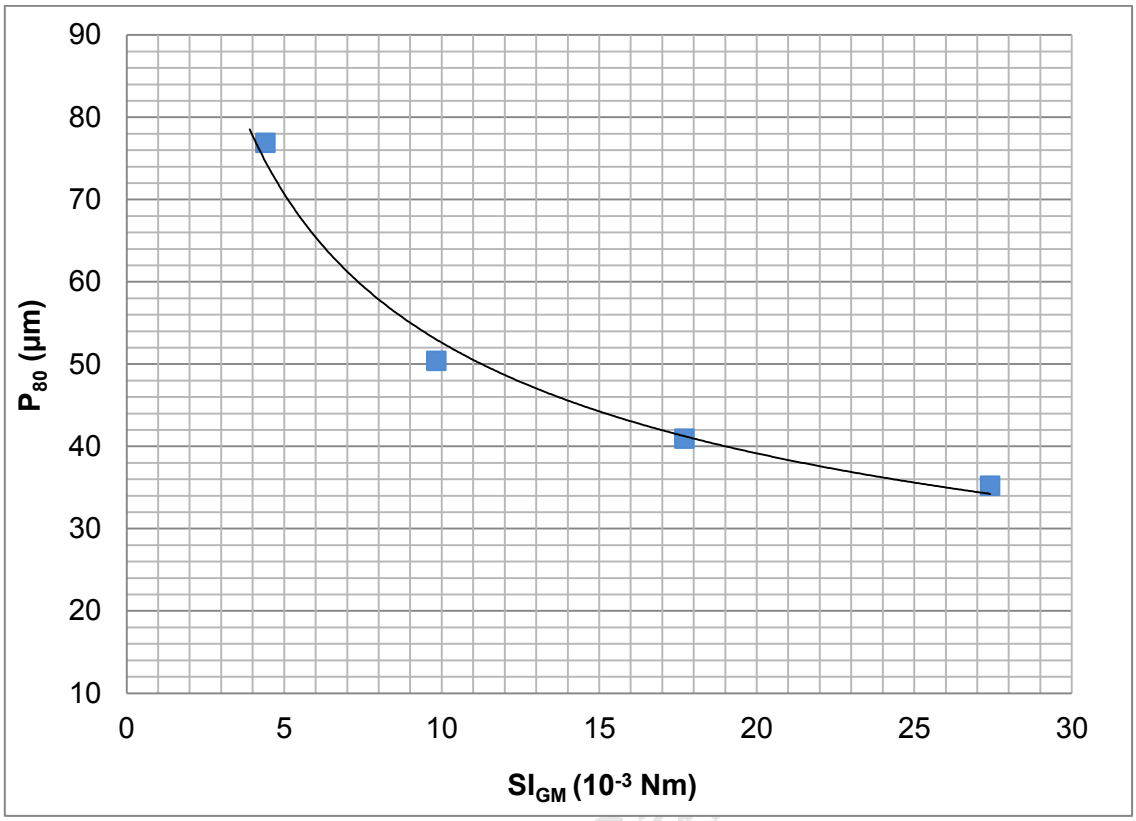

Figure 61: Effect of media stress intensity on the P_{80} at 40wt% solids concentration and 102 seconds milling time.

4.5.3. Effect of media stress intensity on the energy efficiency

The stress intensity describes the energy utilized at a single stress event. This energy facilitates particle breakage. The stress intensity therefore has an influence on energy efficiency. The media stress intensity was calculated using Equation 7 in Section 2.5.7. Figure 62 shows the effect of stress intensity of the grinding media on product based specific energy. Figure 62 shows that the specific energy required to produce both sub 25µm and sub 38µm products decreases rapidly with increase in grinding media stress intensity from 4.41×10^{-3} – 9.83×10^{-3} Nm. This is because the increase in the grinding media stress intensity increases the stress energy and the probability of particle fracture. This leads to an increase in the rate of breakage and consequently the amount of product, resulting in a decrease in the product based specific energy. When the stress intensity increases further, the rate of decrease in the product based specific energy declines. This was observed for both sub 25µm and sub 38µm product. This is due to the decrease in the rate of production of sub 25µm and sub 38µm products. Since these tests were done in a batch system, the fine material being produced was not continuously removed. This could have led to shielding of breakable coarse particles by the fine particles at high stress intensities. In addition, the decrease in the amount of product could be attributed to the grinding media size eventually

being too large for efficient media-particle contacts as particles are continuously being broken at high stress intensities.

The results obtained in this thesis work are in agreement with Kwade and Schwedes (2002) in the comminution of limestone in a horizontal stirred mill. They observed that the energy required to obtain a product, 50% passing 2μm (P_{50} = 2μm), decreased with increase in the stress intensity. However, Kwade and Schwedes (2002) observed an optimum stress intensity where the size based specific energy is a minimum. A number of researchers (Jankovic, 2003; Kwade and Schwedes, 2002; Becker *et al*., 2001) have revealed that an optimum stress intensity exists with respect to grind and energy consumption. If this energy is too small then a number of events are necessary for particle breakage which could result in a decrease in the breakage rate (Jankovic, 2003). However, if this energy is higher than necessary, the surplus goes to waste (Jankovic, 2003). The optimum stress intensity was not observed in this thesis work possibly due to the range of operating variables not being large enough.

It can therefore be concluded that, the stress intensity influences the specific energy required to produce a sub 25μm and sub 38μm Merensky product in a batch vertical stirred mill. The stress intensity can also be used to assess energy efficiency in vertical stirred mills.

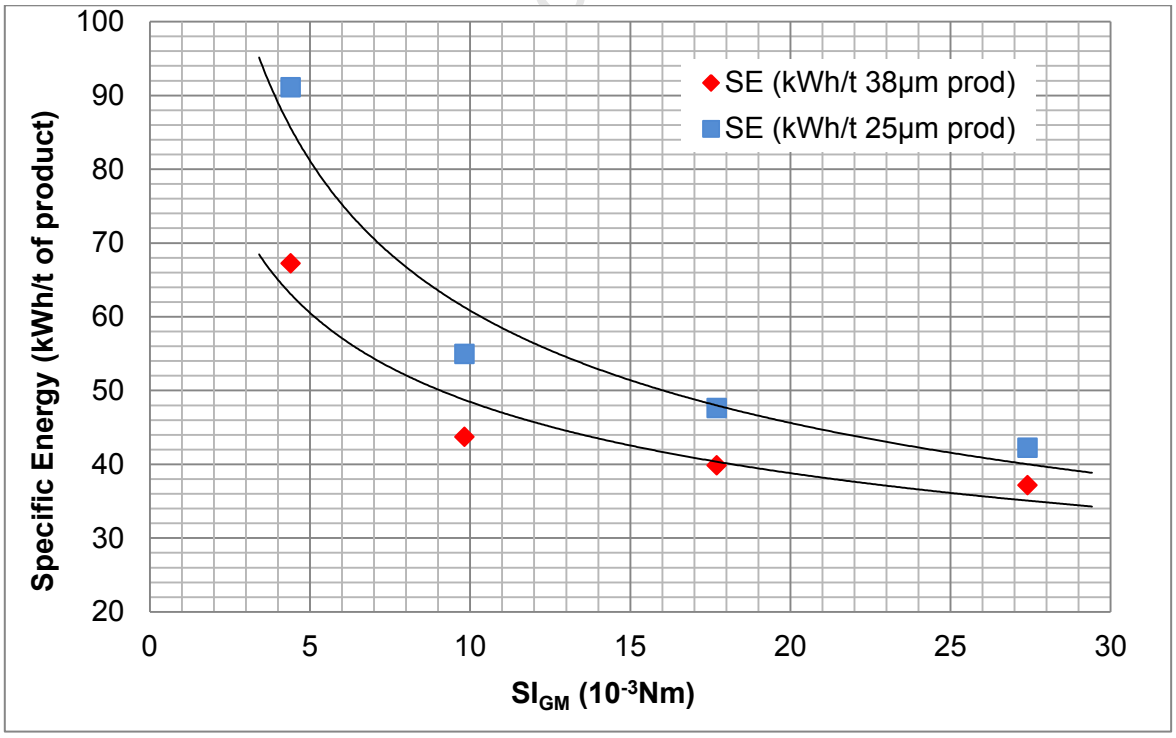

Figure 62: Effect of the Stress Intensity of the grinding media on the product based specific energy at 40wt% solids concentration and 102 seconds milling time.

4.5.4. Effect of the modified stress intensity (taking into account slurry density) on the specific energy required to produce a sub 25µm and sub 38µm product.

The media stress intensity was calculated using Equation 8 in Section 2.5.7. Figure 63 shows the influence of the stress intensity using the model from Kwade *et al*. (1996) on the specific energy required to produce sub 25µm and sub 38µm particles. From Figure 63, it can be seen that as the stress intensity increases, the specific energy to produce sub 25µm and sub 38µm gradually decreases to a minimum. A further increase in the stress intensity results in an increase in the size based specific energy for both the sub 25µm and sub 38µm. The trend observed in Figure 63 is similar to that reported by Kwade *et al*. (1996) from their work on grinding in a stirred mill. When the stress intensity increases from 0.003Nm to 0.015Nm due to increase in impeller speed at constant solids concentration, there appears to be a gradual decrease in the specific energy to produce sub 25µm and sub 38µm particles. The decrease in size based specific energy can be attributed to an increase in production of sub 25µm and sub 38µm particles as a result of increased stressing of particles. The size based specific energy reaches a minimum at a stress intensity of 0.015Nm. As the stress intensity increases beyond this point, the size based specific energy also increases.

It has been shown in Figure 63 that the stress intensity above 0.015Nm increases in the direction of decreasing solids concentration. This is because the stress intensity in this case, is proportion to the difference between the grinding media density and the slurry density (ρ_{GM} - ρ_{sl}). Therefore as the solids concentration decreases, the slurry density decreases and so the stress intensity increases when all other variables are kept constant. However, it has previously been shown that at lower solids concentrations, the grind and energy efficiency is poor (He and Forssberg, 2007; Zheng et al., 1996). Although the stress intensity is increasing, media-particle contact is insufficient hence energy is wasted. The optimum stress intensity for this set up appears to be at 0.015Nm which corresponds to the highest impeller speed (586rpm) and the highest solids concentration tested (80wt% solids). A number of researchers (Jankovic, 2003; Kwade and Schwedes, 2002; Becker *et al*., 2001) have revealed that an optimum stress intensity exists with respect to grind and energy consumption. Below the optimum stress intensity, the energy is too low and a number of breakage events are necessary for particle fragmentation which could result in a decrease in the breakage rate (Jankovic, 2003). However, if this energy is higher than necessary, the surplus goes to waste (Jankovic, 2003).

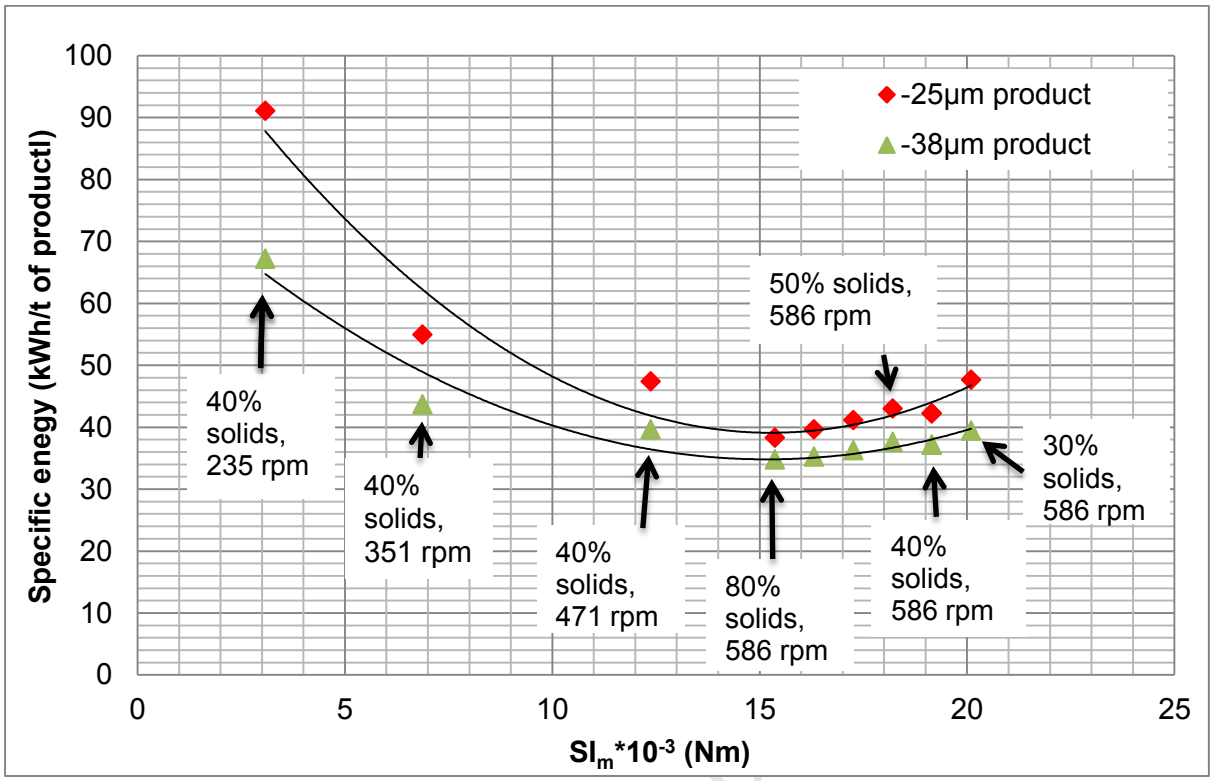

Figure 63: Effect of the modified stress intensity on the specific energy required to produce sub 25µm and sub 38µm.

4.6. Assessing reproducibility of results

This section assesses the reproducibility of test results presented in this thesis based on specific energy and grind. The standard deviations and standard errors for repeat tests are presented and used to assess the reproducibility of results.

4.6.1. Statistical indicators for reproducibility

The standard deviation describes the degree of spread of data from the mean. A low standard deviation would indicate that the results obtained from repeat tests fall close to the mean. A high standard deviation would indicate data scattered significantly away from the mean. The standard error on the other hand, serves as an indication of how reliable the data mean is. A low standard error value would indicate that the mean from the repeated tests is a more precise representation of the true value of the mean.

4.6.2. Reproducibility of results based on specific energy input

In this section, the reproducibility of tests carried out based on specific energy results is presented. Table 15 shows values relating to experimental repeats for various tests. Duplicate runs were conducted for selected tests. The standard deviation and standard error were calculated using Equation 10 and 11, respectively and are shown in Table 15.

$$SD_{SE} = \sqrt{\frac{\sum_{i=1}^{n}(SE_i - \overline{SE})^2}{n-1}} \qquad \textbf{Equation 10}$$

Where:

SD_{SE} : Standard deviation of the specific energy.

SE_i : Specific energy of test i.

$\overline{SE}$: Average specific energy from two tests done at same conditions.

n: Number of tests at same conditions.

$$Se_{SE} = \frac{SD_{SE}}{\sqrt{n}} \qquad \textbf{Equation 11}$$

Where:

Se_{P80} : Standard error in P_{80}.

It can be seen that the standard deviation and consequently standard errors of the repeated tests are low. The low standard deviation indicates that the results obtained from repeat test do not differ significantly. In addition, the low standard error values are an indication that the mean values for the specific energies are reliable. Therefore, it can be concluded that the results are reproducible.

Table 15: Reproducibility of test results based on specific energy input

Variable	Grind time (s)	Specific energy, SE (kWh/t)						
% Solids		Test no.	SE 1	Test no.	SE 2	Average	Standard deviation	Standard Error
30	102	1	13.8	5	13.7	13.8	0.07	0.05
40	102	2	15.0	6	15.0	15.0	0.00	0.00
50	102	3	15.7	7	15.8	15.8	0.07	0.05
60	102	4	15.9	8	15.8	15.9	0.07	0.05
Speed								
235 rpm	102	9	8.7	13	8.8	8.8	0.07	0.05
351 rpm	102	10	11.4	14	11.4	11.4	0.00	0.00
471 rpm	102	11	13.6	15	14.6	14.1	0.71	0.50
586 rpm	102	12	15	16	15	15	0.00	0.00
Disk stirrer								
471 rpm	102	17	8.6	20	10.2	9.4	1.13	0.80
586 rpm	102	18	8.2	21	8.5	8.4	0.21	0.15
40%	102	19	8.5	22	8.2	8.4	0.21	0.15

4.6.3. Reproducibility of results based on grind

In this section, the reproducibility of tests carried out based on grind results is presented. Table 16 shows the standard deviation and standard error of the P_{80} values from various tests calculated using Equations 12 and 13, respectively.

$$SD_{P80} = \sqrt{\frac{\sum_{i=1}^{n}(P80_i - \overline{P80})^2}{n-1}} \qquad \textbf{Equation 12}$$

Where:

SD_{P80} : Standard deviation of the P_{80}.

$P80_i$: P_{80} of test i.

$\overline{P80}$: Average P_{80} from two tests done at same conditions.

n: Number of tests at same conditions.

$$Se_{P80} = \frac{SD_{P80}}{\sqrt{n}}$$ **Equation 13**

Where:

Se_{P80} : Standard error in P_{80}.

The standard deviation and standard errors appear to be low, an indication that the results are reproducible. In close scrutiny, the standard deviation and standard error values shown in Table 16 appear to be higher than those shown in Table 15. This is because the P_{80} values were obtained from product size distributions. The particle size characterization technique used to obtain the size distributions was sieving. Sieving is the most widely used method for sizing material coarser than about 25µm with the Tyler and U.S. standard sieve series commonly utilized (Hogg, 2003: 35). Although the same procedure was used for all samples, sieving is inherently susceptible to errors since it depends on the probability of a particle going through the aperture of a given size for a set time (Hogg, 2003: 38). In addition, errors in the grind results could also be linked to the performance of the mill. Although contacts may be similar, they do not occur in the same way for all particles resulting in some deviations in the results.

Table 16: Reproducibility of test results based on grind results

Variable	Grind time (s)	**P_{80} (µm)**						
% Solids		Test no.	y_1	Test no	y_2	Average	Standard deviation	Standard Error
30	102	1	34.2	5	34.4	34.3	0.15	0.11
40	102	2	25.5	6	28.4	26.9	2.07	1.47
50	102	3	24.7	7	24.4	24.5	0.19	0.13
60	102	4	22.2	8	20.7	21.5	1.08	0.77
Speed								
235 rpm	102	9	65.3	13	64.0	64.6	0.95	0.67
351 rpm	102	10	42.1	14	42.7	42.4	0.45	0.32
471 rpm	102	11	35.2	15	31.7	33.4	2.46	1.74
586 rpm	102	12	25.5	16	28.4	26.9	2.07	1.47
Disk stirrer								
471 rpm	102	17	51.7	20	55.7	53.7	2.83	2.00
586 rpm	102	18	48.7	21	48.6	48.6	0.06	0.04
40%	102	19	48.6	22	48.7	48.6	0.06	0.04

CHAPTER FIVE: CONCLUSIONS AND RECOMMENDATIONS

Conclusions and recommendations based on the results are presented in this chapter.

5.1. Introduction

The objective of this thesis was to investigate the effect of operating variables on energy consumption in stirred mills. A number of variables were selected. These included solids concentration, stirrer speed, media size, media density, impeller type and residence time. From the main findings, the conclusions and recommendations have been drawn and presented in this chapter.

5.2. Key observations

A number of observations were made from the test work. These include the following;

i. The solids concentration influenced the specific energy consumption. An increase in the solids concentration from 30wt% to 80wt% resulted in an increase in the specific energy consumption.
ii. In the range of impeller speeds tested (251rpm – 586rpm), the specific energy increased with an increase in the impeller speed.
iii. For the range of solids concentrations, 30wt% to 50wt%, using the pin impeller resulted in a higher specific energy consumption compared to the disk impeller.
iv. For the impeller speeds in the range 351rpm to 586rpm, the specific energy consumption was higher when the pin stirrer was used compared to the disk stirrer.
v. For the same media type, the specific energy consumption was higher when fine media was used compared to coarse media.
vi. A finer product and lower specific energy consumption were obtained when fine media was used compared to coarse media.
vii. Low density media (-6.7mm + 5.6mm) gave a finer product compared to high density media of adjacent size range (-8mm + 6.7mm).
viii. Breakage rates in a vertical stirred mill increase with increase in the specific energy input, solids concentration and impeller speed. The effect of solids concentration has the least effect on breakage rates compared to specific energy input and impeller speed. In addition, it was observed that the breakage rates decrease with decrease in particle size for all conditions tested.
ix. At constant residence time, the fineness of grind increases with increase in the stress intensity from 4.41×10^{-3} to 27.41×10^{-3}Nm. In addition specific energies required to produce sub 25µm and 38µm material decreased with an increase in the media

stress intensity from 4.41×10^{-3} to 27.41×10^{-3}Nm. An optimum stress intensity with respect to specific energy required to produce sub 25µm and 38µm was observed to be 0.015Nm at the conditions tested in this thesis.

5.3. Conclusions

In line with the objectives of this thesis project, the following conclusions were drawn;

- In batch milling of Merensky in a vertical stirred mill, the energy efficiency increases with increase in solids concentration ranging from 30wt% to 80wt%.
- The energy efficiency increases with increase in impeller speed between 251rpm and 586rpm.
- Using a pin stirrer results in a higher specific energy consumption compared to a disk stirrer when both the solids concentration and impeller speed were varied.
- For high density media (-8mm + 6.7mm and -13.2mm + 11mm), the fine media is more energy efficient than the coarse media. When fine media is used, the specific energy consumption is about 33% less than when coarse media is used.
- For the media sizes tested, the specific energy when high density media was used was higher than when low density media was used. This was due to the greater mass of the high density media to make up 70% of mill volume. However, with respect to grind, media density was not an influencing factor. This was because low density media (+5.6 – 6.7mm) gave a finer product compared to high density media (+6.7 – 8mm).
- The perfect mixing model approach can be used to assess the performance of a stirred mill. The breakage rates in vertical stirred mill increase with increase in the specific energy input, impeller speed and solids concentration. The solids concentration has the least influence on the breakage rates compared to specific energy and impeller speed.
- The media stress intensity approach can be used to assess the influence of design and operating variables at constant residence time. For the batch milling of Merensky in a vertical stirred mill at constant residence time, the fineness of grind increases with increase in the stress intensity from 4.41×10^{-3} to 27.41×10^{-3}Nm. It can also be concluded that the specific energies required to produce sub 25µm and 38µm material decreases with increase in the media stress intensity from 4.41×10^{-3} to 27.41×10^{-3}Nm. When solids concentration is considered, an optimum stress intensity with respect to energy efficiency exists at constant residence time. This was

observed to be 0.015Nm for the conditions tested. The optimum stress intensity was observed when the impeller speed and solids concentration were highest, 586 rpm and 80wt%, respectively.

5.4. Recommendations

The objective of this thesis was to evaluate the effects of design and operating variables on energy consumption in stirred mills. Based on the results and conclusions drawn, the following recommendations are proposed;

- Additional test work should be carried out to investigate the effect of media size on energy consumption and grind in stirred mills. A wider range of media sizes should be selected preferable between 2mm and 6.7mm.

- Tests at higher impeller speeds (600rpm to 1500rpm) should be carried out to assess the effect of high stirrer rates on energy consumption and grind efficiency.

- A model can be developed to predict the performance of the mill in relation to specific energy.

6. REFERENCES

Altun, O., Benzer, H. and Enderle, U., 2013. Effects of operating parameters on the efficiency of dry stirred milling. *Minerals Engineering, 43–44: 58–66.*

Austin, L. G., 1982. Rate Equations for Non-Linear Breakage in Mills Due to Material Effects. *Powder Technology. 31: 127 - 133.*

Austin, L. G., Shoji, K. and Luckie, P. T., 1976. The Effect of Ball Size on Mill Performance. *Powder Technology. 14:71 - 79.*

Becker, M., Kwade, A. and Schwedes, J., 2001. Stress intensity in stirred media mills and its effect on specific energy requirement. *International Journal of Mineral Processing, 61: 189–208.*

Becker, M. and Schwedes, J., 1999. Comminution of ceramics in stirred media mills and wear of grinding beads. *Powder Technology. 105: 374 - 381.*

Bernhardt, C., Reinsch, E. and Husemann, K., 1999. The influence of suspension properties on ultra-fine grinding in stirred ball mills. *Powder Technology 105: 357–361.*

Bilgili, E., Hamey, R. and Scarlett, B., 2006. Nano-milling of pigment agglomerates using a wet stirred media mill: Elucidation of the kinetics and breakage mechanisms. *Chemical Engineering Science. 61: 149 – 157.*

Blecher, L. and Schwedes, J., 1996. Energy distribution and particle trajectories in a grinding chamber of a stirred ball mill. *International Journal of Mineral Processing, 44 - 45: 617 - 627.*

Bruckard, W. J., Sparrow, G. J. and Woodcock, J. T., 2011. A review of the effects of the grinding environment on the flotation of copper sulphides. *International Journal of Mineral Processing. 100: 1–13.*

Chaponda, B., 2011. *Effect of operating variables on IsaMillTM performance using Platinum bearing Ores. MSc. Thesis,* Cape Town: University of Cape town.

Choi, H., Lee, W., Kim, D. U., Kumar, S., Kim, S. S., Chung, H. S., Kim, J. H. and Ahn, Y. C., 2010. Effect of grinding aids on the grinding energy consumed during grinding of calcite in a stirred ball mill. *Minerals Engineering. 23: 54 – 57.*

Conway-Baker, J., Barley, R. W., Williams, R. A., Jia, X., Kostuch, J., McLoughlin, B. and Parker, D. J., 2002. Measurement of the motion of grinding media in a vertically stirred mill using positron emission particle tracking (PEPT). *Minerals Engineering, 15: 53 - 59.*

Ding, Z., Yin, Z., Liu, L. and Chen, Q., 2007. Effect of grinding parameters on the rheology of pyrite–heptane slurry in a laboratory stirred media mill. *Minerals Engineering 20: 701–709.*

Durant, A. C., 2012. *Developing a methodology that incoporates ceramic media properties to model power draw in a M4 IsamillTM. MSc. Thesis,* Cape Town: University of Cape Town.

Eksi, D., Benzer, H. A., Sargin, A. and Genc, O., 2011. A new method for determination of fine particle breakage. *Minerals Engineering 24: 216–220.*

Ellis, S., 2003. *Ultra fine grinding - A practical alternative to oxidative treatment of refractory gold ores.* s.l., s.n.

Eskom, 2013. *The Energy Efficiency Series- Towards an energy efficient mining sector.* [Online] Available at: http://www.eskom.co.za/sites/idm/Documents/121040ESKD_Mining_Brochure_paths.pdf [Accessed 23 November 2013].

Fadhel, H. B. and Frances, C., 2001. Wet batch grinding of alumina hydrate in a stirred bead mill. *Powder Technology, 119: 257 - 268.*

Farber, B. Y., Durant, B. and Bedesi, N., 2011. Effect of media size and mechanical properties on milling efficiency and media consumption. *Minerals Engineering, 24: 367–372.*

Feng, D. and Aldrich, C., 1999. Effect of particle size on flotation performance of complex sulphide ores. *Minerals Engineering, 12(7): 721 - 731.*

Feng, D. and van Deventer, J. S. J., 2010. The effect of iron contaminants on thiosulphate leaching of gold. *Minerals Engineering, 23: 399 - 406.*

Fourie, N. K., 2008. *Maximising value through Isamill grinding technology.* s.l., s.n., pp. 186-197.

Frances, C., 2004. On modelling of submicronic wet milling processes in bead mills. *Powder Technology. 143–144: 253– 263.*

Fuerstenau, D. W., De, A. and Kapur, P. C., 2004. Linear and nonlinear particle breakage processes in comminution systems. *International Journal of Mineral Processing, 74: 317 - 327.*

Gao, M. and Forssberg, E., 1995. Prediction of product size distributions for a stirred ball mill. *Powder Technology, 84: 101 - 106.*

Gao, M. W., Forssberg, K. S. E. and Weller, K. R., 1996. Power predictions for a pilot scale stirred ball mill. *International Journal of Mineral Processing, 44 - 45; 641 - 652.*

Gao, M., Young, M. and Allum, P., 2002. *Isamill fine grinding technology and its industrial applications at Mount Isa Mines,* Brisbane: s.n.

Gaudin, A., 1939. *Principles of Mineral Dressing.* New York: McGraw-Hill Book Company, Inc..

Grano, S., 2009. The critical importance of the grinding environment on fine particle recovery in flotation. *Minerals Engineering. 22:386–394.*

Graves, G. A. and Boehm, T., 2007. Mill media considerations for high energy mills. *Minerals Engineering, 20: 342 - 347.*

Harbort, G., Hourn, M. and Murphy, A., 1998. *IsaMill Ultrafine Grinding for a Sulphide Leach Process,* s.l.: MIM Process Technologies.

He, M. and Forssberg, E., 2007. Influence of slurry rheology on stirred media milling of quartzite. *International Journal of Mineral Processing,,* pp. 84: 240 - 251.

Hennart, S. L. A., Wildeboer, W., van Hee, P. and Meesters, G., 2009. Identification of the grinding mechanisms and their origin in a stirred ball mill using population balances. *Chemical Engineering Science 64: 4123 - 4130.*

Herbst, J. A., Lo, Y. C. and Flintoff, B., 2003. Size reduction and liberation. In: M. C. Fuerstenau and K. N. Han, eds. *Principles of Mineral Processing.* Colorado: Society for Mining, Metallurgy and Exploration, Inc (SME), pp. 61 - 110.

Hogg, R., 2003. Particle Characterization . In: M. C. Fuerstenau and K. N. Han, eds. *Principles of Mineral Processing.* Colorado: Society for Mining, Metallurgy and Exploration, Inc (SME), pp. 9 - 60.

Hogg, R. and Cho, H., 2000. A Revew of Breakage Behaviour in Fine Grinding by Stirred-Media Mills. *KONA. 18: ,* pp. 9 - 19.

Jankovic, A., 2001. Media stress intensity analysis for vertical stirred mills. *Minerals Engineering, 14(10): 1177 - 1186.*

Jankovic, A., 2003. Variables affecting the fine grinding of minerals using stirred mills. *Minerals Engineering, 16: 337 - 345.*

Jankovic, A., 2008. *A Review of Regrinding and Fine Grinding Technology - the Facts and Myths,* Asia-Pacific: Metsominerals.

Jankovic, A. and Sinclair, S., 2006. The shape of product size distributions in stirred mills. *Minerals Engineering, 19: 1528 - 1536.*

Jayasundara, C. J., Yang, R. Y., Guo, B. Y., Yu, A. B., Govender, I., Mainza, A., van der Westhuizen, A. and Rubenstein, J., 2011. CFD–DEM modelling of particle flow in IsaMills – Comparison between simulations and PEPT measurements. *Minerals Engineering. 24: 181–187.*

Jayasundara, C. T., 2007. *Numerical and experimental studies of granular dynamics in Isamill: Phd Thesis,* s.l.: Centre for Computer Simulation and Modelling of Particulate Systems, School of Materials Science and Engineering, The University of New South Wales.

Jayasundara, C. T., Yang, R. Y., Guo, B. Y., Yu, A. B. and Rubenstein, J., 2009. Effect of slurry properties on particle motion in IsaMills. *Minerals Engineering. 22: 886–892.*

Jayasundara, C. T., Yang, R. and Yu, A., 2012. Effect of the size of media on grinding performance in stirred mills. *Minerals Engineering 33: 66–71.*

Jayasundara, C. T., Yang, R. Y., Yu, A. B. and Curry, D., 2008. Discrete particle simulatioin of particle flow in IsaMill- Effect of grinding medium properties. *Chemical Engineering Journal, 135: 103 - 112.*

Jayasundara, C. T., Yang, R. Y., Yu, A. B. and Rubenstein, J., 2010. Effects of disc rotation speed and media loading on particle flow and grinding performance in a horizontal stirred mill. *International Journal of Mineral Processing, 96: 27–35.*

Kalra, R., 1999. *Overview on Alternative Methods for Fine and Ultra-Fine Grinding,* Perth : IIR Conference, Crushing and Grinding 99.

Kapur, P. C., Pande, D. and Fuerstenau, D. W., 1997. Analysis of single-particle breakage by impact grinding. *International Journal of Mineral Processing, 49: 223 - 236.*

Kelly, E. G. and Spottiswood, D., 1982. *Introduction to mineral processing.* New York: John Wiley and Sons .

King, R., 1982. Flotation of fine particles. In: *Principles of flotation.* Johannesburg: South African Institute of Mining and Metallurgy, pp. 215-225.

King, R. P., 2001. *Modeling and simulation of mineral processing systems.* Oxford: Butterworth-Heinemann.

Kwade, A., 1999a. Wet comminution in stirred media mills - research and its practical application. *Power Technology, 105: 14 - 20.*

Kwade, A., 1999b. Determination of the most important grinding mechanism in stirred media mills by calculating stress intensity and stress number. *Powder Technology, 105: 382 - 388.*

Kwade, A., 2004. Mill selection and process optimization using a physical. *International Journal of Mineral Processing, 74: 93 - 101.*

Kwade, A., Blecher, L. and Schwedes, J., 1996. Motion and stress intensity of grinding beads in a stirred media mill. Part 2: Stress intensity and its effect on comminution. *Powder Technology, 81: 69 - 76.*

Kwade, A. and Schwedes, J., 2002. Breaking characteristics of different materials and their effect on stress intensity and stress number in stirred media mills. *Powder Technology, 122: 109 - 121.*

Lane, G. L., 1999. CFD Modelling of a stirred bead mill for fine grinding. *CSIRO Minerals.*

Latchireddi, S. and Rajamani, R. K., 2006. *The influence of shell, grate, and pulp lifters on SAG mill performance,* s.l.: SME ANNUAL MEETING AND EXHIBIT PROCEEDINGS.

Latchireddi, S. and Rajamani, R. K., n.d. *The influence of shell, grate and pulp lifters on SAG mill performance,* Salt Lake City: Department of Metallurgical Engineering, The University of Utah.

Lichter, J. and Davey, G., 2006. Selection and Sizing of Ultrafine and Stirred Grinding Mills. In: S. K. Kawatra, ed. *Advances in Comminution.* Colorado: Society for Mining, Metallurgy and Exploration Inc, pp. 69 - 85.

Liddell, K. S., McRae, L. B. and Dunne, R. C., 1986. Process routes for beneficiation of noble metals from Merensky and UG-2 ores.. *Mintek Review, 4: 33 - 44.*

Little, W. and Van De Ruit, L., 2012. *Effect of impeller speed, impeller type and media density on the energy efficiency of a vertical stirred mill. BSc. Thesis,,* Cape Town: University of Cape Town.

Lowrison, G. C., 1974. *Crushing and Grinding. The size reduction of solid materials.* s.l.:Hazell Watson and Viney Ltd..

Mankosa, M. J., Adel, G. T. and Yoon, R. H., 1986. Effect of Media Size in Stirred Ball Mill Grinding of Coal. *Powder Technology, 49: 75 - 82 75.*

Mankosa, M. J., Adel, G. T. and Yoon, R. H., 1989. Effect of Operating Parameters in Stirred Ball Mill Grinding of Coal. *Powder Technology, 59: 255 - 260.*

Ma, Z., Hu, S., Zhang, S. and Pan, X., 1998. Breakage behavior of quartz in a laboratory stirred ball mill. *Powder Technology, 100: 69 - 73.*

Metso, 2010. *Stirred mills: Vertimill and Stirred media detritor,* s.l.: Metso Minerals Industries, Inc..

Muzenda, E., Afolabi, A. S., Abdulkareem, A. S. and Ntuli, F., 2011. Effect of pH on the Recovery and Grade of Base Metal Sulphides (PGMs) by Flotation. *World Congress on Engineering and Computer Science, 2.*

Napier-Munn, T. J., Morell, S., Morrison, R. D. and Kojovic, T., 2005. *Mineral Comminution Circuits: Their Operation and Optimisation.* Brisbane: : Julius Kruttschnitt Mineral Research Centre.

Nel, E., Valenta, M. and Naude, N., 2005. Influence of open circuit regrind milling on UG-2 ore composition and mineralogy at Impala's UG-2 concentrator. *Minerals Engineering, 18: 785 - 790.*

Nell, J., 2004. Melting of platinum group metal concentrates in South Africa. *South African Institute of Mining and Metallurgy, 423 - 428.*

Ntsele, C. and Allen, J., 2012. Technology selection of stirred mills for energy efficiency in primary and regrinding applications for the platinum industry. *The Southern African Institute of Mining and Metallurgy, 781 - 808.*

Orumwense, O. A., 1992. The kinetics of fine grinding in an annular ball mill. *Powder Technology. 73:101-108.*

Paterson, A. J. C., 2004. High density slurry and paste tailings, transport systems. *The South African Institute of Mining and Metallurgy, 159 - 166.*

Pease, J. D., 2007. *Coarse IsaMilling at McArthur.* Brisbane, s.n.

Pease, J. D., Young, M. F. and Curry, D. C., 2005. *Fine Grinding as Enabling Technology – The IsaMill,* s.l.: s.n.

Peng, Y. and Grano, S., 2010. Effect of iron contamination from grinding media on the flotation of sulphide minerals of different particle size. *International Journal of Mineral Processing. 97:1–6.*

Rule, C. M., 2011. Stirred milling — new comminution technology in the PGM industry. *The Journal of The Southern African Institute of Mining and Metallurgy. 111: 101 - 107.*

Rule, C. M., Knopjes, L. and Atkinson, R. J., 2008. Ultra fine grinding of intermediate flotation concentrates in the PGM industry at the Pt Mile operation on Anglo Platinum tailings. *Third International Platinum Conference ' Platinum in Transformation' , The Southern African Institute of Mining and Metallurgy.*

Samanli, S. and Cuhadaroglu, D. a. H. J. Y., 2011. An investigation of particle size variation in stirred mills in terms of breakage kinetics,. *Energy Sources, Part A: Recovery, Utilization, and Environmental Effects, 33:6, 549-561.*

Schouwstra, R. P., Kinloch, E. D. and Lee, C. A., 2000. A Short Geological Review of the. *Platinum Metals Rev, 44 (1): 33 - 39.*

Schumacher, B. A., Shines, K. C., Burton, J. V. and Papp, M. L., 1990. *A comparison of soil sample homogenization techniques,* Las Vegas, Nevada: Lockheed Engineering and Sciences Company, Inc..

Shi, F., Morrison, R., Cervelling, A., Burns, F., Musa, F., 2009. Comparison of energy efficiency between ball mills and stirred mills in coarse grinding. *Minerals Engineering, 22: 673 - 680.*

Sinnott, M., Cleary, P. W. and Morrison, R. D., 2011. Slurry flow in a tower mill. *Minerals Engineering. 24: 152–159.*

Sun, Y., Dong, M., Mao, y. and Fan, D., 2009. *Analysis on grinding media motion in ball mill by Discrete Element Method.* Brasov, World Scientific and Engineering Academy and Society, pp. 227 - 231.

Taveres, L. M. and King, R. P., 1998. Single-particle fracture under impact loading. *International Journal of Mineral Processing, 54: 1–28.*

Theuerkauf, J. and Schwedes, J., 1999. Theoretical and experimental investigation on particle and fluid motion in stirred media mills. *Powder Technology, 105: 406–412.*

Toraman, O. and Katırcıoglu, D., 2011. A study on the effect of process parameters in stirred ball mill. *Advanced Powder Technology 22: 26–30.*

Tüzün, M., Loveday, B. and Hinde, A., 1995. Effect of pin tip velocity, ball density and ball size on grinding kinetics in a stirred ball mill. *International Journal of Mineral Processing, 43: 179 - 191.*

Valenta, M. M., 2007. Balancing the reagent suite to optimise grade and recovery. *Minerals Engineering, 20: 979 - 985.*

Van Der Westhuizen, A. P., Govender, I., Mainza, A. N. and Rubenstein, J., 2011. Tracking the motion of media particles inside an IsaMill™ using PEPT. *Minerals Engineering. 24: 195–204.*

Varinot, C., Berthiaux, H. and Dodds, J., 1999. Prediction of the product size distribution in associations of stirred bead mills. *Powder Technology, 105: 228–236.*

Varinot, C., Hiltgun, S., Pons, M. N. and Dodds, J., 1997. Identification of the fragmentation mechanisms in wet-phase fine grinding in a stirred bead mill. *Chemical Engineering Science, 52 (20): 3605 - 3612.*

Wang, Y. and Forssberg, E., 2000. Product size distribution in stirred media mills. *Minerals Engineering, 13(4): 459 - 465.*

Weedon, D. M., 2001. A Perfect Mixing Matrix Model For Ball Mills. *Minerals Engineering. 14 (10): 1225-1236.*

Weller, K. and Gao, M., 1999. Ultra-fine grinding. *AJM Crushing and Grinding Conference, Kalgoorlie.*

Weller, K., Spencer, S., Gao, M. and Liu, Y., 2000. Tracer studies and breakage testing in pilot - scale stirred mills. *Minerals Engineering.*

Wesseldijk, Q. I., Reuter, M. A., Bradshaw, D. J. and Harris, P. J., 1999. The floatation behaviour of chromite with respect to the beneficiation of UG2 ore. *Minerals Engineering, 12 (10): 1177 - 1184.*

Wills, B., 1997. *Mineral Processing Technology.* London: Butterworth-Heinemann.

Xiao, Z. and Laplante, A. R., 2004. Characterizing and recovering the platinum group minerals—a review. *Minerals Engineering, 17: 961 - 979.*

Yue, J. and Klein, B., 2006. Effects of bead size on ultrafine grinding in a stirred bead mill. In: *Advances in Comminution.* Littleton, Colorado: Society for Mining, Metallurgy and Exploration, Inc (SME), pp. 87 - 98.

Zheng, J., Harris, C. C. and Somasundaran, P., 1996. A study on grinding and energy input in stirred media mills. *Power Technology, 86: 171 - 178.*

7. APPENDIX

7.1. Grind curve test

Figure 64 shows the size distributions of feed material milled at different specific energy inputs. It can be observed from Figure 64 that the greater the specific energy input, the finer the grind. The spacing between the size distributions is seen to decrease with increase in specific energy input, a possible indication of decrease in the rate of material breakage.

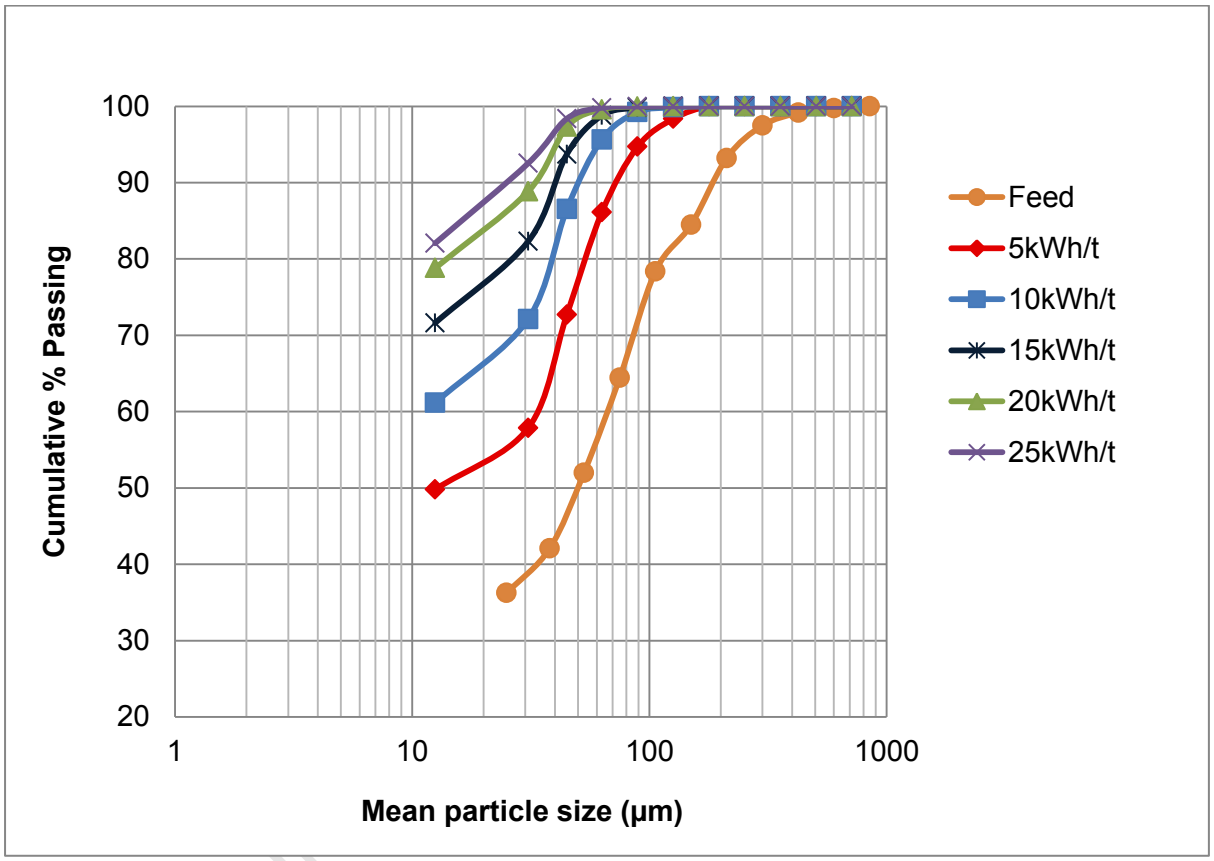

Figure 64: Product size distributions for various specific energy input.

Table 17: Product size distribution raw data at 5kWh/t

Mass Wet Screened	**283.92**	**g**			
5kWh/t					
Size Passing (µm)	Sample Mass (g)	Filter paper mass (g)	Net sample mass (g)	% Mass Passing	Cum % Passing
850	0.00	0.00	0.00	0.00	100.00
600	0.00	0.00	0.00	0.00	100.00
425	0.00	0.00	0.00	0.00	100.00
300	0.00	0.00	0.00	0.00	100.00
212	4.42	0.00	4.42	1.65	100.00
150	9.82	0.00	9.82	3.66	98.35
106	23.07	0.00	23.07	8.59	94.70
75	36.08	0.00	36.08	13.43	86.11
53	39.85	0.00	39.85	14.83	72.68
38	21.61	0.00	21.61	8.04	57.85
25	152.98	19.19	133.79	49.80	49.80
Total			**268.64**	**100**	

Table 18: Product size distribution raw data at 10kWh/t

Mass Wet Screened	**289.95**	**g**			
10kWh/t					
Size Passing (µm)	Sample Mass (g)	Filter paper mass (g)	Net sample mass (g)	% Mass Passing	Cum % Passing
850	0.00	0.00	0.00	0.00	100.00
600	0.00	0.00	0.00	0.00	100.00
425	0.00	0.00	0.00	0.00	100.00
300	0.00	0.00	0.00	0.00	100.00
212	0.39	0.00	0.39	0.14	100.00
150	1.61	0.00	1.61	0.58	99.86
106	10.67	0.00	10.67	3.82	99.28
75	26.60	0.00	26.60	9.53	95.46
53	38.71	0.00	38.71	13.87	85.93
38	31.83	0.00	31.83	11.41	72.05
25	190.78	21.57	169.21	60.64	60.64
Total			**279.02**	**100**	

Table 19: Product size distribution raw data at 15kWh/t

Mass Wet Screened	**277.61**	**g**		
15kWh/t				
Size Passing (µm)	Sample Mass (g)	Filter paper mass (g)	Net sample mass (g)	% Mass Passing	Cum % Passing
850	0.00	0.00	0.00	0.00	100.00
600	0.00	0.00	0.00	0.00	100.00
425	0.00	0.00	0.00	0.00	100.00
300	0.00	0.00	0.00	0.00	100.00
212	0.00	0.00	0.00	0.00	100.00
150	0.50	0.00	0.50	0.19	100.00
106	2.44	0.00	2.44	0.91	99.81
75	14.06	0.00	14.06	5.27	98.90
53	27.76	0.00	27.76	10.40	93.63
38	29.46	0.00	29.46	11.04	83.23
25	210.16	17.54	192.62	72.19	72.19
Total			**266.84**	**100**	

Table 20: Product size distribution raw data at 20kWh/t

Mass Wet Screened	**276.00**	**g**		
20kWh/t				
Size Passing (µm)	Sample Mass (g)	Filter paper mass (g)	Net sample mass (g)	% Mass Passing	Cum % Passing
850	0.00	0.00	0.00	0.00	100.00
600	0.00	0.00	0.00	0.00	100.00
425	0.00	0.00	0.00	0.00	100.00
300	0.00	0.00	0.00	0.00	100.00
212	0.08	0.00	0.08	0.03	100.00
150	0.09	0.00	0.09	0.03	99.97
106	0.98	0.00	0.98	0.36	99.94
75	6.60	0.00	6.60	2.42	99.58
53	23.27	0.00	23.27	8.54	97.16
38	27.53	0.00	27.53	10.10	88.62
25	230.80	16.72	214.08	78.52	78.52
Total			**272.63**	**100**	

Table 21: Product size distribution raw data at 25kWh/t

Mass Wet Screened	**313.91**	**g**			
25kWh/t					
Size Passing (µm)	Sample Mass (g)	Filter paper mass (g)	Net sample mass (g)	% Mass Passing	Cum % Passing
850	0.00	0.00	0.00	0.00	100.00
600	0.00	0.00	0.00	0.00	100.00
425	0.00	0.00	0.00	0.00	100.00
300	0.00	0.00	0.00	0.00	100.00
212	0.00	0.00	0.00	0.00	100.00
150	0.08	0.00	0.08	0.03	100.00
106	0.52	0.00	0.52	0.17	99.97
75	4.42	0.00	4.42	1.43	99.81
53	18.10	0.00	18.10	5.85	98.38
38	32.44	0.00	32.44	10.48	92.53
25	276.06	21.98	254.08	82.06	82.06
Total			**309.64**	**100**	

Table 22: Product size distribution raw data for repeat test at 10kWh/t

Mass Wet Screened	**278.83**	**g**			
10kWh/t Repeat					
Size Passing (µm)	Sample Mass (g)	Filter paper mass (g)	Net sample mass (g)	% Mass Passing	Cum % Passing
850	0.00	0.00	0.00	0.00	100.00
600	0.00	0.00	0.00	0.00	100.00
425	0.00	0.00	0.00	0.00	100.00
300	0.00	0.00	0.00	0.00	100.00
212	0.40	0.00	0.40	0.15	100.00
150	1.80	0.00	1.80	0.66	99.85
106	9.18	0.00	9.18	3.37	99.19
75	23.68	0.00	23.68	8.69	95.82
53	40.70	0.00	40.70	14.93	87.13
38	28.73	0.00	28.73	10.54	72.20
25	187.95	19.92	168.03	61.66	61.66
Total			**272.52**	**100**	

Table 23: Product size distribution raw data for repeat test at 15kWh/t

Mass Wet Screened		**289.56**	**g**		
15kWh/t Repeat					
Size Passing (µm)	Sample Mass (g)	Filter paper mass (g)	Net sample mass (g)	% Mass Passing	Cum % Passing
850	0.00	0.00	0.00	0.00	100.00
600	0.00	0.00	0.00	0.00	100.00
425	0.00	0.00	0.00	0.00	100.00
300	0.00	0.00	0.00	0.00	100.00
212	0.00	0.00	0.00	0.00	100.00
150	0.39	0.00	0.39	0.14	100.00
106	3.30	0.00	3.30	1.19	99.86
75	13.40	0.00	13.40	4.84	98.67
53	34.48	0.00	34.48	12.46	93.82
38	28.52	0.00	28.52	10.31	81.36
25	215.23	18.64	196.59	71.05	71.05
Total			**276.68**	**100**	

Table 24: Product size distribution raw data for repeat test at 20kWh/t

Mass Wet Screened		**296.06**	**g**		
20kWh/t Repeat					
Size Passing (µm)	Sample Mass (g)	Filter paper mass (g)	Net sample mass (g)	% Mass Passing	Cum % Passing
850	0.00	0.00	0.00	0.00	100.00
600	0.00	0.00	0.00	0.00	100.00
425	0.00	0.00	0.00	0.00	100.00
300	0.00	0.00	0.00	0.00	100.00
212	0.00	0.00	0.00	0.00	100.00
150	0.10	0.00	0.10	0.03	100.00
106	0.98	0.00	0.98	0.34	99.97
75	6.26	0.00	6.26	2.17	99.63
53	24.25	0.00	24.25	8.39	97.46
38	28.87	0.00	28.87	9.99	89.07
25	242.85	14.25	228.60	79.08	79.08
Total			**289.06**	**100**	

7.2. Effect of test variables on product size distribution

7.2.1. Solids concentration tests

Figure 65 shows the product size distribution of material milled at different solids concentration. It can be observed that over the range of solids concentration tested, an increase in the solids concentration results a finer grind.

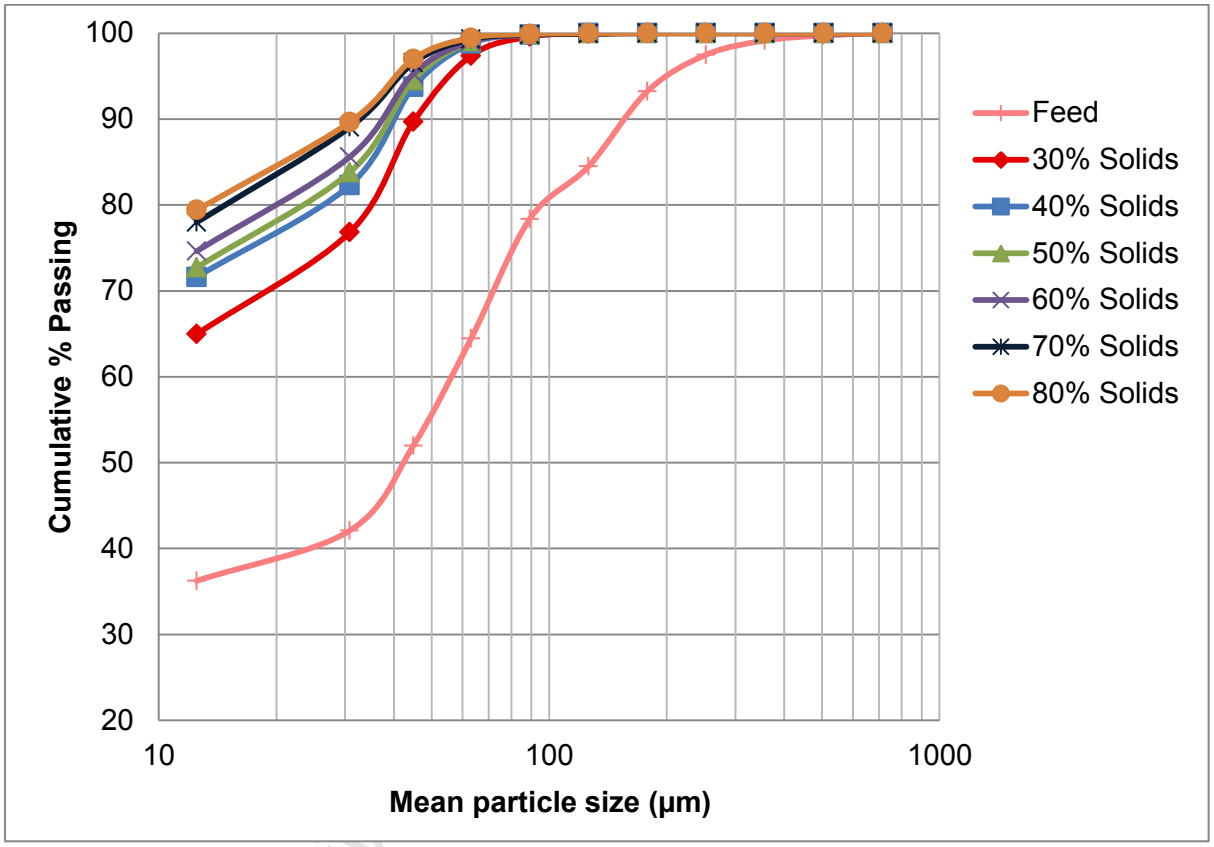

Figure 65: Product size distribution at various solids concentration.

Table 25: Product size distribution raw data at 30% solids

Mass Wet Screened	**295.35**	**g**			
30% Solids					
Size Passing (µm)	Sample Mass (g)	Filter paper mass (g)	Net sample mass (g)	% Mass Passing	Cum % Passing
850	0.00	0.00	0.00	0.00	100.00
600	0.00	0.00	0.00	0.00	100.00
425	0.00	0.00	0.00	0.00	100.00
300	0.00	0.00	0.00	0.00	100.00
212	0.20	0.00	0.20	0.07	100.00
150	1.02	0.00	1.02	0.36	99.93
106	6.28	0.00	6.28	2.21	99.57
75	23.71	0.00	23.71	8.36	97.36
53	33.56	0.00	33.56	11.83	89.00
38	34.43	0.00	34.43	12.14	77.17
25	208.57	24.12	184.45	65.03	65.03
Total			**283.65**	**100.00**	

Table 26: Product size distribution raw data at 40% solids

Mass Wet Screened	**277.61**	**g**			
40% Solids					
Size Passing (µm)	Sample Mass (g)	Filter paper mass (g)	Net sample mass (g)	% Mass Passing	Cum % Passing
850	0.00	0.00	0.00	0.00	100.00
600	0.00	0.00	0.00	0.00	100.00
425	0.00	0.00	0.00	0.00	100.00
300	0.00	0.00	0.00	0.00	100.00
212	0.00	0.00	0.00	0.00	100.00
150	0.50	0.00	0.50	0.19	100.00
106	2.44	0.00	2.44	0.91	99.81
75	14.06	0.00	14.06	5.27	98.90
53	27.76	0.00	27.76	10.40	93.63
38	29.46	0.00	29.46	11.04	83.23
25	210.16	17.54	192.62	72.19	72.19
Total			**266.84**	**100**	

Table 27: Product size distribution raw data at 50% solids

Mass Wet Screened		**307.88**	**g**		
50% Solids					
Size Passing (µm)	Sample Mass (g)	Filter paper mass (g)	Net sample mass (g)	% Mass Passing	Cum % Passing
850	0.00	0.00	0.00	0.00	100.00
600	0.00	0.00	0.00	0.00	100.00
425	0.00	0.00	0.00	0.00	100.00
300	0.00	0.00	0.00	0.00	100.00
212	0	0.00	0.00	0.00	100.00
150	0.32	0.00	0.32	0.11	100.00
106	2.64	0.00	2.64	0.90	99.89
75	14.38	0.00	14.38	4.92	98.99
53	30.12	0.00	30.12	10.31	94.07
38	32.7	0.00	32.70	11.19	83.76
25	236.18	24.15	212.03	72.57	72.57
Total			**292.19**	**100**	

Table 28: Product size distribution raw data at 60% solids

Mass Wet Screened		**301.8**	**g**		
60% Solids					
Size Passing (µm)	Sample Mass (g)	Filter paper mass (g)	Net sample mass (g)	% Mass Passing	Cum % Passing
850	0.00	0.00	0.00	0.00	100.00
600	0.00	0.00	0.00	0.00	100.00
425	0.00	0.00	0.00	0.00	100.00
300	0.00	0.00	0.00	0.00	100.00
212	0	0.00	0.00	0.00	100.00
150	0.6	0.00	0.60	0.20	100.00
106	1.96	0.00	1.96	0.67	99.80
75	11.43	0.00	11.43	3.88	99.13
53	29.52	0.00	29.52	10.02	95.25
38	32.89	0.00	32.89	11.17	85.23
25	237.42	19.33	218.09	74.06	74.06
Total			**294.49**	**100**	

Table 29: Product size distribution raw data at 70% solids

Mass Wet Screened		**301.98**	**g**		
70% Solids					
Size Passing (µm)	Sample Mass (g)	Filter paper mass (g)	Net sample mass (g)	% Mass Passing	Cum % Passing
850	0.00	0.00	0.00	0.00	100.00
600	0.00	0.00	0.00	0.00	100.00
425	0.00	0.00	0.00	0.00	100.00
300	0.00	0.00	0.00	0.00	100.00
212	0.21	0.00	0.21	0.07	100.00
150	0.3	0.00	0.30	0.10	99.93
106	1.57	0.00	1.57	0.53	99.83
75	8.09	0.00	8.09	2.76	99.29
53	22.03	0.00	22.03	7.50	96.54
38	32.45	0.00	32.45	11.05	89.03
25	248.42	19.48	228.94	77.98	77.98
Total			**293.59**	**100**	

Table 30: Product size distribution raw data at 80% solids

Mass Wet Screened		**292.83**	**g**		
80% Solids					
Size Passing (µm)	Sample Mass (g)	Filter paper mass (g)	Net sample mass (g)	% Mass Passing	Cum % Passing
850	0.00	0.00	0.00	0.00	100.00
600	0.00	0.00	0.00	0.00	100.00
425	0.00	0.00	0.00	0.00	100.00
300	0.00	0.00	0.00	0.00	100.00
212	0	0.00	0.00	0.00	100.00
150	0.3	0.00	0.30	0.10	100.00
106	1.26	0.00	1.26	0.44	99.90
75	7.03	0.00	7.03	2.45	99.46
53	21.1	0.00	21.10	7.37	97.00
38	29.26	0.00	29.26	10.22	89.63
25	247.09	19.66	227.43	79.42	79.42
Total			**286.38**	**100**	

Table 31: Product size distribution raw data at 30% solids repeat test

Mass Wet Screened	**291.29**	**g**			
30% Solids Repeat					
Size Passing (µm)	Sample Mass (g)	Filter paper mass (g)	Net sample mass (g)	% Mass Passing	Cum % Passing
850	0.00	0.00	0.00	0.00	100.00
600	0.00	0.00	0.00	0.00	100.00
425	0.00	0.00	0.00	0.00	100.00
300	0.00	0.00	0.00	0.00	100.00
212	0.19	0.00	0.19	0.07	100.00
150	0.87	0.00	0.87	0.31	99.93
106	6.33	0.00	6.33	2.25	99.62
75	19.76	0.00	19.76	7.02	97.38
53	39.15	0.00	39.15	13.90	90.36
38	32.58	0.00	32.58	11.57	76.45
25	201.04	18.35	182.69	64.88	64.88
Total			**281.57**	**100.00**	

Table 32: Product size distribution raw data at 40% solids repeat test

Mass Wet Screened	**289.56**	**g**			
40% Solids Repeat					
Size Passing (µm)	Sample Mass (g)	Filter paper mass (g)	Net sample mass (g)	% Mass Passing	Cum % Passing
850	0.00	0.00	0.00	0.00	100.00
600	0.00	0.00	0.00	0.00	100.00
425	0.00	0.00	0.00	0.00	100.00
300	0.00	0.00	0.00	0.00	100.00
212	0.00	0.00	0.00	0.00	100.00
150	0.39	0.00	0.39	0.14	100.00
106	3.30	0.00	3.30	1.19	99.86
75	13.40	0.00	13.40	4.84	98.67
53	34.48	0.00	34.48	12.46	93.82
38	28.52	0.00	28.52	10.31	81.36
25	215.23	18.64	196.59	71.05	71.05
Total			**276.68**	**100**	

Table 33: Product size distribution raw data at 50% solids repeat test

Mass Wet Screened		**287.52**	**g**		
50% Solids Repeat					
Size Passing (µm)	Sample Mass (g)	Filter paper mass (g)	Net sample mass (g)	% Mass Passing	Cum % Passing
850	0.00	0.00	0.00	0.00	100.00
600	0.00	0.00	0.00	0.00	100.00
425	0.00	0.00	0.00	0.00	100.00
300	0.00	0.00	0.00	0.00	100.00
212	0.00	0.00	0.00	0.00	100.00
150	0.31	0.00	0.31	0.11	100.00
106	2.29	0.00	2.29	0.82	99.89
75	11.35	0.00	11.35	4.08	99.06
53	30.98	0.00	30.98	11.14	94.98
38	30.47	0.00	30.47	10.96	83.84
25	221.64	19.02	202.62	72.88	72.88
Total			**278.02**	**100**	

Table 34: Product size distribution raw data at 60% solids repeat test

Mass Wet Screened		**287.67**	**g**		
60% Solids Repeat					
Size Passing (µm)	Sample Mass (g)	Filter paper mass (g)	Net sample mass (g)	% Mass Passing	Cum % Passing
850	0.00	0.00	0.00	0.00	100.00
600	0.00	0.00	0.00	0.00	100.00
425	0.00	0.00	0.00	0.00	100.00
300	0.00	0.00	0.00	0.00	100.00
212	0.00	0.00	0.00	0.00	100.00
150	0.46	0.00	0.46	0.17	100.00
106	2.49	0.00	2.49	0.90	99.83
75	10.02	0.00	10.02	3.64	98.93
53	25.76	0.00	25.76	9.35	95.29
38	29.68	0.00	29.68	10.77	85.94
25	225.93	18.86	207.07	75.17	75.17
Total			**275.48**	**100**	

7.2.2. Impeller speed tests

Figure 66 shows the product size distributions of material milled at different impeller speeds. It is evident that over the range tested, the higher the impeller speed, the finer the grind.

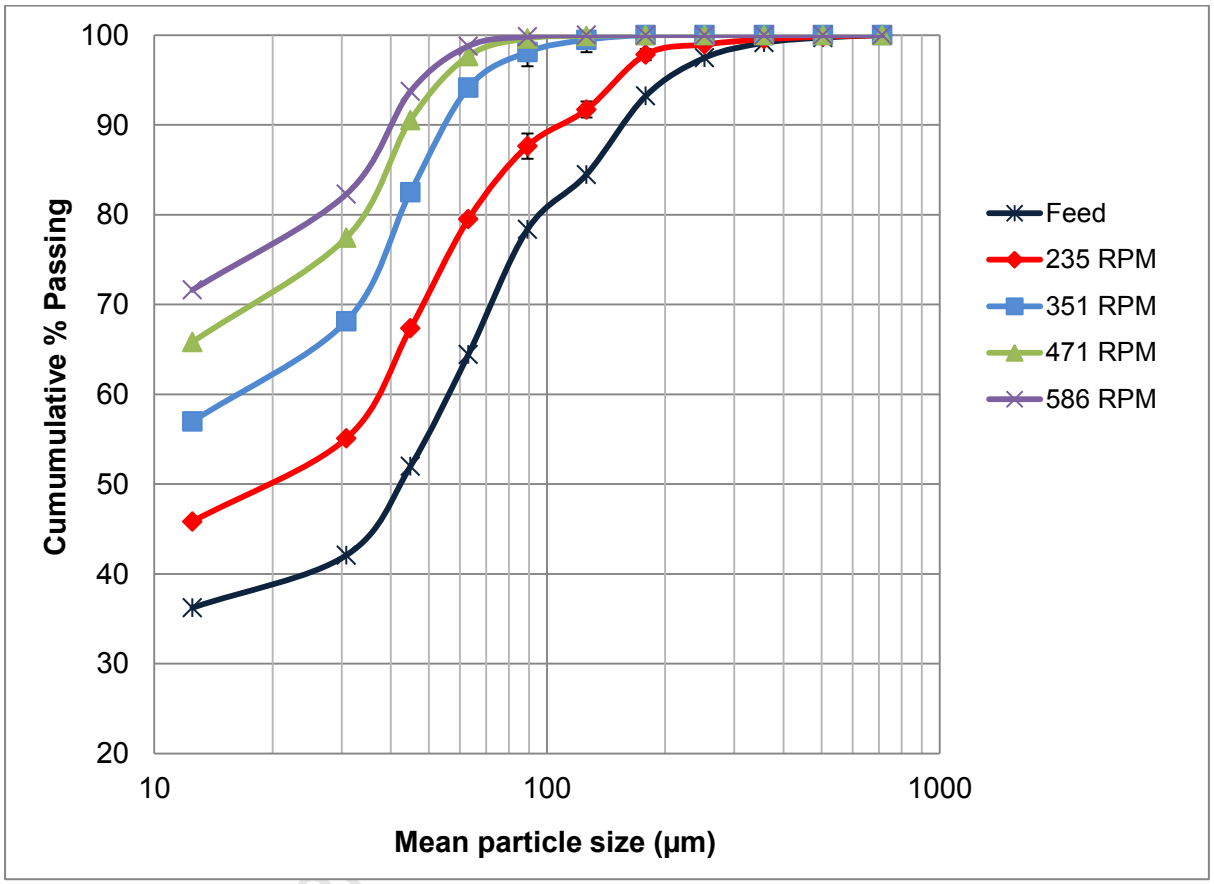

Figure 66: Product size distributions of material milled at different impeller speeds.

Table 35: Product size distribution raw data at 20.1Hz

Mass Wet Screened	**301.08**	**g**		
20.1 Hz				
Size Passing (µm)	Sample Mass (g)	Filter paper mass (g)	Net sample mass (g)	% Mass Passing	Cum % Passing
850	0.43	0.00	0.43	0.14	100.00
600	0.93	0.00	0.93	0.31	99.86
425	1.58	0.00	1.58	0.52	99.55
300	3.22	0.00	3.22	1.06	99.03
212	19.05	0.00	19.05	6.26	97.98
150	12.74	0.00	12.74	4.19	91.72
106	25.09	0.00	25.09	8.24	87.53
75	38.26	0.00	38.26	12.57	79.29
53	38.06	0.00	38.06	12.50	66.72
38	29.79	0.00	29.79	9.79	54.21
25	159.44	24.22	135.22	44.43	44.43
Total			**304.37**	**100.00**	

Table 36: Product size distribution raw data at 30Hz

Mass Wet Screened	**300.82**	**g**		
30 Hz				
Size Passing (µm)	Sample Mass (g)	Filter paper mass (g)	Net sample mass (g)	% Mass Passing	Cum % Passing
850	0.00	0.00	0.00	0.00	100.00
600	0.00	0.00	0.00	0.00	100.00
425	0.00	0.00	0.00	0.00	100.00
300	0.00	0.00	0.00	0.00	100.00
212	1.35	0.00	1.35	0.47	100.00
150	2.80	0.00	2.80	0.98	99.53
106	13.01	0.00	13.01	4.54	98.55
75	32.04	0.00	32.04	11.18	94.01
53	41.09	0.00	41.09	14.33	82.84
38	28.51	0.00	28.51	9.95	68.50
25	186.42	18.56	167.86	58.56	58.56
Total			**286.66**	**100.00**	

Table 37: Product size distribution raw data at 40.2Hz

Mass Wet Screened		**302.42**	**g**		
40.2 Hz					
Size Passing (µm)	Sample Mass (g)	Filter paper mass (g)	Net sample mass (g)	% Mass Passing	Cum % Passing
850	0.00	0.00	0.00	0.00	100.00
600	0.00	0.00	0.00	0.00	100.00
425	0.00	0.00	0.00	0.00	100.00
300	0.00	0.00	0.00	0.00	100.00
212	0.30	0.00	0.30	0.10	100.00
150	0.90	0.00	0.90	0.31	99.90
106	7.11	0.00	7.11	2.45	99.59
75	21.63	0.00	21.63	7.44	97.14
53	40.83	0.00	40.83	14.05	89.70
38	32.01	0.00	32.01	11.01	75.65
25	206.54	18.68	187.86	64.64	64.64
Total			**290.64**	**100.00**	

Table 38: Product size distribution raw data at 50Hz

Mass Wet Screened		**277.61**	**g**		
50 Hz					
Size Passing (µm)	Sample Mass (g)	Filter paper mass (g)	Net sample mass (g)	% Mass Passing	Cum % Passing
850	0.00	0.00	0.00	0.00	100.00
600	0.00	0.00	0.00	0.00	100.00
425	0.00	0.00	0.00	0.00	100.00
300	0.00	0.00	0.00	0.00	100.00
212	0.00	0.00	0.00	0.00	100.00
150	0.50	0.00	0.50	0.19	100.00
106	2.44	0.00	2.44	0.91	99.81
75	14.06	0.00	14.06	5.27	98.90
53	27.76	0.00	27.76	10.40	93.63
38	29.46	0.00	29.46	11.04	83.23
25	210.16	17.54	192.62	72.19	72.19
Total			**266.84**	**100.00**	

Table 39: Product size distribution raw data at 20.1Hz repeat test

Mass Wet Screened	**296.38**	**g**			
20.1 Hz Repeat					
Size Passing (µm)	Sample Mass (g)	Filter paper mass (g)	Net sample mass (g)	% Mass Passing	Cum % Passing
850	0.55	0.00	0.55	0.19	100.00
600	0.80	0.00	0.80	0.27	99.81
425	1.91	0.00	1.91	0.65	99.54
300	3.46	0.00	3.46	1.17	98.90
212	17.72	0.00	17.72	6.00	97.72
150	11.66	0.00	11.66	3.95	91.72
106	23.76	0.00	23.76	8.05	87.77
75	34.70	0.00	34.70	11.76	79.72
53	35.36	0.00	35.36	11.98	67.96
38	25.76	0.00	25.76	8.73	55.98
25	155.40	15.94	139.46	47.25	47.25
Total			**295.14**	**97.72**	

Table 40: Product size distribution raw data at 30Hz repeat test

Mass Wet Screened	**238.48**	**g**			
30 Hz repeat					
Size Passing (µm)	Sample Mass (g)	Filter paper mass (g)	Net sample mass (g)	% Mass Passing	Cum % Passing
850	0.00	0.00	0.00	0.00	100.00
600	0.00	0.00	0.00	0.00	100.00
425	0.00	0.00	0.00	0.00	100.00
300	0.00	0.00	0.00	0.00	100.00
212	1.25	0.00	1.25	0.56	100.00
150	3.99	0.00	3.99	1.77	99.44
106	7.60	0.00	7.60	3.38	97.67
75	27.22	0.00	27.22	12.10	94.29
53	32.37	0.00	32.37	14.38	82.20
38	27.95	0.00	27.95	12.42	67.81
25	158.70	34.05	124.65	55.39	55.39
Total			**225.03**	**100**	

Table 41: Product size distribution raw data at 40.2Hz repeat test

Mass Wet Screened		**303.49**	**g**		
40.2 Hz Repeat					
Size Passing (µm)	Sample Mass (g)	Filter paper mass (g)	Net sample mass (g)	% Mass Passing	Cum % Passing
850	0.00	0.00	0.00	0.00	100.00
600	0.00	0.00	0.00	0.00	100.00
425	0.00	0.00	0.00	0.00	100.00
300	0.00	0.00	0.00	0.00	100.00
212	0.23	0.00	0.23	0.08	100.00
150	0.72	0.00	0.72	0.24	99.92
106	4.37	0.00	4.37	1.47	99.68
75	20.46	0.00	20.46	6.88	98.21
53	35.95	0.00	35.95	12.08	91.34
38	36.41	0.00	36.41	12.24	79.26
25	230.56	31.13	199.43	67.02	67.02
Total			**297.57**	**100**	

Table 42: Product size distribution raw data at 50Hz repeat test

Mass Wet Screened		**289.56**	**g**		
50 Hz Repeat					
Size Passing (µm)	Sample Mass (g)	Filter paper mass (g)	Net sample mass (g)	% Mass Passing	Cum % Passing
850	0.00	0.00	0.00	0.00	100.00
600	0.00	0.00	0.00	0.00	100.00
425	0.00	0.00	0.00	0.00	100.00
300	0.00	0.00	0.00	0.00	100.00
212	0.00	0.00	0.00	0.00	100.00
150	0.39	0.00	0.39	0.14	100.00
106	3.30	0.00	3.30	1.19	99.86
75	13.40	0.00	13.40	4.84	98.67
53	34.48	0.00	34.48	12.46	93.82
38	28.52	0.00	28.52	10.31	81.36
25	215.23	18.64	196.59	71.05	71.05
Total			**276.68**	**100**	

7.2.3. Disk stirrer tests

Figure 67 shows the product size distribution for the disk stirrer tests at different solids concentrations. From the product size distributions, it appears that over the range of solids concentration tested, there are no significant changes in the grind with increasing solids concentration. This is shown by the product size distributions at 30%, 40% and 50% solids almost layered on top of each other (refer to Figure 67).

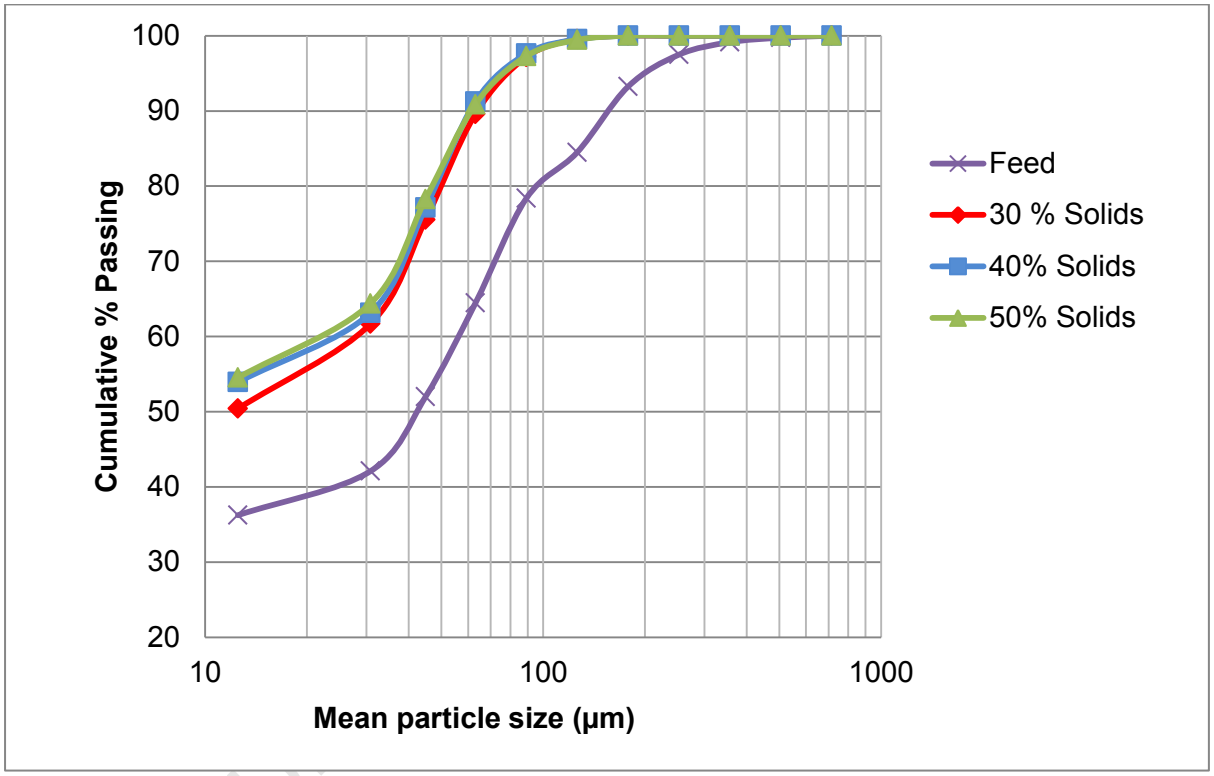

Figure 67: Product size distributions for disk stirrer tests at different solids concentration.

Table 43: Product size distribution raw data at 30% solids for disk impeller tests.

Mass Wet Screened	**289**	**g**		
30% Solids				
Size Passing (µm)	Sample Mass (g)	Filter paper mass (g)	Net sample mass (g)	% Mass Passing	Cum % Passing
850	0.00	0.00	0.00	0.00	100.00
600	0.00	0.00	0.00	0.00	100.00
425	0.00	0.00	0.00	0.00	100.00
300	0.00	0.00	0.00	0.00	100.00
212	1.30	0.00	1.30	0.46	100.00
150	6.67	0.00	6.67	2.37	99.54
106	21.34	0.00	21.34	7.58	97.17
75	39.68	0.00	39.68	14.09	89.59
53	38.98	0.00	38.98	13.84	75.51
38	31.75	0.00	31.75	11.27	61.67
25	165.40	23.44	141.96	50.40	50.40
Total			**281.68**	**100.00**	

Table 44: Product size distribution raw data at 40% solids for disk impeller tests

Mass Wet Screened			**291.17**	**g**	
40% Solids					
Size Passing (µm)	Sample Mass (g)	Filter paper mass (g)	Net sample mass (g)	% Mass Passing	Cum % Passing
850	0.00	0.00	0.00	0.00	100.00
600	0.00	0.00	0.00	0.00	100.00
425	0.00	0.00	0.00	0.00	100.00
300	0.00	0.00	0.00	0.00	100.00
212	1.32	0.00	1.32	0.48	100.00
150	5.26	0.00	5.26	1.92	99.52
106	17.46	0.00	17.46	6.37	97.60
75	38.7	0.00	38.70	14.11	91.24
53	38.39	0.00	38.39	14.00	77.13
38	25.26	0.00	25.26	9.21	63.13
25	165.98	18.06	147.92	53.92	53.92
Total			**274.31**	**100**	

Table 45: Product size distribution raw data at 50% solids for disk impeller tests

Mass Wet Screened	**292.14**	**g**		
50% Solids				
Size Passing (µm)	Sample Mass (g)	Filter paper mass (g)	Net sample mass (g)	% Mass Passing	Cum % Passing
850	0.00	0.00	0.00	0.00	100.00
600	0.00	0.00	0.00	0.00	100.00
425	0.00	0.00	0.00	0.00	100.00
300	0.00	0.00	0.00	0.00	100.00
212	1.55	0.00	1.55	0.56	100.00
150	6.01	0.00	6.01	2.16	99.44
106	17.92	0.00	17.92	6.43	97.29
75	35.16	0.00	35.16	12.61	90.86
53	38.67	0.00	38.67	13.87	78.25
38	27.5	0.00	27.50	9.86	64.38
25	170.6	18.57	152.03	54.52	54.52
Total			**278.84**	**100**	

Table 46: Product size distribution raw data at 30Hz for disk impeller tests

Mass Wet Screened	**303.72**	**g**		
30 Hz				
Size Passing (µm)	Sample Mass (g)	Filter paper mass (g)	Net sample mass (g)	% Mass Passing	Cum % Passing
850	0.00	0.00	0.00	0.00	100.00
600	0.00	0.00	0.00	0.00	100.00
425	0.00	0.00	0.00	0.00	100.00
300	0.00	0.00	0.00	0.00	100.00
212	9.09	0.00	9.09	3.17	100.00
150	13.69	0.00	13.69	4.77	96.83
106	30.54	0.00	30.54	10.64	92.06
75	35.62	0.00	35.62	12.41	81.42
53	31.1	0.00	31.10	10.84	69.01
38	35.28	0.00	35.28	12.29	58.18
25	180.79	49.09	131.70	45.89	45.89
Total			**287.02**	**100**	

Table 47: Product size distribution raw data at 40Hz for disk impeller tests

Mass Wet Screened	**298.06**	**g**		
40 Hz				
Size Passing (µm)	Sample Mass (g)	Filter paper mass (g)	Net sample mass (g)	% Mass Passing	Cum % Passing
850	0.00	0.00	0.00	0.00	100.00
600	0.00	0.00	0.00	0.00	100.00
425	0.00	0.00	0.00	0.00	100.00
300	0.00	0.00	0.00	0.00	100.00
212	3.06	0.00	3.06	1.08	100.00
150	7.10	0.00	7.10	2.50	98.92
106	24.06	0.00	24.06	8.48	96.42
75	36.01	0.00	36.01	12.69	87.94
53	42.71	0.00	42.71	15.05	75.26
38	21.94	0.00	21.94	7.73	60.21
25	166.65	17.70	148.95	52.48	52.48
Total			**283.83**	**100**	

Table 48: Product size distribution raw data at 50Hz for disk impeller tests

Mass Wet Screened	**304.84**	**g**		
50 Hz				
Size Passing (µm)	Sample Mass (g)	Filter paper mass (g)	Net sample mass (g)	% Mass Passing	Cum % Passing
850	0.00	0.00	0.00	0.00	100.00
600	0.00	0.00	0.00	0.00	100.00
425	0.00	0.00	0.00	0.00	100.00
300	0.00	0.00	0.00	0.00	100.00
212	1.40	0.00	1.40	0.47	100.00
150	4.97	0.00	4.97	1.67	99.53
106	22.51	0.00	22.51	7.54	97.87
75	38.92	0.00	38.92	13.04	90.32
53	41.06	0.00	41.06	13.76	77.28
38	28.51	0.00	28.51	9.55	63.52
25	179.99	18.91	161.08	53.97	53.97
Total			**298.45**	**100**	

Table 49: Product size distribution raw data at 40Hz for disk impeller repeat tests

Mass Wet Screened	**306.78**	**g**		
40 Hz Repeat				
Size Passing (µm)	Sample Mass (g)	Filter paper mass (g)	Net sample mass (g)	% Mass Passing	Cum % Passing
850	0.00	0.00	0.00	0.00	100.00
600	0.00	0.00	0.00	0.00	100.00
425	0.00	0.00	0.00	0.00	100.00
300	0.00	0.00	0.00	0.00	100.00
212	3.76	0.00	3.76	1.29	100.00
150	10.51	0.00	10.51	3.61	98.71
106	26.5	0.00	26.50	9.09	95.10
75	43.15	0.00	43.15	14.80	86.01
53	39.42	0.00	39.42	13.52	71.21
38	23.86	0.00	23.86	8.19	57.68
25	161.54	17.27	144.27	49.50	49.50
Total			**291.47**	**100**	

Table 50: Product size distribution raw data at 50Hz for disk impeller repeat tests

Mass Wet Screened	**291.17**	**g**		
50 Hz Repeat				
Size Passing (µm)	Sample Mass (g)	Filter paper mass (g)	Net sample mass (g)	% Mass Passing	Cum % Passing
850	0.00	0.00	0.00	0.00	100.00
600	0.00	0.00	0.00	0.00	100.00
425	0.00	0.00	0.00	0.00	100.00
300	0.00	0.00	0.00	0.00	100.00
212	1.32	0.00	1.32	0.48	100.00
150	5.26	0.00	5.26	1.92	99.52
106	17.46	0.00	17.46	6.37	97.60
75	38.7	0.00	38.70	14.11	91.24
53	38.39	0.00	38.39	14.00	77.13
38	25.26	0.00	25.26	9.21	63.13
25	165.98	18.06	147.92	53.92	53.92
Total			**274.31**	**100**	

Figure 68 shows the product size distributions for disk stirrer tests at various impeller speeds. An increase in impeller speed appears to improve grind. The effect is however minimal.

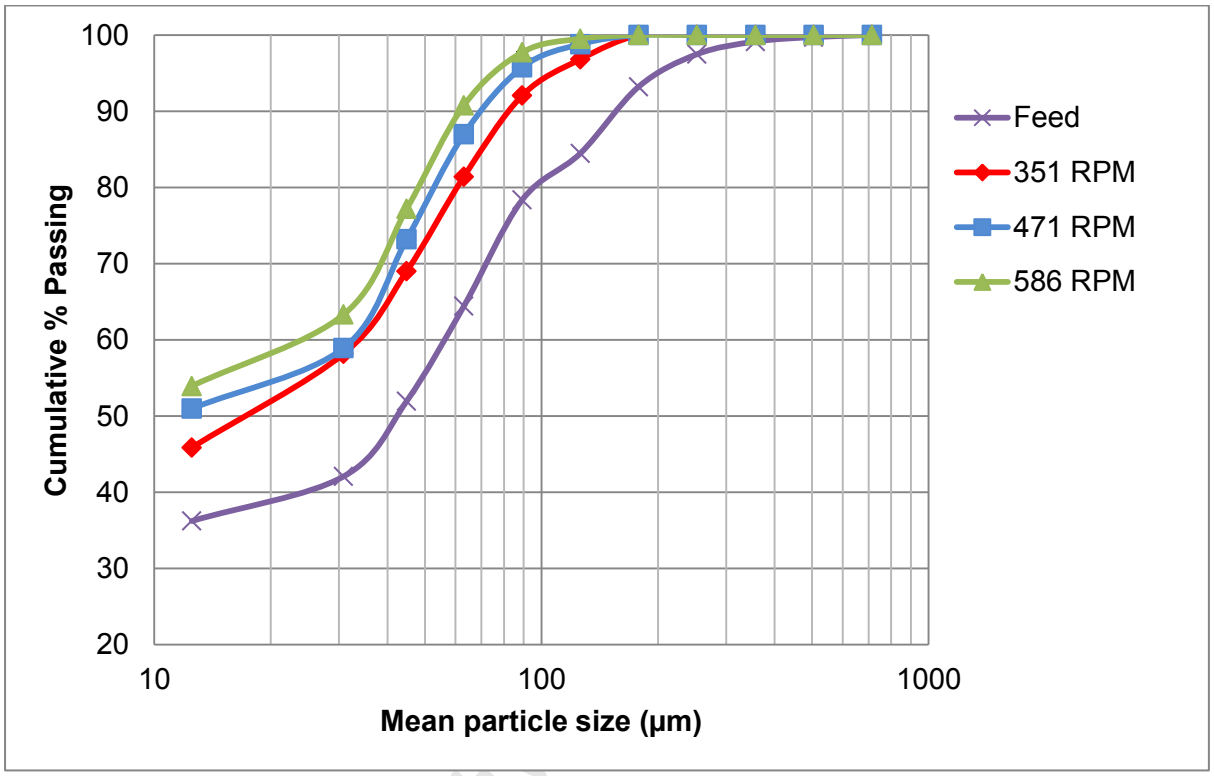

Figure 68: Product size distributions for disk stirrer tests at different impeller speed.

7.2.4. Grinding media size and density tests

7.2.4.1. High Density (HD) media tests

Table 51: Product size distribution raw data for 12.6kg HD media at 22.6kWh/t

Mass Wet Screened		**292.48**	**g**		
		Batch time	1min 42secs		
HD +11.2 - 13.2 mm SE=22.6kWh/t, Media=12.6kg					
Size Passing (µm)	Sample Mass (g)	Filter paper mass (g)	Net sample mass (g)	% Mass Passing	Cum % Passing
850	0.00	0.00	0.00	0.00	100.00
600	0.00	0.00	0.00	0.00	100.00
425	0.00	0.00	0.00	0.00	100.00
300	0.00	0.00	0.00	0.00	100.00
212	0.33	0.00	0.33	0.12	100.00
150	2.50	0.00	2.50	0.91	99.88
106	12.70	0.00	12.70	4.62	98.97
75	27.11	0.00	27.11	9.86	94.35
53	36.23	0.00	36.23	13.18	84.49
38	25.97	0.00	25.97	9.45	71.31
25	200.28	30.26	170.02	61.86	61.86
Total			**274.86**	**100.00**	

Table 52: Product size distribution raw data for 12.6kg HD media at 15kWh/t

Mass Wet Screened	**299.75**	**g**		
HD +11.2 - 13.2 mm SE=15kWh/t, Media=12.6kg				
Size Passing (µm)	Sample Mass (g)	Filter paper mass (g)	Net sample mass (g)	% Mass Passing	Cum % Passing
850	0.00	0.00	0.00	0.00	100.00
600	0.00	0.00	0.00	0.00	100.00
425	0.00	0.00	0.00	0.00	100.00
300	0.00	0.00	0.00	0.00	100.00
212	0.60	0.00	0.60	0.21	100.00
150	4.02	0.00	4.02	1.41	99.79
106	17.06	0.00	17.06	5.99	98.38
75	33.69	0.00	33.69	11.83	92.38
53	40.63	0.00	40.63	14.27	80.55
38	26.05	0.00	26.05	9.15	66.28
25	181.41	18.79	162.62	57.13	57.13
Total			**284.67**	**100**	

Table 53: Product size distribution raw data for 5.5kg HD media at 15kWh/t

Mass Wet Screened	**297.94**	**g**		
HD +11.2 - 13.2 mm SE=15kWh/t, Media=5.5kg				
Size Passing (µm)	Sample Mass (g)	Filter paper mass (g)	Net sample mass (g)	% Mass Passing	Cum % Passing
850	0.00	0.00	0.00	0.00	100.00
600	0.00	0.00	0.00	0.00	100.00
425	0.00	0.00	0.00	0.00	100.00
300	0.00	0.00	0.00	0.00	100.00
212	0.54	0.00	0.54	0.19	100.00
150	5.26	0.00	5.26	1.89	99.81
106	21.8	0.00	21.80	7.82	97.92
75	40.8	0.00	40.80	14.63	90.10
53	38.82	0.00	38.82	13.92	75.47
38	23.95	0.00	23.95	8.59	61.55
25	166.11	18.44	147.67	52.96	52.96
Total			**278.84**	**100**	

Table 54: Product size distribution raw data for 5.5kg +6.7-8mm HD media at 15kWh/t

Mass Wet Screened	**285.85**	**g**		
HD +6.7-8mm, 15kWh/t, Media Mass=5.5kg,				
Size Passing (µm)	Sample Mass (g)	Filter paper mass (g)	Net sample mass (g)	% Mass Passing	Cum % Passing
850	0.00	0.00	0.00	0.00	100.00
600	0.00	0.00	0.00	0.00	100.00
425	0.00	0.00	0.00	0.00	100.00
300	0.00	0.00	0.00	0.00	100.00
212	0	0.00	0.00	0.00	100.00
150	0.24	0.00	0.24	0.09	100.00
106	2.92	0.00	2.92	1.11	99.91
75	17.42	0.00	17.42	6.62	98.80
53	36.5	0.00	36.50	13.88	92.17
38	27.1	0.00	27.10	10.31	78.29
25	197.07	18.29	178.78	67.99	67.99
Total			**262.96**	**100**	

Table 55: Product size distribution raw data for 12.6kg +11.2-13.2mm HD media repeat test at 22.1kWh/t

Mass Wet Screened	**289.08**	**g**		
HD +11.2 - 13.2 mm Repeat SE=22.1kWh/t				
Size Passing (µm)	Sample Mass (g)	Filter paper mass (g)	Net sample mass (g)	% Mass Passing	Cum % Passing
850	0.00	0.00	0.00	0.00	100.00
600	0.00	0.00	0.00	0.00	100.00
425	0.00	0.00	0.00	0.00	100.00
300	0.00	0.00	0.00	0.00	100.00
212	0.32	0.00	0.32	0.11	100.00
150	2.78	0.00	2.78	0.98	99.89
106	13.40	0.00	13.40	4.71	98.91
75	31.92	0.00	31.92	11.22	94.20
53	35.37	0.00	35.37	12.43	82.99
38	29.12	0.00	29.12	10.23	70.56
25	190	18.3	171.7	60.33	60.33
Total			**284.61**	**100.00**	

Table 56: Product size distribution raw data for 12.6kg +11.2-13.2mm HD media repeat test at 15kWh/t

Mass Wet Screened	**296.62**	**g**		
HD +11.2 - 13.2 mm Repeat SE=15kWh/t				
Size Passing (µm)	Sample Mass (g)	Filter paper mass (g)	Net sample mass (g)	% Mass Passing	Cum % Passing
850	0.00	0.00	0.00	0.00	100.00
600	0.00	0.00	0.00	0.00	100.00
425	0.00	0.00	0.00	0.00	100.00
300	0.00	0.00	0.00	0.00	100.00
212	0.80	0.00	0.80	0.28	100.00
150	4.92	0.00	4.92	1.74	99.72
106	19.07	0.00	19.07	6.75	97.97
75	33.28	0.00	33.28	11.79	91.22
53	40.03	0.00	40.03	14.18	79.44
38	24.65	0.00	24.65	8.73	65.26
25	177.85	18.22	159.63	56.53	56.53
Total			**282.38**	**100**	

Table 57: Product size distribution raw data for 5.5kg +11.2-13.2mm HD media repeat test at 15kWh/t

Mass Wet Screened	**302.25**	**g**		
HD +11.2 - 13.2 mm SE=15kWh/t, Media=5.5kg Repeat				
Size Passing (µm)	Sample Mass (g)	Filter paper mass (g)	Net sample mass (g)	% Mass Passing	Cum % Passing
850	0.00	0.00	0.00	0.00	100.00
600	0.00	0.00	0.00	0.00	100.00
425	0.00	0.00	0.00	0.00	100.00
300	0.00	0.00	0.00	0.00	100.00
212	0.46	0.00	0.46	0.16	100.00
150	4.96	0.00	4.96	1.76	99.84
106	22.70	0.00	22.70	8.08	98.07
75	41.32	0.00	41.32	14.70	89.99
53	41.45	0.00	41.45	14.75	75.29
38	21.78	0.00	21.78	7.75	60.54
25	167.65	19.27	148.38	52.79	52.79
Total			**281.05**	**100**	

Table 58: Product size distribution raw data for 5.5kg +6.7-8mm HD media repeat test at 15kWh/t

Mass Wet Screened		**g**		
HD +6.7-8mm, 15kWh/t Repeat Media Mass=5.5kg,				
Size Passing (µm)	Sample Mass (g)	Filter paper mass (g)	Net sample mass (g)	% Mass Passing	Cum % Passing
850	0.00	0.00	0.00	0.00	100.00
600	0.00	0.00	0.00	0.00	100.00
425	0.00	0.00	0.00	0.00	100.00
300	0.00	0.00	0.00	0.00	100.00
212	0.21	0.00	0.21	0.07	100.00
150	0.40	0.00	0.40	0.14	99.93
106	2.62	0.00	2.62	0.91	99.79
75	15.54	0.00	15.54	5.38	98.88
53	39.92	0.00	39.92	13.83	93.50
38	33.92	0.00	33.92	11.75	79.66
25	209.83	13.84	195.99	67.91	67.91
Total			**288.6**	**100**	

7.2.4.2. Low Density (LD) media tests

Table 59: Product size distribution raw data for 5.5kg +2.80-4.75mm LD media at 13kWh/t

Mass Wet Screened		**288.09**	**g**		
Batch time	5min 11.23 secs				
LD +2.80 - 4.75 mm SE=13.0kWh/t, Media=5.50kg, 5:11:23					
Size Passing (µm)	Sample Mass (g)	Filter paper mass (g)	Net sample mass (g)	% Mass Passing	Cum % Passing
850	0.00	0.00	0.00	0.00	100.00
600	0.00	0.00	0.00	0.00	100.00
425	0.00	0.00	0.00	0.00	100.00
300	0.00	0.00	0.00	0.00	100.00
212	3.18	0.00	3.18	1.14	100.00
150	1.03	0.00	1.03	0.37	98.86
106	1.41	0.00	1.41	0.51	98.49
75	4.52	0.00	4.52	1.62	97.99
53	14.96	0.00	14.96	5.36	96.37
38	26.61	0.00	26.61	9.53	91.01
25	245.38	18.00	227.38	81.47	81.47
Total			**279.09**	**100.00**	

Table 60: Product size distribution raw data for 5.5kg +2.80-4.75mm LD media at 4.5kWh/t

Mass Wet Screened		**278.53**	**g**		
Batch time	1min 42secs				
LD +2.80 - 4.75 mm SE=4.5kWh/t, Media=5.50kg					
Size Passing (µm)	Sample Mass (g)	Filter paper mass (g)	Net sample mass (g)	% Mass Passing	Cum % Passing
850	0.24	0.00	0.24	0.09	100.00
600	0.85	0.00	0.85	0.32	99.91
425	1.7	0.00	1.70	0.63	99.59
300	3.04	0.00	3.04	1.13	98.96
212	16.38	0.00	16.38	6.09	97.83
150	9.24	0.00	9.24	3.44	91.74
106	16.75	0.00	16.75	6.23	88.31
75	28.58	0.00	28.58	10.63	82.08
53	31.81	0.00	31.81	11.83	71.45
38	18.57	0.00	18.57	6.90	59.63
25	158.3	16.50	141.80	52.72	52.72
Total			**268.96**	**97.83**	

Table 61: Product size distribution raw data for 5.5kg +5.6-6.7mm LD media at 15kWh/t

Mass Wet Screened		**303.84**	**g**		
Batch time	5min 11.23 secs				
LD +5.6 - 6.7mm SE=15.0kWh/t, Media=5.50kg,					
Size Passing (µm)	Sample Mass (g)	Filter paper mass (g)	Net sample mass (g)	% Mass Passing	Cum % Passing
850	0.00	0.00	0.00	0.00	100.00
600	0.00	0.00	0.00	0.00	100.00
425	0.00	0.00	0.00	0.00	100.00
300	0.00	0.00	0.00	0.00	100.00
212	0.00	0.00	0.00	0.00	100.00
150	0.41	0.00	0.41	0.14	100.00
106	1.13	0.00	1.13	0.38	99.86
75	8.78	0.00	8.78	2.93	99.49
53	31.69	0.00	31.69	10.59	96.55
38	37.03	0.00	37.03	12.37	85.96
25	238.52	18.32	220.20	73.59	73.59
Total			**299.24**	**100.00**	

Table 62: Product size distribution raw data for 5.5kg +6.7-8mm LD media at 5.8kWh/t

Mass Wet Screened		**282.47**	**g**		
Batch time	1min 42secs				
LD +6.7 - 8mm SE=5.8kWh/t, Media=5.50kg,					
Size Passing (µm)	Sample Mass (g)	Filter paper mass (g)	Net sample mass (g)	% Mass Passing	Cum % Passing
850	0.00	0.00	0.00	0.00	100.00
600	0.00	0.00	0.00	0.00	100.00
425	0.00	0.00	0.00	0.00	100.00
300	0.00	0.00	0.00	0.00	100.00
212	1.40	0.00	1.40	0.51	100.00
150	5.18	0.00	5.18	1.89	99.49
106	22.70	0.00	22.70	8.30	97.60
75	39.68	0.00	39.68	14.50	89.30
53	42.32	0.00	42.32	15.47	74.80
38	25.30	0.00	25.30	9.25	59.33
25	151.66	14.61	137.05	50.09	50.09
Total			**273.63**	**100.00**	

Table 63: Product size distribution raw data for 5.5kg +2.80-4.75mm LD media repeat test at 13.3kWh/t

Mass Wet Screened		**289.97**	**g**		
LD +2.80 - 4.75 mm SE=13.3kWh/t, Media=5.50kg, Repeat					
Size Passing (µm)	Sample Mass (g)	Filter paper mass (g)	Net sample mass (g)	% Mass Passing	Cum % Passing
850	0.00	0.00	0.00	0.00	100.00
600	0.00	0.00	0.00	0.00	100.00
425	0.00	0.00	0.00	0.00	100.00
300	0.00	0.00	0.00	0.00	100.00
212	3.70	0.00	3.70	1.32	100.00
150	0.64	0.00	0.64	0.23	98.68
106	0.90	0.00	0.90	0.32	98.46
75	2.64	0.00	2.64	0.94	98.14
53	10.84	0.00	10.84	3.85	97.20
38	20.50	0.00	20.50	7.29	93.34
25	268.13	26.06	242.07	86.06	86.06
Total			**281.29**	**100.00**	

Table 64: Product size distribution raw data for 5.5kg +2.80-4.75mm LD media repeat test at 4.5kWh/t

Batch time	1min 42secs				
Mass Wet Screened		**293.06**	**g**		
LD +2.80 - 4.75 mm SE=4.5kWh/t, Media=5.50kg, Repeat					
Size Passing (µm)	Sample Mass (g)	Filter paper mass (g)	Net sample mass (g)	% Mass Passing	Cum % Passing
850	0.28	0.00	0.28	0.10	100.00
600	0.85	0.00	0.85	0.29	99.90
425	1.92	0.00	1.92	0.66	99.61
300	4.27	0.00	4.27	1.46	98.96
212	21.24	0.00	21.24	7.26	97.50
150	11.71	0.00	11.71	4.00	90.23
106	19.98	0.00	19.98	6.83	86.23
75	37.98	0.00	37.98	12.99	79.39
53	28.9	0.00	28.90	9.88	66.41
38	25.44	0.00	25.44	8.70	56.52
25	155.33	15.50	139.83	47.82	47.82
Total			**292.40**	**97.50**	

Table 65: Product size distribution raw data for 5.5kg +5.6-6.7mm LD media repeat test at 15kWh/t

Mass Wet Screened		**252.04**	**g**		
LD +5.6 - 6.7mm SE=15.0kWh/t, Media=5.50kg,Repeat					
Size Passing (µm)	Sample Mass (g)	Filter paper mass (g)	Net sample mass (g)	% Mass Passing	Cum % Passing
850	0.00	0.00	0.00	0.00	100.00
600	0.00	0.00	0.00	0.00	100.00
425	0.00	0.00	0.00	0.00	100.00
300	0.00	0.00	0.00	0.00	100.00
212	0.00	0.00	0.00	0.00	100.00
150	0.46	0.00	0.46	0.18	100.00
106	1.50	0.00	1.50	0.60	99.82
75	9.35	0.00	9.35	3.76	99.21
53	26.72	0.00	26.72	10.74	95.45
38	36.93	0.00	36.93	14.84	84.72
25	189.27	15.41	173.86	69.87	69.87
Total			**248.82**	**100.00**	

Table 66: Product size distribution raw data for 5.5kg +6.7-8mm LD media repeat test at 5.8kWh/t

Batch time	1min 42secs				
Mass Wet Screened		**290.14**	**g**		
LD +6.7 - 8mm SE=5.8kWh/t, Media=5.50kg,Repeat					
Size Passing (µm)	Sample Mass (g)	Filter paper mass (g)	Net sample mass (g)	% Mass Passing	Cum % Passing
850	0.00	0.00	0.00	0.00	100.00
600	0.00	0.00	0.00	0.00	100.00
425	0.00	0.00	0.00	0.00	100.00
300	0.00	0.00	0.00	0.00	100.00
212	1.35	0.00	1.35	0.50	100.00
150	6.30	0.00	6.30	2.32	99.50
106	23.34	0.00	23.34	8.59	97.19
75	40.99	0.00	40.99	15.08	88.60
53	41.21	0.00	41.21	15.16	73.52
38	22.09	0.00	22.09	8.13	58.36
25	152.40	15.85	136.55	50.23	50.23
Total			**271.83**	**100.00**	

7.3. Development of stress model equations

The stress number in batch grinding processes is proportional to the number of grinding media contacts, N_C and the probability that sufficient stress is applied to a particle trapped between grinding media, P_S. The stress number has an inverse relationship with the number of product particles in the milling chamber, N_P. The expression describing the stress number is shown in Equation 14 (Kwade and Schwedes, 2002; Fadhel and Frances, 2001; Kwade, 1999a):

$$SN = \frac{N_c P_s}{N_p} \qquad \textbf{Equation 14}$$

(from Kwade and Schwedes, 2002).

The number of media interactions is said to be proportional to the number of revolutions,n, grinding time, t_G and grinding media inside the milling chamber, N_{GM}. This is described by Equation 15.

$$N_c \propto n \times t_G \times N_{GM} \qquad \textbf{Equation 15}$$

(from Kwade and Schwedes, 2002).

In Equation 8, grinding media inside the milling chamber can be estimated from the grinding chamber volume,V_{GC}, diameter of the grinding media, d_{GM}, the voidage of grinding media filling, ε and the filling ratio of the grinding media, φ_{GM}. This is shown in Equation 16.

$$N_G = \frac{V_{GC}\varphi_{GM}(1-\varepsilon)}{\frac{\pi}{6}d_{GM}^3} \qquad \textbf{Equation 16}$$

(from Kwade and Schwedes, 2002).

According to Kwade and Schwedes (2002), the likelihood that a particle is trapped between grinding media and sufficiently stressed partially depends on the type of comminution process. It is said that this probability is proportional to the grinding media surface (Equation 17) in the case of de-agglomeration and disintegration of microorganisms (Kwade and Schwedes, 2002)

$$P_s \propto d_{GM}^2 \qquad \textbf{Equation 17}$$

(from Kwade and Schwedes, 2002).

In the case of comminution of crystalline materials, this probability is said to be proportional to the volume between two grinding beads where a particle is like to be trapped which is in turn proportional to the diameter of the grinding media (Kwade and Schwedes, 2002):

$$P_s \propto d_{GM}$$ **Equation 18**

(from Kwade and Schwedes, 2002).

The number of feed particles can be estimated from the ratio of the total volume of particles to the average volume of one feed particle as shown in Equation 19 (Kwade and Schwedes, 2002).

$$N_p \propto \frac{V_{p,top}}{V_p} = \frac{(1-\varphi_{GM}(1-\varepsilon))}{V_p} c_v$$ **Equation 19**

(from Kwade and Schwedes, 2002).

Combining Equations 16 – 19, Equations 20 and 21 can be obtained.

$$SN = \frac{\varphi_{GM}(1-\varepsilon)}{(1-\varphi_{GM}(1-\epsilon))c_v} \frac{nt}{d_{GM}}$$ **Equation 20**

(from Kwade and Schwedes, 2002).

$$SN = \frac{\varphi_{GM}(1-\varepsilon)}{(1-\varphi_{GM}(1-\epsilon))c_v} \frac{nt}{d_{GM}^2}$$ **Equation 21**

(from Kwade and Schwedes, 2002).

In addition to the stress number, the stress intensity has also been identified as a considerable factor that influences particle fragmentation (Jankovic, 2003; Kwade and Schwedes, 2002; Kwade, 1999a).

A proportionality expression to describe the stress intensity, SI, in terms of the stress intensity of the grinding media SI_{GM}, has been derived for a disc type stirred mill and is expressed in equation 22 (Kwade and Schwedes, 2002; Kwade, 1999a):

$$SI \propto SI_{GM} = d_{GM}^3 \rho_{GM} v_t^2$$ **Equation 22**

Some of the major assumptions used in deriving equation 3 are as follows:

- The tangential velocity of the grinding beads is proportional to the circumferential speed of stirrer discs.
- Only single particle stressing occurs, hence the stressed particle volume is independent of the grinding media size.
- The diameter of the stirrer disks is constant.